

This discussion paper is/has been under review for the journal Atmospheric Chemistry and Physics (ACP). Please refer to the corresponding final paper in ACP if available.

# Air–snow transfer of nitrate on the East Antarctic plateau – Part 2: An isotopic model for the interpretation of deep ice-core records

J. Erbland<sup>1,2</sup>, J. Savarino<sup>1,2</sup>, S. Morin<sup>3</sup>, J. L. France<sup>4,\*</sup>, M. M. Frey<sup>5</sup>, and M. D. King<sup>4</sup>

<sup>1</sup>Université Grenoble Alpes, LGGE, 38000 Grenoble, France

<sup>2</sup>CNRS, LGGE, 38000 Grenoble, France

<sup>3</sup>Météo-France – CNRS, CNRM – GAME UMR 3589, CEN, Grenoble, France

<sup>4</sup>Department of Earth Sciences, Royal Holloway University of London, Egham, Surrey, TW20 0EX, UK

<sup>5</sup>British Antarctic Survey, Natural Environment Research Council, Cambridge, UK

\* now at: School of Environmental Sciences, University of East Anglia, Norwich, NR4 7TJ, UK

Received: 9 January 2015 – Accepted: 23 February 2015 – Published: 10 March 2015

Correspondence to: J. Savarino (joel.savarino@ujf-grenoble.fr)

Published by Copernicus Publications on behalf of the European Geosciences Union.

Title Page

Abstract

Introduction

Conclusions

References

Tables

Figures

◀

▶

◀

▶

Back

Close

Full Screen / Esc

Printer-friendly Version

Interactive Discussion



## Abstract

Unraveling the modern budget of reactive nitrogen on the Antarctic plateau is critical for the interpretation of ice core records of nitrate. This requires accounting for nitrate recycling processes occurring in near surface snow and the overlying atmospheric boundary layer. Not only concentration measurements, but also isotopic ratios of nitrogen and oxygen in nitrate, provide constraints on the processes at play. However, due to the large number of intertwined chemical and physical phenomena involved, numerical modelling is required to test hypotheses in a quantitative manner. Here we introduce the model “TRAnsfer of Atmospheric Nitrate Stable Isotopes To the Snow” (TRANSITS), a novel conceptual, multi-layer and one-dimensional model representing the impact of processes operating on nitrate at the air–snow interface on the East Antarctic plateau, in terms of concentrations (mass fraction) and the nitrogen ( $\delta^{15}\text{N}$ ) and oxygen isotopic composition ( $^{17}\text{O}$ -excess,  $\Delta^{17}\text{O}$ ) in nitrate. At the air–snow interface at Dome C (DC, 75°06' S, 123°19' E), the model reproduces well the values of  $\delta^{15}\text{N}$  in atmospheric and surface snow (skin layer) nitrate as well as in the  $\delta^{15}\text{N}$  profile in DC snow including the observed extraordinary high positive values (around +300‰) below 20 cm. The model also captures the observed variability in nitrate mass fraction in the snow. While oxygen data are qualitatively reproduced at the air–snow interface at DC and in East Antarctica, the simulated  $\Delta^{17}\text{O}$  values underestimate the observed  $\Delta^{17}\text{O}$  values by a few %. This is explained by the simplifications made in the description of the atmospheric cycling and oxidation of  $\text{NO}_2$ . The model reproduces well the sensitivity of  $\delta^{15}\text{N}$ ,  $\Delta^{17}\text{O}$  and the apparent fractionation constants ( $^{15}\varepsilon_{\text{app}}$ ,  $^{17}E_{\text{app}}$ ) to the snow accumulation rate. Building on this development, we propose a framework for the interpretation of nitrate records measured from ice cores. Measurement of nitrate mass fractions and  $\delta^{15}\text{N}$  in the nitrate archived in an ice core, may be used to derive information about past variations in the total ozone column and/or the primary inputs of nitrate above Antarctica as well as in nitrate trapping efficiency (defined as the ratio between the archived nitrate flux and the primary nitrate input flux). The  $\Delta^{17}\text{O}$  of

## Air–snow transfer of nitrate on the East Antarctic plateau

J. Erbland et al.

[Title Page](#)

[Abstract](#)

[Introduction](#)

[Conclusions](#)

[References](#)

[Tables](#)

[Figures](#)

◀

▶

[Back](#)

[Close](#)

[Full Screen / Esc](#)

[Printer-friendly Version](#)

[Interactive Discussion](#)



nitrate could then be corrected from the impact of cage recombination effects associated with the photolysis of nitrate in snow. Past changes in the relative contributions of the  $\Delta^{17}\text{O}$  in the primary inputs of nitrate and the  $\Delta^{17}\text{O}$  in the locally cycled  $\text{NO}_2$  could then be determined. Therefore, information about the past variations in the local and long range processes operating on reactive nitrogen species could be obtained from ice cores collected in low accumulation regions such as the Antarctic plateau.

## 1 Introduction

Ice cores from the East Antarctic plateau provide long-term archives of Earth's climate and atmospheric composition such as past relative changes in local temperatures and global atmospheric  $\text{CO}_2$  levels (EPICA community members, 2004, for example). Soluble impurities have been used in such cores as tracers of biogeochemical processes. As the end product of the atmospheric oxidation of  $\text{NO}_x$  ( $\text{NO} + \text{NO}_2$ ), nitrate ( $\text{NO}_3^-$ ) is a major ion found in Antarctic snow (Wolff, 1995). Its primary origins are a combination of inputs from the stratosphere and from low latitude sources (Legrand and Delmas, 1986; Legrand and Kirchner, 1990). Stratospheric inputs of nitrate are believed to be mostly caused by the sedimentation of Polar Stratospheric Clouds (PSCs) in winter (Seinfeld and Pandis, 1998; Jacob, 1999). The interpretation of nitrate deep ice-core records remains elusive (e.g. Wolff et al., 2010) mainly because its deposition to the snow is not irreversible (Traversi et al., 2014 and references therein) at low accumulation sites such as Dome C or Vostok ( $78^\circ 27' \text{ S}, 106^\circ 50' \text{ E}$ , elevation 3488 m.a.s.l.).

### 1.1 Nitrate recycling

Nitrate loss from snow can occur through the physical release of  $\text{HNO}_3$  (via evaporation and/or desorption, also referred to as simply "evaporation") or through the UV-photolysis of the  $\text{NO}_3^-$  ion (Röthlisberger et al., 2000). At wavelengths ( $\lambda$ ) below 345 nm,  $\text{NO}_3^-$  photolyses to form  $\text{NO}_2$  (Chu and Anastasio, 2003) or  $\text{NO}_2^-$  ion (Chu and

ACPD

15, 6887–6966, 2015

## Air–snow transfer of nitrate on the East Antarctic plateau

J. Erbland et al.

[Title Page](#)

[Abstract](#)

[Introduction](#)

[Conclusions](#)

[References](#)

[Tables](#)

[Figures](#)



[Back](#)

[Close](#)

[Full Screen / Esc](#)

[Printer-friendly Version](#)

[Interactive Discussion](#)



Anastasio, 2007) which can form HONO at pH < 7. Nitrate photolysis is quantitatively represented by its rate constant ( $J$ ) expressed as follows:

$$J = \int \phi(\lambda, T) \sigma(\lambda, T) I(\lambda, \theta, z) d\lambda \quad (1)$$

with  $\phi$  the quantum yield,  $\sigma$  the absorption cross section of  $\text{NO}_3^-$ ,  $I$  the actinic flux,

- 5  $\lambda$  the wavelength,  $T$  the temperature,  $\theta$  the solar zenith angle and  $z$  the depth. Two recent laboratory studies have investigated nitrate photolysis in DC snow. Meusinger et al. (2014) have reported the quantum yields for the photolysis of either photolabile or buried nitrate. The terms “photolabile” and “buried” were introduced by Meusinger et al. (2014) as different “domains”, i.e. different physico-chemical properties of the 10 region around the nitrate chromophore. Berhanu et al. (2014a) have reported the absorption cross-section of  $^{14}\text{NO}_3^-$  and  $^{15}\text{NO}_3^-$  in Antarctic snow at a given temperature, using a new semi-empirical zero point energy shift ( $\Delta\text{ZPE}$ ) model.

Nitrate deposition to the snow can occur through various mechanisms including co-condensation and dry deposition (Röthlisberger et al., 2000; Frey et al., 2009). Within 15 the snowpack, nitrate can be contained as  $\text{HNO}_3$  in the gas phase, adsorbed on the surface or dissolved in the snow ice matrix. It can be exchanged between these compartments by adsorption, desorption or diffusion processes (Dominé et al., 2007) which can lead to a redistribution of nitrate inside the snowpack, a process which tends to smooth the nitrate mass fraction profiles (Wagenbach et al., 1994). Phase change 20 and recrystallization processes (snow metamorphism) can further promote the mobility of nitrate thus potentially modify the location of nitrate (Dominé and Shepson, 2002; Kaempfer and Plapp, 2009), with implications for its availability for photolysis and desorption processes (Dominé and Shepson, 2002). For instance, it is more available for photolysis when adsorbed on the snow ice matrix surface where cage recombination 25 effects are less likely to occur (Chu and Anastasio, 2003; Meusinger et al., 2014 and references therein).

The photolysis of nitrate has been identified to be an important mechanism for nitrate mass loss in the snow on the Antarctic plateau (Frey et al., 2009; France et al.,

<a href="#">Title Page</a>	
<a href="#">Abstract</a>	<a href="#">Introduction</a>
<a href="#">Conclusions</a>	<a href="#">References</a>
<a href="#">Tables</a>	<a href="#">Figures</a>
<a href="#">◀</a>	<a href="#">▶</a>
<a href="#">◀</a>	<a href="#">▶</a>
<a href="#">Back</a>	<a href="#">Close</a>
<a href="#">Full Screen / Esc</a>	
<a href="#">Printer-friendly Version</a>	
<a href="#">Interactive Discussion</a>	



2011). As a consequence, the release of nitrogen oxides through this process leads to a complex recycling of nitrate at the air–snow interface (Davis et al., 2008). Here we refer to “nitrate recycling” as the combination of nitrate photolysis in snow and the production of  $\text{NO}_x$ , the subsequent atmospheric gas-phase chemistry to form atmospheric nitrate from  $\text{NO}_x$ , its partial dry or wet deposition and the export of the remaining. Davis et al. (2008) and Frey et al. (2009) suggested the following conceptual model for nitrate recycling in the atmosphere–snow system for the Antarctic plateau where annual snow accumulation rates are low. The stratospheric component of nitrate is deposited to the surface in late winter, in a shallow surface snow layer of approximately uniform concentration (Savarino et al., 2007). The increase in surface UV radiation in spring initiates a photolysis-driven redistribution process of  $\text{NO}_3^-$ , which continues throughout the sunlit season resulting in the almost complete depletion of the bulk snow nitrate reservoir. In summer, this results in a strongly asymmetric distribution of total  $\text{NO}_3^-$  within the atmosphere–snow column as previously noted by Wolff et al. (2002), with the majority of the mass of nitrate residing in a “skin layer” (the top mm of snow, often under form of surface hoar) and only a small fraction in the atmospheric column above it or in the snow below.

## 1.2 Nitrogen cycles overlapping at the air–snow interface at Dome C

Figure 1 shows the two nitrogen cycles, which overlap at the air–snow interface at Dome C. The first cycle concerns  $\text{NO}_2$ , which is formed by the oxidation of NO and destroyed by photolysis or by oxidation to form  $\text{HNO}_3$ . Kukui et al. (2014) have measured a median photolytic rate constant of  $\text{NO}_2$  of  $1.3 \times 10^{-2} \text{ s}^{-1}$  at DC from 19 December 2011 to 10 January 2012 which gives a photochemical lifetime of  $\text{NO}_2$  of  $\tau_{\text{photo}}(\text{NO}_2) \approx 77 \text{ s}$ . The main summertime oxidation channel of NO is  $\text{NO} + \text{O}_3$  with a chemical lifetime of NO of  $\tau_{\text{NO+O}_3} \approx 5.7 \text{ min}$  for the median mixing ratio of  $\text{O}_3$  of 23.7 ppb (Kukui et al., 2014). The  $\text{NO} + \text{O}_3$  oxidation channel is therefore the limitation reaction in the  $\text{NO}/\text{NO}_2$  cycling. Considering the oxidation by OH as the main sink of  $\text{NO}_2$  around summer solstice, we find a chemical lifetime of  $\text{NO}_2$  of  $\tau_{\text{NO}_2+\text{OH}} \approx 58 \text{ min}$

[Title Page](#)

[Abstract](#)

[Introduction](#)

[Conclusions](#)

[References](#)

[Tables](#)

[Figures](#)

[◀](#)

[▶](#)

[◀](#)

[▶](#)

[Back](#)

[Close](#)

[Full Screen / Esc](#)

[Printer-friendly Version](#)

[Interactive Discussion](#)



for temperature, pressure and OH mixing ratios ( $3.1 \times 10^6$  molecule cm $^{-3}$ ) observed over the same period (Kukui et al., 2014). The ratio  $\tau_{\text{NO}_2+\text{OH}}/\tau_{\text{NO}+\text{O}_3}$  indicates that, in summertime conditions, NO<sub>2</sub> is photochemically cycled approximately 10 times before being converted into HNO<sub>3</sub>. In the atmosphere, HNO<sub>3</sub> does not accumulate much as observed from the low nitrate atmospheric concentrations at Dome C (Frey et al., 2009; Erbland et al., 2013). This is due to the fact that the chemical lifetime of NO<sub>2</sub> is of the same order of magnitude as the deposition/export lifetime of HNO<sub>3</sub> (approximately 3.5 h at South Pole, Huey et al., 2004). Therefore, nitric acid quickly deposits after its formation in the atmosphere and this results in a cycle at the air–snow interface where snow NO<sub>3</sub><sup>-</sup> is converted to NO<sub>2</sub> which is ultimately oxidized to gas-phase HNO<sub>3</sub>, which deposits on the snow surface.

The second cycle concerns NO<sub>3</sub><sup>-</sup> in the snow photic zone (the zone of active photochemistry), which corresponds to ca. 50 cm, i.e. 3 times the observed typical e-folding depth (France et al., 2011), a depth below which 95 % of the UV radiation is lost. There, it accumulates by deposition of atmospheric HNO<sub>3</sub> and is removed by UV photolysis or is “archived” below the photic zone. The lifetime of nitrate in the top 50 cm against photolysis can be calculated as  $\tau_{\text{photo}}(\text{NO}_3^-) = m_{50\text{ cm}}(\text{NO}_3^-)/F(\text{NO}_2)$  (Sect. 3.1.1 in Jacob, 1999), with  $m_{50\text{ cm}}(\text{NO}_3^-)$  the integrated mass of nitrate per unit horizontal surface area in the top 50 cm of the snowpack and  $F(\text{NO}_2)$ , the annual potential flux of photolytically-produced NO<sub>2</sub> per unit horizontal surface area. The lifetime of nitrate in the top 50 cm against archival can be calculated as  $\tau_{\text{arch}}(\text{NO}_3^-) = m_{50\text{ cm}}(\text{NO}_3^-)/\text{FA}$  (Jacob, 1999), with FA, the archived nitrate mass flux per unit horizontal surface area. Using representative annual values for the above physical (potential NO<sub>2</sub> flux, France et al., 2011; updated  $\phi$  value, Meusinger et al., 2014; archived nitrate flux, Frey et al., 2009; Erbland et al., 2013,), it is found that nitrate in snow is cycled on average  $\approx 120$  times in the snow photic zone before being buried below the photic zone.

<a href="#">Title Page</a>	<a href="#">Abstract</a>	<a href="#">Introduction</a>
<a href="#">Conclusions</a>	<a href="#">References</a>	
<a href="#">Tables</a>	<a href="#">Figures</a>	
<a href="#">◀</a>	<a href="#">▶</a>	
<a href="#">◀</a>	<a href="#">▶</a>	
<a href="#">Back</a>	<a href="#">Close</a>	
<a href="#">Full Screen / Esc</a>		
	<a href="#">Printer-friendly Version</a>	
	<a href="#">Interactive Discussion</a>	



## 1.3 Isotopic signatures of processes involved in nitrate recycling

The post-depositional processes as described above thus strongly imprint the stable isotopic composition of nitrate in snow at low accumulation sites (Blunier et al., 2005; Frey et al., 2009; Erbland et al., 2013). Nitrate is composed of N and O atoms and has the following stable isotope ratios:  $^{15}\text{N}/^{14}\text{N}$ ,  $^{17}\text{O}/^{16}\text{O}$  and  $^{18}\text{O}/^{16}\text{O}$  from which isotopic enrichment values  $\delta^{15}\text{N}$ ,  $\delta^{17}\text{O}$ ,  $\delta^{18}\text{O}$  can be computed. The  $\delta$  scale is defined as  $\delta = R_{\text{spl}}/R_{\text{ref}} - 1$  with  $R$  denoting the isotope ratios, the references being  $\text{N}_2\text{--AIR}$  for N and VSMOW for O. The quantification of the integrated isotopic effects of post-depositional processes is achieved by calculating apparent fractionation constants ( $^{15}\varepsilon_{\text{app}}$ ,  $^{17}\varepsilon_{\text{app}}$  and  $^{18}\varepsilon_{\text{app}}$ ) from isotopic and mass fraction profiles of nitrate in the top decimeters of snow (Blunier et al., 2005; Frey et al., 2009; Erbland et al., 2013). For instance,  $^{15}\varepsilon_{\text{app}}$  is calculated from the following equation, which represents a Rayleigh model and assumes a single loss process and the immediate and definitive removal of the lost nitrate fraction:

$$^{15}\ln(\delta^{15}\text{N}_f + 1) = ^{15}\varepsilon_{\text{app}} \cdot \ln f + \ln(\delta^{15}\text{N}_0 + 1) \quad (2)$$

with  $\delta^{15}\text{N}_f$  and  $\delta^{15}\text{N}_0$  the  $\delta$ -value in the remaining and initial snow nitrate,  $f$  is the remaining mass fraction. Comparing apparent fractionation constants obtained in the field to the fractionation constants associated with the physical and photochemical nitrate loss processes has demonstrated that the UV-photolysis of nitrate is the dominant mass loss process on the Antarctic plateau (Erbland et al., 2013). As a consequence,  $^{15}\text{N}$  in nitrate archived beyond the photic zone on plateau sites depends on  $^{15}\varepsilon_{\text{pho}}$ , the  $^{15}\text{N}/^{14}\text{N}$  fractionation constant associated with nitrate photolysis (Frey et al., 2009; Erbland et al., 2013) and the magnitude of the loss ( $f$ ) (Eq. 2). Because of its link with the residence time of nitrate in the photic zone, a strong relationship has been found between the snow accumulation rate ( $A$ ) and the degree of isotopic fractionation  $\delta^{15}\text{N}$  in the archived (asymptotic, "as.") nitrate (Freyer et al., 1996; Erbland et al., 2013). At a given actinic flux  $I$ , the  $^{15}\text{N}/^{14}\text{N}$  fractionation constant induced by nitrate photolysis

Title Page

Abstract

Introduction

Conclusions

References

Tables

Figures

◀

▶

◀

▶

Back

Close

Full Screen / Esc

Printer-friendly Version

Interactive Discussion



is calculated as the ratio of the photolysis rate constants:

$$^{15}\varepsilon_{\text{pho}} = \frac{J'}{J} - 1 \quad (3)$$

with  $J$  and  $J'$  the photolytic rate constants of  $^{14}\text{NO}_3^-$  and  $^{15}\text{NO}_3^-$  respectively. The Rayleigh distillation model applied to a single process in an open system gives the  $\delta^{15}\text{N}$  values in the emitted and remaining fractions as follows:

$$\delta^{15}\text{N}_{\text{rem}} = (1 + \delta^{15}\text{N}_0) \times f^{^{15}\varepsilon} - 1 \quad (4)$$

$$\delta^{15}\text{N}_{\text{emi}} = (1 + \delta^{15}\text{N}_0) \times \frac{1 - f^{^{15}\varepsilon+1}}{1 - f} - 1 \quad (5)$$

with  $f$  the remaining nitrate mass fraction,  $^{15}\varepsilon$  the fractionation constant and  $\delta^{15}\text{N}_0$  which represents the  $\delta^{15}\text{N}$  in the initial nitrate.

The three stable isotopes of oxygen allow to define a unique tracer,  $\Delta^{17}\text{O} = \delta^{17}\text{O} - 0.52 \times \delta^{18}\text{O}$  which is referred to as “oxygen isotope anomaly” or also “ $^{17}\text{O}$ -excess”. An apparent fractionation constant ( $^{17}F_{\text{app}}$ ) can be computed for  $\Delta^{17}\text{O}$  using Eq. (2), similarly to what can be done for isotopic enrichment values ( $\delta$ ). Most oxygen-bearing species feature  $\Delta^{17}\text{O} = 0\%$  but some species such as atmospheric nitrate can partially inherit the large positive oxygen isotope anomaly transferred from ozone thus reflecting the relative contribution of various oxidants involved in its formation (Michalski et al., 2003; Morin et al., 2007, 2008, 2009, 2011; Kunasek et al., 2008; Alexander et al., 2009).

Erblund et al. (2013) documented year-round measurements of  $\Delta^{17}\text{O}$  in atmospheric and skin layer nitrate at Dome C and on the Antarctic plateau, which revealed a photolytically driven isotopic equilibrium between the two compartments, i.e. the  $\Delta^{17}\text{O}$  atmospheric signal is mostly conserved in the skin layer. In contrast to  $\delta^{15}\text{N}$ , post-depositional processes have a small impact on  $\Delta^{17}\text{O}$  in nitrate snow profiles (Frey et al., 2009) so that a large portion of the atmospheric signature is transferred in snow

Title Page

Abstract

Introduction

Conclusions

References

Tables

Figures

◀

▶

◀

▶

Back

Close

Full Screen / Esc

Printer-friendly Version

Interactive Discussion



## 1.4 Goals of this article

In this paper, we test the nitrate recycling theory and evaluate it in light of the field isotopic measurements presented in Erbland et al. (2013) and obtained at the air–snow interface at Dome C as well as in several shallow snow pits collected at this site and on a large portion of the East Antarctic plateau. Testing this theory requires the building of a numerical model which represents nitrate recycling at the air–snow interface and describes the evolution of the nitrogen and oxygen stable isotopic composition of nitrate with various constraints from key environmental variables such as the solar zenith angle and the available UV radiation. Various models have been developed to investigate the physical and chemical processes involving nitrate in snow and their impact on the atmospheric chemistry in Antarctica (Wang et al., 2007; Liao and Tan, 2008; Boxe and Saiz-Lopez, 2008) and in Greenland (Jarvis et al., 2008, 2009; Kunasek et al., 2008; Thomas et al., 2011; Zatko et al., 2013). Those models are adapted to short time periods (hours to day typically) and focus on processes at play in the atmosphere and in the near-surface snowpack. In this article, we present a new model called TRANSITS (“T<sup>R</sup>ansfer of Atmospheric Nitrate Stable Isotopes To the Snow”), which shares some hypotheses with the modeling effort of Wolff et al. (2002) and the conceptual model of Davis et al. (2008). Together with a more realistic representation of some processes,

<a href="#">Title Page</a>	
<a href="#">Abstract</a>	<a href="#">Introduction</a>
<a href="#">Conclusions</a>	<a href="#">References</a>
<a href="#">Tables</a>	<a href="#">Figures</a>
<a href="#">◀</a>	<a href="#">▶</a>
<a href="#">◀</a>	<a href="#">▶</a>
<a href="#">Back</a>	<a href="#">Close</a>
<a href="#">Full Screen / Esc</a>	
<a href="#">Printer-friendly Version</a>	
<a href="#">Interactive Discussion</a>	



[Title Page](#)[Abstract](#)[Introduction](#)[Conclusions](#)[References](#)[Tables](#)[Figures](#)[◀](#)[▶](#)[◀](#)[▶](#)[Back](#)[Close](#)[Full Screen / Esc](#)[Printer-friendly Version](#)[Interactive Discussion](#)

the main novelty brought by the TRANSITS model is the incorporation of the oxygen and nitrogen stable isotopic ratios in nitrate as a diagnostic and evaluation tool in the ideal case of the East Antarctic plateau where snow accumulation rates are low and where nitrate mass loss can be mostly attributed to UV-photolysis. The following key questions are addressed in this work:

- 5 1. Is the theory behind the TRANSITS model compatible with the available field measurements?
2. What controls the mass and isotopic composition ( $\delta^{15}\text{N}$  and  $\Delta^{17}\text{O}$ ) of the archived nitrate?
- 10 3. The model is first described. Then it is evaluated by comparing its outputs to observations in the case of simulations at the air–snow interface at Dome C as well as in East Antarctic sites. A framework for the interpretation of the nitrate isotope record in deep ice cores is then given in light of sensitivity tests of the model.

## 2 Description of the TRANSITS model

### 15 2.1 Overview

TRANSITS is a multi-layer, 1-D isotopic model which represents a snow and atmosphere column with an arbitrary surface area taken sufficiently large to neglect local lateral air mass movement (i.e. at the scale of the East Antarctic plateau). The snowpack is set to a constant height of one meter divided into 1000 layers of a 1 mm thickness.

- 20 4. The atmospheric boundary layer (ABL) is represented by a single box of a constant height.

The aim of the model is to conceptually represent nitrate recycling at the air–snow interface (UV-photolysis of  $\text{NO}_3^-$ , emission of  $\text{NO}_x$ , local oxidation, deposition of  $\text{HNO}_3$ ) and to model the impact on nitrogen and oxygen stable isotopic ratios in nitrate in both reservoirs. For the sake of simplicity, we will focus on  $\Delta^{17}\text{O}$  and  $\delta^{15}\text{N}$ ;  $\delta^{18}\text{O}$  is

<a href="#">Title Page</a>	
<a href="#">Abstract</a>	<a href="#">Introduction</a>
<a href="#">Conclusions</a>	<a href="#">References</a>
<a href="#">Tables</a>	<a href="#">Figures</a>
<a href="#">◀</a>	<a href="#">▶</a>
<a href="#">◀</a>	<a href="#">▶</a>
<a href="#">Back</a>	<a href="#">Close</a>
<a href="#">Full Screen / Esc</a>	
<a href="#">Printer-friendly Version</a>	
<a href="#">Interactive Discussion</a>	

not included in the TRANSITS model. The TRANSITS model is neither a snowpack nor a gas-phase chemistry model and it does not aim at representing all the mechanisms responsible for nitrate mobility neither at the snowpack scale nor at the snow microstructure scale.

Figure 2 provides an overview of the TRANSITS model. The loss of nitrate from snow is assumed to only occur through UV-photolysis, because the physical release of  $\text{HNO}_3$  is negligible (Erbland et al., 2013). TRANSITS does not treat different nitrate domains in snow and it is hypothesized that its photolysis only produces  $\text{NO}_2$ .  $\text{NO}_2$  undergoes local cycling with NO which modifies its oxygen isotope composition while the N atom is preserved. One computed year is divided into 52 time steps of approximately one week ( $\Delta t = 606\,877$  s), a time step sufficiently long to assume quantitative oxidation of  $\text{NO}_2$  into  $\text{HNO}_3$ . The chosen time step also allows to operate at the annual timescale, which is best suited to long simulation durations. For simplicity, we assume that  $\text{NO}_2$  oxidation occurs through reaction with OH radicals. The deposition of atmospheric  $\text{HNO}_3$  is assumed to occur by the uptake at the surface of the snowpack. Nitrate diffusion is assumed to occur in the snowpack and is solved at a time step of 4 h within each main model time step. Below one meter, a depth where the actinic flux is always negligible, the nitrate is archived. Table 1 provides a glossary of the acronyms used in this paper, as well as their definition.

## 2.2 Mass balance equations

In each box, the model solves the general “mass-balance” equation, which describes the temporal evolution of the concentration of the species  $X$  (i.e. nitrate or  $\text{NO}_2$ ):

$$\frac{d}{dt}[X] = \sum_i P_i - \sum_j L_j \quad (6)$$



The mass-balance equations also apply to the products  $[X] \times \delta^{15}\text{N}$  and  $[X] \times \Delta^{17}\text{O}$  (Morin et al., 2011):

$$\frac{d}{dt}([X] \times \delta^{15}\text{N}) = \sum_i (P_i \times \delta^{15}\text{N}_i(X)) - (\sum_j (L_j \times (\delta^{15}\text{N}(X) - 15\varepsilon_j))) \quad (7)$$

$$\frac{d}{dt}([X] \times \Delta^{17}\text{O}) = \sum_i (P_i \times \Delta^{17}\text{O}_i(X)) - (\sum_j L_j) \times \Delta^{17}\text{O}(X) \quad (8)$$

5 where  $P_i$  and  $L_j$  respectively represent sources and sinks rates (in  $\text{cm}^{-3} \text{s}^{-1}$ ) and  $\delta^{15}\text{N}_i(X)$  and  $\Delta^{17}\text{O}_i(X)$  the isotopic compositions of the  $i$  sources. A  $^{15}\text{N}/^{14}\text{N}$  fractionation constant ( $^{15}\varepsilon_j$ ) can be associated with loss process  $j$ . Within each compartment, incoming fluxes are positive and outgoing fluxes are negative. The concentration of nitrate in a snow layer is handled as “nitrate mass fraction” which is denoted  $\omega(\text{NO}_3^-)$ .

10 For simplicity, fluxes will be hereafter denoted “FY”, with “Y” a chain of capital letters. The primary input of nitrate to the modeled atmosphere is denoted FPI and is a combination of a stratospheric flux (FS) and the horizontal long distance transport (FT) of nitrate. Therefore,  $\text{FPI} = \text{FS} + \text{FT}$ . The two primary origins of nitrate are defined by constant  $\Delta^{17}\text{O}$  and  $\delta^{15}\text{N}$  signatures denoted  $\Delta^{17}\text{O}(\text{FS})$ ,  $\Delta^{17}\text{O}(\text{FT})$ ,  $\delta^{15}\text{N}(\text{FS})$  and  $\delta^{15}\text{N}(\text{FT})$ . The secondary source of nitrate to the atmosphere is the local oxidation of  $\text{NO}_2$  occurring after nitrate photolysis in the snow (FP).

15 Nitrate is removed from the atmospheric box via two processes. Large scale horizontal air masses movement can lead to a loss of nitrate, hereafter named “horizontal export flux” (FE). The FE flux is modeled as a constant fraction of all incoming nitrate fluxes to the atmosphere  $\text{FE} = f_{\text{exp}} \times (\text{FP} + \text{FS} + \text{FT})$ . The export of nitrate is assumed to preserve the  $\Delta^{17}\text{O}$  and  $\delta^{15}\text{N}$  values. Nitrate can also be lost via deposition (FD) to the snow, which is the sole nitrate source to the snowpack. This flux is obtained by solving the mass balance in the atmospheric box and is added to the topmost layer of the snowpack at each model time step.

<a href="#">Title Page</a>	
<a href="#">Abstract</a>	<a href="#">Introduction</a>
<a href="#">Conclusions</a>	<a href="#">References</a>
<a href="#">Tables</a>	<a href="#">Figures</a>
<a href="#"></a>	<a href="#"></a>
<a href="#"></a>	<a href="#"></a>
<a href="#">Full Screen / Esc</a>	
<a href="#">Printer-friendly Version</a>	
<a href="#">Interactive Discussion</a>	



The loss of nitrate from the snowpack is assumed to occur through nitrate UV-photolysis only. Within the snowpack, nitrate is redistributed by macroscopic diffusion, which is assumed to preserve  $\Delta^{17}\text{O}$  and  $\delta^{15}\text{N}$ .

## 2.3 Physical properties of the atmosphere and the snowpack

- 5 The constant height of the ABL is denoted  $h_{\text{AT}}$ . This single atmospheric box is assumed to be well mixed at all times which is justified at the time resolution of the model (ca. one week). Hereafter we denote  $\gamma(\text{NO}_3^-)$  the nitrate concentration in the atmospheric box. In TRANSITS, the time evolution of this variable is prescribed.

Physical properties of the snowpack influencing radiative transfer in snow are fixed,  
10 according to a typical Dome C snowpack with a constant layering throughout the year as defined in France et al. (2011): it is made of 11 and 21 cm of soft and hard wind-  
pack snow at the top and hoar-like snow below with their respective snow densities,  
scattering and absorption coefficients at 350 nm. At Dome C, the e-folding attenuation  
depths (denoted  $\eta$ ) for the three snow layers are fairly constant in the range 350–  
15 400 nm (France et al., 2011) and this observation can be extended to the 320–350 nm  
range. The snow optical properties taken at 350 nm are therefore assumed to be valid  
for the whole 280–350 nm range of interest for nitrate photolysis. This hypothesis is  
supported twofold. First, e-folding attenuation depths measured at Alert, Nunavut show  
no significant sensitivity to wavelengths in the 310–350 nm range (King and Simpson,  
20 2001). Second,  $\eta$  values measured in a recent laboratory study only show a weak  
(10 %) decrease from 350 to 280 nm (Meusinger et al., 2014). Under Dome C conditions,  
the absorption of UV by impurities is small and the depth attenuation of UV  
light is mostly driven by light scattering (France et al., 2011). As a consequence,  $\eta$  is  
assumed to be independent on the impurities content in the snow, in this case, nitrate  
itself.

While optical calculations are based on a realistic snowpack, nitrate mass and isotopic computations are performed assuming a constant density of snow ( $\rho$ ), which simplifies the computation. This simplification has no impact on the optical behavior

<a href="#">Title Page</a>	
<a href="#">Abstract</a>	<a href="#">Introduction</a>
<a href="#">Conclusions</a>	<a href="#">References</a>
<a href="#">Tables</a>	<a href="#">Figures</a>
<a href="#">◀</a>	<a href="#">▶</a>
<a href="#">◀</a>	<a href="#">▶</a>
<a href="#">Back</a>	<a href="#">Close</a>
<a href="#">Full Screen / Esc</a>	
<a href="#">Printer-friendly Version</a>	
<a href="#">Interactive Discussion</a>	



of the snowpack because it is assumed to be independent on the nitrate fractions. However, the snow density being constant means that the snowpack does not undergo densification. For simplicity, we also hypothesize that no sublimation, wind redistribution, melt nor flow occur and that the surface of the snowpack is assumed to be flat and insensitive to erosion.

5

## 2.4 Parameterization of chemical processes

Figure 3 provides an overview of the physical and chemical processes included in TRANSITS as well as the parameters and input variables of interest for each process. Table 2 lists the chemical and physical processes included or not in the model. A description of the parameterization of each process is given below.

10

### 2.4.1 Nitrate UV-photolysis

Nitrate photolysis is at the core of the model. At each time step, the photolyzed nitrate mass in a layer equals  $e^{-J\Delta t} \times m$ , where  $m$  is the initial nitrate mass in the layer and  $J$ , the photolysis rate constant of  $\text{NO}_3^-$  (Eq. 1). The UV actinic fluxes ( $I$ ) required for the calculation of  $J$  have been computed in the 280–350 nm range using offline runs of the TUV-snow radiative-transfer model (Lee-Taylor and Madronich, 2012). TUV-snow has been run for the DC location and snowpack for various dates (i.e. solar zenith angle,  $\theta$ ), assuming a clear aerosols-free sky and using the extraterrestrial irradiance from Chance and Kurucz (2010) and a constant Earth–Sun distance as that of 27 December 2010. Ozone profiles from 25 to 500 DU with a resolution of 25 DU have been used to run the radiative transfer model. Next, we denote  $k$  the “photic zone compression factor”, which represents variations of depth of the photic zone under the effect of changes in physical properties of the snowpack due to snow metamorphism or in chemical properties. In Eq. (1), the term “ $z$ ” is therefore replaced by “ $z/k$ ”. A typical Dome C snowpack is represented by  $k$  value of 1. Lower  $k$  values mean that the UV radiation is extinguished more rapidly with depth. Last, we denote  $q$  the “actinic flux

15

20

25

ACPD

15, 6887–6966, 2015

Air–snow transfer of  
nitrate on the East  
Antarctic plateau

J. Erbland et al.

<a href="#">Title Page</a>	
<a href="#">Abstract</a>	<a href="#">Introduction</a>
<a href="#">Conclusions</a>	<a href="#">References</a>
<a href="#">Tables</a>	<a href="#">Figures</a>
<a href="#">◀</a>	<a href="#">▶</a>
<a href="#">◀</a>	<a href="#">▶</a>
<a href="#">Back</a>	<a href="#">Close</a>
<a href="#">Full Screen / Esc</a>	
<a href="#">Printer-friendly Version</a>	
<a href="#">Interactive Discussion</a>	



## Air–snow transfer of nitrate on the East Antarctic plateau

J. Erbland et al.

[Title Page](#)

[Abstract](#)

[Introduction](#)

[Conclusions](#)

[References](#)

[Tables](#)

[Figures](#)

[◀](#)

[▶](#)

[◀](#)

[▶](#)

[Back](#)

[Close](#)

[Full Screen / Esc](#)

[Printer-friendly Version](#)

[Interactive Discussion](#)



enhancement factor”, which accounts for variations in the actinic flux received at the snow surface and hence at depth. This parameter represents changes in the actinic flux emitted from the Sun or changes in the Earth–Sun distance due to variations in the Earth’s orbit. In Eq. (1), the term “ $I$ ” is therefore replaced by “ $q \times I$ ”. In the modern DC case,  $q$  is set to 1.

Another key control on  $J$  is the quantum yield ( $\phi$ ), a parameter which is strongly governed by nitrate location in the snow ice matrix and which corresponds to nitrate availability to photolysis. Nitrate is assumed to deposit to the snow under the form of  $\text{HNO}_3$  but its adsorption and/or dissociation to  $\text{NO}_3^- + \text{H}^+$  are not explicitly represented. Indeed, modeling nitrate location in the snow is well beyond the scope of the present study. For the sake of simplicity, we assume that nitrate location in the snow ice matrix is constant. Therefore,  $\phi$  is set to a constant value.

Nitrate photolysis is assumed to only produce  $\text{NO}_2$ . We acknowledge that other volatile nitrogen species such as NO or HONO may be produced. However, the photolysis of HONO in the atmosphere would rapidly produce NO which would contribute to the  $\text{NO}/\text{NO}_2$  cycle and hence have a nil impact in terms of N mass balance.

In the model,  ${}^{15}\varepsilon_{\text{pho}}$  is explicitly calculated at each time step and in each snow layer using Eq. (3). Because the layering of the physical properties of snow is fixed,  ${}^{15}\varepsilon_{\text{pho}}$  is constant with time. Earlier, we have hypothesized that the scattering and absorption properties of each layer of the snowpack are kept constant in the 280–350 nm range. This results in the independency of  ${}^{15}\varepsilon_{\text{pho}}$  with depth, in agreement with the laboratory study of Berhanu et al. (2014a) and the field study of Berhanu et al. (2014b). Therefore, the modeled  ${}^{15}\varepsilon_{\text{pho}}$  is entirely determined by the spectral distribution of the UV radiation received at the surface of the snowpack. The Rayleigh fractionation model applied to nitrate photolysis allows calculating the  $\delta^{15}\text{N}$  in the photolyzed and the remaining nitrate applying Eqs. (4) and (5) with the use of  ${}^{15}\varepsilon_{\text{pho}}$ . Nitrate photolysis is assumed to be a mass dependent process so that the  $\Delta^{17}\text{O}$  in the initial, photolyzed and remaining nitrate is the kept same.

## 2.4.2 Cage effect

A constant fraction of the photolyzed nitrate (denoted  $f_{\text{cage}}$ ) is assumed to undergo cage recombination so that the photo-fragment  $\text{NO}_2$  reacts back with OH to re-form  $\text{HNO}_3$ . This results in an apparent remaining nitrate mass fraction denoted  $f_{\text{app}}$  which writes:  $f_{\text{app}} = f + f_{\text{cage}} \times (1 - f)$  and, consequently, to a lower apparent quantum yield. In the cage effect process, OH is assumed to undergo an isotopic exchange with the water molecules of the ice lattice, so that the recombined  $\text{HNO}_3$  contains an oxygen atom originating from  $\text{H}_2\text{O}$  and featuring  $\Delta^{17}\text{O}(\text{H}_2\text{O}) = 0\text{\textperthousand}$  (McCabe et al., 2005).

## 2.4.3 Emission of $\text{NO}_2$ and photochemical steady-state

The total photolytic flux (FP) represents the potential emission of  $\text{NO}_2$  from the snow to the atmosphere and is the sum of the photolytic fluxes from each snow layer. A simple isotopic mass balance is applied to calculate the  $\delta^{15}\text{N}$  and  $\Delta^{17}\text{O}$  of the photolytic loss flux FP. The extraction of  $\text{NO}_2$  from the snowpack is assumed to preserve its chemical and isotopic integrity, i.e. it does not undergo any chemical reaction or any isotopic fractionation. FP represents the potential flux of  $\text{NO}_2$  in accordance with the terminology used in France et al. (2011).

Before its conversion to  $\text{HNO}_3$ ,  $\text{NO}_2$  originating from the snowpack undergoes numerous photolytic destruction and reformation (Fig. 1). We assume that summer conditions prevail during the whole sunlit season. Atmospheric chemistry is not explicitly simulated but only conceptually represented.  $\Delta^{17}\text{O}(\text{NO}_2)$  is calculated following the approach of Morin et al. (2011), i.e. assuming photochemical steady-state (PSS) of  $\text{NO}_x$  (when the lifetime of  $\text{NO}_x$  is shorter than 10 min), an assumption which is valid for most of the sunlit season ( $\tau(\text{NO}_2) < 10$  min from 27 September to 7 March). We therefore denote  $\Delta^{17}\text{O}(\text{NO}_2, \text{PSS})$ , the  $\Delta^{17}\text{O}$  value harbored by  $\text{NO}_2$  after its local cycling, which is represented by (Morin et al., 2008, 2011):

$$\Delta^{17}\text{O}(\text{NO}_2, \text{PSS}) = \alpha \times \Delta^{17}\text{O}_{\text{O}_3+\text{NO}}(\text{NO}_2) \quad (9)$$

Title Page

Abstract

Introduction

Conclusions

References

Tables

Figures

|◀

▶|

◀

▶

Back

Close

Full Screen / Esc

Printer-friendly Version

Interactive Discussion



with  $\alpha$ , a variable which accounts for the perturbation of the Leighton cycle by various radicals such as peroxy radicals ( $\text{RO}_2$ ) and halogen oxides. For simplicity, we only consider  $\text{BrO}$ ,  $\text{HO}_2$  and  $\text{CH}_3\text{O}_2$  as the species perturbing the Leighton cycle. The  $\alpha$  variable is calculated at each time step as in Eq. (10) assuming  $\Delta^{17}\text{O}(\text{HO}_2) = \Delta^{17}\text{O}(\text{CH}_3\text{O}_2) = 0\text{\textperthousand}$  (Morin et al., 2011). Recent observations at DC seem to support the assumption  $\Delta^{17}\text{O}(\text{CH}_3\text{O}_2) = 0\text{\textperthousand}$  because  $\text{CH}_3\text{O}_2$  may entirely originate from the reaction  $\text{R} + \text{O}_2$  or photolysis of species ( $\text{CH}_3\text{CHO}$ ) featuring  $\Delta^{17}\text{O} = 0\text{\textperthousand}$  (Kukui et al., 2014). The assumption  $\Delta^{17}\text{O}(\text{HO}_2) = 0\text{\textperthousand}$  is also supported by the same observations although 5 % of  $\text{HO}_2$  originate from the reaction  $\text{O}_3 + \text{OH}$  which leads to  $\Delta^{17}\text{O}(\text{HO}_2) > 0\text{\textperthousand}$ . For simplicity, we stick to the assumption  $\Delta^{17}\text{O}(\text{HO}_2) = 0\text{\textperthousand}$ .

$$\alpha = \frac{k_{\text{O}_3+\text{NO}} \cdot [\text{O}_3] + k_{\text{BrO+NO}} \cdot [\text{BrO}]}{k_{\text{O}_3+\text{NO}} \cdot [\text{O}_3] + k_{\text{HO}_2+\text{NO}} \cdot [\text{HO}_2] + k_{\text{CH}_3\text{O}_2+\text{NO}} \cdot [\text{CH}_3\text{O}_2] + k_{\text{BrO+NO}} \cdot [\text{BrO}]} \quad (10)$$

with temperature- and pressure-dependent kinetic rate constants from Atkinson et al. (2004, 2006, 2007) and the mixing ratios of  $\text{O}_3$ ,  $\text{BrO}$ ,  $\text{HO}_2$  and  $\text{CH}_3\text{O}_2$  at ground. Savarino et al. (2008) have measured that  $\text{O}_3$  preferentially transfers one of its terminal O atom when oxidizing NO with a probability of 92 % which translates in the following equation:

$$\Delta^{17}\text{O}_{\text{O}_3+\text{NO}}(\text{NO}_2) = 1.18 \times \Delta^{17}\text{O}(\text{O}_3)_{\text{bulk}} + 6.6 \times 10^{-3} \quad (11)$$

with  $\Delta^{17}\text{O}(\text{O}_3)_{\text{bulk}}$ , the isotopic anomaly of local bulk ozone. The O atom in  $\text{BrO}$  originates from the terminal oxygen atom of ozone through its reaction with bromine (Morin et al., 2007 and references therein). For simplicity, we assume that the O atom transferred during the NO oxidation by  $\text{O}_3$  and  $\text{BrO}$  is identical.

#### 2.4.4 Local oxidation of $\text{NO}_2$

$\text{NO}_2$  is directly converted to  $\text{HNO}_3$  with the preservation of the N atom. However, a local additional oxygen atom is incorporated. This is a reasonable assumption given the

<a href="#">Title Page</a>	
<a href="#">Abstract</a>	<a href="#">Introduction</a>
<a href="#">Conclusions</a>	<a href="#">References</a>
<a href="#">Tables</a>	<a href="#">Figures</a>
<a href="#">◀</a>	<a href="#">▶</a>
<a href="#">◀</a>	<a href="#">▶</a>
<a href="#">Back</a>	<a href="#">Close</a>
<a href="#">Full Screen / Esc</a>	
<a href="#">Printer-friendly Version</a>	
<a href="#">Interactive Discussion</a>	



<a href="#">Title Page</a>	
<a href="#">Abstract</a>	<a href="#">Introduction</a>
<a href="#">Conclusions</a>	<a href="#">References</a>
<a href="#">Tables</a>	<a href="#">Figures</a>
<a href="#">◀</a>	<a href="#">▶</a>
<a href="#">◀</a>	<a href="#">▶</a>
<a href="#">Back</a>	<a href="#">Close</a>
<a href="#">Full Screen / Esc</a>	
<a href="#">Printer-friendly Version</a>	
<a href="#">Interactive Discussion</a>	

short chemical lifetime of NO<sub>x</sub> (in the order of hours) in comparison with the approximately one-week time step used in the model. The Δ<sup>17</sup>O of HNO<sub>3</sub> is given by Eq. (12).

$$\Delta^{17}\text{O}(\text{HNO}_3) = \frac{2}{3}\Delta^{17}\text{O}(\text{NO}_2) + \frac{1}{3}\Delta^{17}\text{O}(\text{add. O}) \quad (12)$$

Similarly to the local cycling of NO<sub>2</sub>, the local oxidation of this species is only conceptually represented. For simplicity, we assume that the formation of HNO<sub>3</sub> only occurs through the pure daytime channel, i.e. the reaction of NO<sub>2</sub> and OH: Δ<sup>17</sup>O(add. O) = Δ<sup>17</sup>O(OH).

According to Kukui et al. (2014), the photolysis of HONO accounts for 56 % of the total atmospheric primary radical production at Dome C. The other two main OH production channels are HO<sub>2</sub> + NO (33 %) and H<sub>2</sub>O<sub>2</sub> photolysis (7 %) (Kukui et al., 2014), both of which can be considered to lead to OH with a nil <sup>17</sup>O-excess given the fact that Δ<sup>17</sup>O(HO<sub>2</sub>) = 0 ‰ and Δ<sup>17</sup>O(H<sub>2</sub>O<sub>2</sub>) = Δ<sup>17</sup>O(HO<sub>2</sub>) (Morin et al., 2011). Reaction channels involving ozone in the formation of OH represent less than 4 %. For simplicity, we assume that 60 % of OH is produced by HONO photolysis and that the other 40 % lead to Δ<sup>17</sup>O(OH) = 0 ‰. The Δ<sup>17</sup>O of OH therefore writes:

$$\Delta^{17}\text{O}(\text{OH}) = 0.6 \cdot \Delta^{17}\text{O}(\text{HONO}) \quad (13)$$

with Δ<sup>17</sup>O(HONO) = Δ<sup>17</sup>O(NO<sub>2</sub><sup>-</sup>) = Δ<sup>17</sup>O(photo. NO<sub>3</sub><sup>-</sup>) where NO<sub>2</sub><sup>-</sup> is one of the product of NO<sub>3</sub><sup>-</sup> photolysis.

## 2.5 Parameterization of physical processes

### 2.5.1 Snow accumulation

The snow accumulation thickness depends on the snow accumulation rate ( $A$ ) as well as on snow density ( $\rho$ ). Older layers are buried preserving their nitrate mass and isotopic composition. Immediately after snow accumulation, the modeled snowpack is resampled at a 1 mm resolution.



## 2.5.2 Nitrate deposition to the snow

The deposited flux (FD) and its isotopic composition ( $\Delta^{17}\text{O}(\text{FD})$  and  $\delta^{15}\text{N}(\text{FD})$ ) are obtained by solving Eqs. (6) to Eq. (8) (Fig. 3). For the sake of simplicity, the downward deposition flux is modeled assuming a pure physical diffusion of  $\text{HNO}_3$  in the top layer of the snowpack. The deposition process is assumed to preserve  $\Delta^{17}\text{O}$ . This process is associated with a  $^{15}\text{N}/^{14}\text{N}$  fractionation constant ( $^{15}\varepsilon_{\text{dep}}$ ).

## 2.5.3 Nitrate diffusion in the snowpack

Nitrate diffusion in the snowpack leads to changes in nitrate mass fraction and isotope profiles in the snowpack, and it is represented by the use of a diffusivity coefficient denoted  $D$  and by a zero-flux boundary condition at the top and at the bottom of the snowpack ( $z = 1 \text{ m}$ ):

$$\begin{cases} \frac{\partial \omega(z,t)}{\partial t} = D \frac{\partial^2 \omega(z,t)}{\partial z^2} \\ \frac{\partial \omega(0,t)}{\partial z} = 0 \\ \frac{\partial \omega(1,t)}{\partial z} = 0 \end{cases} \quad (14)$$

with  $\omega(z,t)$ , the nitrate mass fraction in each layer,  $z$  and  $t$  the space and time variables and  $\frac{\partial \omega(0,t)}{\partial z}$  and  $\frac{\partial \omega(1,t)}{\partial z}$  the nitrate concentration at the top and bottom of the snowpack, respectively. Given the assumption of a constant snow density and a uniform mesh grid, Eq. (14) also applies to the snow mass in the layer ( $m$ ). Equation Eq. (14) is solved at a time step of 4 h. Space and time derivatives are approximated by the finite difference method.

<a href="#">Title Page</a>	
<a href="#">Abstract</a>	<a href="#">Introduction</a>
<a href="#">Conclusions</a>	<a href="#">References</a>
<a href="#">Tables</a>	<a href="#">Figures</a>
<a href="#">◀</a>	<a href="#">▶</a>
<a href="#">◀</a>	<a href="#">▶</a>
<a href="#">Back</a>	<a href="#">Close</a>
<a href="#">Full Screen / Esc</a>	
<a href="#">Printer-friendly Version</a>	
<a href="#">Interactive Discussion</a>	



### 3 Model setup, runs and evaluation

#### 3.1 Method

To evaluate the model, we study its ability to reproduce at best the present-day observations at Dome C and across East Antarctica. To this end, a realistic simulation of 5 TRANSITS is compared to the data observed at the air–snow interface at Dome C and in the top 50 cm of snow in East Antarctica.

##### 3.1.1 Field observations

In this section, we briefly describe the observed data used to evaluate the model. Most of the observed data originate from Erbland et al. (2013). Atmospheric nitrate 10 concentration and isotopic measurements were measured 2 m above ground at Dome C during the years 2007–2008 (Frey et al., 2009) and 2009–2010 (Erbland et al., 2013). In this second study, nitrate mass fraction and isotopic composition have also been measured in the skin layer (the  $(4 \pm 2)$  mm of top snow) and for the 2009–2010 period. Nitrate mass fractions and isotopic profiles are available from three 50 cm snow pits 15 sampled at Dome C during the austral summers 2007–2008 and 2009–2010 (Frey et al., 2009; Erbland et al., 2013). NO<sub>x</sub> emission fluxes were measured at Dome C from 22 December 2009 to 28 January 2010 (Frey et al., 2013).

Forty-five 50 cm deep snow profiles were collected at DC from February 2010 to February 2014 and nitrate mass fractions were measured as in Erbland et al. (2013). 20 These previously unpublished profiles have been collected approximately every month by the DC overwintering team. From the fifty-one 50 cm snow pits collected at DC (45 unpublished and 6 published in Röhlisberger et al., 2000; Frey et al., 2009; France et al., 2011; Erbland et al., 2013), we use the nitrate mass fraction profiles to calculate  $m_{50\text{ cm}}(\text{NO}_3^-)$ , the total mass of nitrate in the top 50 cm of a 1 m<sup>2</sup> section of the 25 snowpack.

[Title Page](#)[Abstract](#)[Introduction](#)[Conclusions](#)[References](#)[Tables](#)[Figures](#)[◀](#)[▶](#)[◀](#)[▶](#)[Back](#)[Close](#)[Full Screen / Esc](#)[Printer-friendly Version](#)[Interactive Discussion](#)



from 21 June to 13 September, the period when the mean air temperature at 50 mb allows the formation of PSCs of type I ( $T < -78^{\circ}\text{C}$ ) (NOAA observations in 2008, available at <http://www.cpc.ncep.noaa.gov/products/stratosphere/polar/polar.shtml>). Transitions before and after the twelve-week  $\text{FS}(t)$  plateau are assumed to be linear and last 4 weeks. The  $\delta^{15}\text{N}(\text{FS})$  value is set to 19‰ as estimated by Savarino et al. (2007) based on computations from chemical mechanisms, fractionation factors, and isotopic measurements. This value is consistent with the value retrieved at 15 km above South Pole and at summer solstice ( $21 \pm 4$ )‰ based on measurements of the atmospheric  $\text{H}^{15}\text{NO}_3/\text{H}^{14}\text{NO}_3$  isotope ratio profile by the Earth observation instrument MIDAS operated onboard of the Environmental Satellite (ENVISAT) (Brizzi et al., 2009). No direct measurement of  $\Delta^{17}\text{O}$  in stratospheric nitrate exists. Savarino et al. (2007) estimated that  $\Delta^{17}\text{O}$  is higher than 40‰ and we set  $\Delta^{17}\text{O}(\text{FS})$  to 42‰.

There is no estimate of the nitrogen mass flux received on the Antarctic continent by long range transport (FT). In the absence of such information and for simplicity, we assume that, annually,  $\text{FS}/\text{FPI} = 50\%$ . This means that the annual fluxes FT and FS are equal. We also assume a constant repartition of FT throughout the year. We agree that this hypothesis is debatable given that air mass movement into the Antarctic plateau may be hampered at times when the polar vortex is strongest. As for the flux, the  $\delta^{15}\text{N}$  and  $\Delta^{17}\text{O}$  of this nitrate source are not known. However, we assume that it features  $\delta^{15}\text{N}(\text{FT}) = 0\%$  and  $\Delta^{17}\text{O}(\text{FT}) = 30\%$ , which represent averaged values for tropospheric nitrate in pristine areas in low/middle latitudes (Morin et al., 2009).

The fraction of nitrate fluxes which is horizontally exported from the atmospheric box is set to a constant value of  $f_{\text{exp}} = 20\%$ .

Annual snow accumulation rates measured at Dome C vary considerably at the inter-annual timescale as a result of snow redistribution by the wind (Libois et al., 2014). For example, years with net ablation are as frequent as 15%. The same process also affects the repartition of snow accumulation rates at a sub-annual timescale. For the sake of simplicity, the annual snow accumulation rate is set to a constant value of  $28 \text{ kg m}^{-2} \text{ a}^{-1}$  (93 mm of snow per year for  $\rho = 300 \text{ kg m}^{-3}$ ) which is representative of

[Title Page](#)[Abstract](#)[Introduction](#)[Conclusions](#)[References](#)[Tables](#)[Figures](#)[◀](#)[▶](#)[◀](#)[▶](#)[Back](#)[Close](#)[Full Screen / Esc](#)[Printer-friendly Version](#)[Interactive Discussion](#)

the Dome C site (Frezzotti et al., 2004; Libois et al., 2014). We also assumed a constant repartition of snow accumulation within the computed year. Snow densities also vary considerably at the decimeter-scale both horizontally and vertically (Libois et al., 2014). To simplify, the snow density has been set to  $300 \text{ kg m}^{-3}$ , the average value found for the snow top layers at Dome C (France et al., 2011). This value is close to the average value ( $316 \text{ kg m}^{-3}$ ) observed in a mean 25 cm depth DC profile (Libois et al., 2014). We note that our choice of snow density for the nitrate mass and isotopic calculations is consistent with that used for the optical calculations in the soft windpack layer at the surface, where most of the action occurs.

The adjustment parameter  ${}^{15}\varepsilon_{\text{dep}}$  (representing the  ${}^{15}\text{N}/{}^{14}\text{N}$  fractionation associated with  $\text{HNO}_3$  deposition) is set to a value of +10‰ in order to reproduce at best the shift in  $\delta^{15}\text{N}$  in the observed atmospheric and skin layer nitrate (Erbland et al., 2013). The diffusivity coefficient is calculated as in Thibert and Domine (1998) with the mean summertime DC temperature (i.e. 237 K in November–December–January).  $D$  is therefore set to  $1.3 \cdot 10^{-11} \text{ cm}^2 \text{ s}^{-1}$ .

The parameter  $\phi$  is set to a constant value of 0.026. The magnitude of the cage effect is adjusted using a constant parameter of  $f_{\text{cage}} = 0.15$ , which means that 15 % of the photolyzed nitrate undergoes cage recombination and isotopic exchange with water. Given the choice of a modeled cage effect of 15 %, we obtain an apparent modeled quantum yield (denoted  $\phi^*$ ) of  $0.85 \times 0.026 \approx 0.022$ , a value smaller than the mean value for buried nitrate (0.05) but higher than the smallest value observed for this domain (0.003) (Meusinger et al., 2014).

We used absorption cross sections of  ${}^{14}\text{NO}_3^-$  and  ${}^{15}\text{NO}_3^-$  in snow recommended by Berhanu et al. (2014a). The TUV-snow model used to model the actinic flux in the DC snowpack was run using constant  $k$  and  $q$  parameters set to 1. An additional input is the ozone column and we used the measurements at Dome C over the 2000–2009 period. The 2000–2005 data were derived from the measurements made by the Earth Probe Total Ozone Mapping Spectrometer (EP/TOMS) and processed by the NASA (data obtained at <http://ozoneaq.gsfc.nasa.gov/>). The 2007–2009 data were obtained

<a href="#">Title Page</a>	<a href="#">Abstract</a>	<a href="#">Introduction</a>
<a href="#">Conclusions</a>	<a href="#">References</a>	
<a href="#">Tables</a>	<a href="#">Figures</a>	
<a href="#">◀</a>	<a href="#">▶</a>	
<a href="#">◀</a>	<a href="#">▶</a>	
<a href="#">Back</a>	<a href="#">Close</a>	
<a href="#">Full Screen / Esc</a>		
<a href="#">Printer-friendly Version</a>		
<a href="#">Interactive Discussion</a>		



# Air–snow transfer of nitrate on the East Antarctic plateau

J. Erbland et al.

from the “Système d’Analyse par Observation Zénithale” (SAOZ) observation network at ground (data obtained at <http://saoz.obs.uvsq.fr/index.html>). Weekly averages have been calculated over the 2000–2009 period and converted to obtain the same resolution (25 DU) than that used for the offline runs of the TUV-snow model (Fig. 4).

The variable  $\alpha$  has been calculated from Eq. (10) using weekly average mixing ratios of O<sub>3</sub> measured at Dome C in 2007–2008 (Legrand et al., 2009). During the OPALe campaign, Frey et al. (2014) have measured BrO mixing ratios of 2–3 pptv. We assume that [BrO] is constant throughout the year and equal to 2.5 pptv. Temperatures and pressures at each time step were calculated from the 3 h observations from the Concordia Automatic Weather Station (AWS 8989) in 2009–2010 (University of Wisconsin-Madison, data available at <ftp://amrc.ssec.wisc.edu/pub/aws/q3h/>, accessed 4 July 2013). Mixing ratios of HO<sub>2</sub> and CH<sub>3</sub>O<sub>2</sub> were deduced from those of RO<sub>2</sub> assuming RO<sub>2</sub> = HO<sub>2</sub> + CH<sub>3</sub>O<sub>2</sub> and [HO<sub>2</sub>]/[RO<sub>2</sub>] = 0.7 (Kukui et al., 2014). Mixing ratios of RO<sub>2</sub> were estimated from their linear relationship with  $J(\text{NO}_2)$ : [RO<sub>2</sub>]/(molecule cm<sup>-3</sup>) =  $7.25 \times 10^9 \times (J(\text{NO}_2)/\text{s}^{-1})$  (Fig. 3b in Kukui et al., 2014). The time series of  $J(\text{NO}_2)$  was calculated with the TUV model for the appropriate solar zenith angle.

There is a lack of measurements of  $\Delta^{17}\text{O}(\text{O}_3)_{\text{bulk}}$  in the Antarctic troposphere. Therefore, we used the constant value of  $\Delta^{17}\text{O}(\text{O}_3)_{\text{bulk}} = 25.2\%$  which represents the mean value observed in the Southern Hemisphere and measured during an Atlantic cruise in April/May 2012 (Vicars and Savarino, 2014).

We note that Frey et al. (2014) have measured high  $[NO_2]/[NO]$  ratios which are not consistent with other measurements available at Dome C. The authors suggest that an unknown mechanism which converts NO into  $NO_2$  or interferences in the  $NO_x$  measurements are responsible for the discrepancy observed. Given that the oxidant budget is not yet fully resolved at DC, we stick to our simple parameterization of the local resetting of the oxygen isotopic composition of  $NO_2$ . We recall that we have made various simplifications in the description of the local cycling and oxidation of  $NO_2$ . These assumptions include:  $\Delta^{17}O(HO_2) = 0\text{\textperthousand}$ , the neglected activity of  $O_3$  when calculating  $\Delta^{17}O(OH)$ , the more complex NO to  $NO_2$  conversion reaction scheme with a potential

6910

A small rectangular icon containing the letters "cc" inside a circle and the letters "BY" below it, indicating a Creative Commons Attribution license.

[Printer-friendly Version](#)

greater influence of O<sub>3</sub> and, eventually, the neglected nighttime NO<sub>2</sub> oxidation pathway at the beginning and end of the sunlit season (involving O<sub>3</sub>). We therefore anticipate that the Δ<sup>17</sup>O values simulated by TRANSITS at DC will represent the lower bound to the observations.

### 5 3.1.3 Simulations across East Antarctica

Sampled sites on the D10-DC-Vostok route are characterized by a wide range of annual snow accumulation rates which gradually drop from 558 kg m<sup>-2</sup> a<sup>-1</sup> close to the coast (D10) to 20 kg m<sup>-2</sup> a<sup>-1</sup> high on the plateau (around Vostok) (Erblan et al., 2013). The simulation of nitrate in East Antarctic snowpacks and the investigation of TRANSITS's ability to reproduce such wide snow accumulation conditions, we consider 10 test sites whose snow accumulation rates are (20, 25, 30, 40, 50, 75, 100, 200, 300, 600) kg m<sup>-2</sup> a<sup>-1</sup>, respectively. For simplicity, we consider that A is the sole variable used to characterize different sites from the coast to the plateau in East Antarctica. All the other parameters and variables are kept the same of those for DC. TRANSITS is therefore run in the DC realistic configuration described above. This means that we do not consider changes in latitude, elevation or ozone column conditions which would impact the TUV-modeled actinic fluxes. Also, the physical, optical and chemical properties of the snowpacks are considered constant. No change in local atmospheric chemistry is taken into account and the horizontal export of nitrogen from locations on the plateau to those close to the coast is not modeled. Last, we hypothesize that the time series of atmospheric nitrate concentrations are the same than that measured at DC. This assumption is supported by the observation of Savarino et al. (2007) who show comparable atmospheric nitrate concentration time series at the coastal Dumont d'Urville station and at DC.

25 The parameters and variables used for the DC realistic simulation as well as those used for the simulations across East Antarctica are given in Table 3.

<a href="#">Title Page</a>	
<a href="#">Abstract</a>	<a href="#">Introduction</a>
<a href="#">Conclusions</a>	<a href="#">References</a>
<a href="#">Tables</a>	<a href="#">Figures</a>
<a href="#">◀</a>	<a href="#">▶</a>
<a href="#">◀</a>	<a href="#">▶</a>
<a href="#">Back</a>	<a href="#">Close</a>
<a href="#">Full Screen / Esc</a>	
<a href="#">Printer-friendly Version</a>	
<a href="#">Interactive Discussion</a>	



### 3.1.4 Model initialization and output data

The 1 m snowpack is initialized with a constant nitrate profile of  $\omega(\text{NO}_3^-) = 50 \text{ ng NO}_3^- \text{ g}^{-1}$ ,  $\Delta^{17}\text{O}(\text{NO}_3^-) = 30\text{\textperthousand}$  and  $\delta^{15}\text{N}(\text{NO}_3^-) = 50\text{\textperthousand}$ . The atmosphere box is initialized with  $\gamma(\text{NO}_3^-) = 5 \text{ ng NO}_3^- \text{ m}^{-3}$  and  $\Delta^{17}\text{O}$  and  $\delta^{15}\text{N}$  values of 30 and 5‰, respectively.

The model is run for a time sufficiently long to allow it to converge (e.g. 25 years for DC conditions). Raw data generated by the model are processed to obtain the time series of concentration and isotopic composition of atmospheric nitrate and in a top skin layer of 4 mm, the depth profiles of mass fraction,  $\delta^{15}\text{N}$  and  $\Delta^{17}\text{O}$  in snow nitrate and the time series of the  $\text{NO}_2$  flux from the snow to the atmosphere.

From the simulated profiles of nitrate mass and isotopic composition in snow, we calculate the apparent fraction constants ( ${}^{15}\varepsilon_{\text{app}}$  and  ${}^{17}E_{\text{app}}$ ) as in Erbland et al. (2013). Also, the nitrate mass and isotopic composition in the top 50 cm are calculated. We recall that the model also computes the simulated mass fraction and isotopic composition in the archived nitrate, which can be compared to the observed asymptotic values.

## 3.2 Results

### 3.2.1 Simulation results at the DC air–snow interface

Figure 5 gives the results at the air–snow interface for the DC-like realistic simulation: simulated nitrate concentrations and  $\delta^{15}\text{N}$  and  $\Delta^{17}\text{O}$  in both the atmospheric and skin layer compartments as well as the simulated fluxes (FD, FE, FP) together with the observations at Dome C in 2007–2008 and 2009–2010. On this figure, the dates of the observed data have been transformed in order to superimpose them all on a one-year period starting on 21 June. Figure 6 gives the snowpack results for the DC-like realistic simulation: simulated nitrate mass fraction and isotopic composition in the top 50 cm of snow and in the archived flux as well as the simulated apparent fractionation constants. In this section, we briefly describe the simulated results.

<a href="#">Title Page</a>	
<a href="#">Abstract</a>	<a href="#">Introduction</a>
<a href="#">Conclusions</a>	<a href="#">References</a>
<a href="#">Tables</a>	<a href="#">Figures</a>
<a href="#">◀</a>	<a href="#">▶</a>
<a href="#">◀</a>	<a href="#">▶</a>
<a href="#">Back</a>	<a href="#">Close</a>
<a href="#">Full Screen / Esc</a>	
<a href="#">Printer-friendly Version</a>	
<a href="#">Interactive Discussion</a>	



Table 4 gives a summary of averages and minimum/maximum of the simulated values in the atmosphere and skin layer. In the following, only the atmospheric and skin layer data observed at DC in 2009–2010 will be compared to TRANSITS simulations.

In the atmosphere, the simulated annual weighted  $\delta^{15}\text{N}$  value ( $-9.8\text{\textperthousand}$ ) is close to the observed value ( $-6.5\text{\textperthousand}$ ). The same is observed in the skin layer (simulated:  $+26.3\text{\textperthousand}$ , observed:  $+18.2\text{\textperthousand}$ ).

Values of  $\delta^{15}\text{N}$  in winter are well reproduced by the model in both the atmosphere and skin layer, including the observed 10‰ shift. The simulated variations and timing of both compartments are consistent with observations. Indeed, the lowest  $\delta^{15}\text{N}$  values in the atmospheric nitrate occur in October (simulated: -25.3‰, observed: -30.8‰) when the stratospheric input has stopped and when the UV radiation becomes significant to encourage the production of isotopically light  $\text{NO}_x$  from the snowpack.  $\delta^{15}\text{N}$  values then gradually start to rise throughout spring and summer to reach a local maximum in January. We observe that the increase in  $\delta^{15}\text{N}$  is faster in the observations than in the simulation. However, maximum values reached in summer are similar (simulated: +5.7‰, observed: +10.8‰). Similar trends are observed in the skin layer although the recovery from the lowest  $\delta^{15}\text{N}$  values in October (simulated: +4.2‰, observed: -11.7‰) occurs at similar rates. Last, we note that large variations of more than 40‰ observed in  $\delta^{15}\text{N}$  measured at DC are not reproduced by the model.

The simulated variations of  $\Delta^{17}\text{O}$  in both compartments are consistent with observations, i.e.  $\Delta^{17}\text{O}$  decreases from high winter values to the lowest values in the middle of summer. However,  $\Delta^{17}\text{O}$  values in skin layer are not well reproduced as observed on Fig. 5: the simulated annual weighted  $\Delta^{17}\text{O}$  value in skin layer is lower than in the observation (28.6 and 31.7‰, respectively). The model does not reproduce as well the small difference in the annual weighted  $\Delta^{17}\text{O}$  values in the atmosphere and the skin layer (simulated: +1.0‰, observed: -2.3‰) but, the simulated annual weighted  $\Delta^{17}\text{O}$  value in the atmosphere is in better agreement with the observations (27.6 and 29.4‰, respectively). When considering the annual variability of the difference in  $\Delta^{17}\text{O}$  in the atmosphere and skin layer, the model reproduces well the important shift in early



October (simulated:  $-7\text{\textperthousand}$ , observed:  $-7\text{\textperthousand}$ ) but not the small negative shift by the end of the summer (simulated: approximately  $+2\text{\textperthousand}$ , observed: approximately  $-2\text{\textperthousand}$ ).

The variations in nitrate mass fractions in the skin layer are well reproduced by the model: deviations from the winter background values occur during the sunlit season to reach a maximum in December. However, the period of values high above background is longer (September to April) for the simulation than in the observations (October/February). Also, the simulated annual average in nitrate mass fractions ( $2953\text{ ng g}^{-1}$ ) is more than 7 times higher than the observed value ( $390\text{ ng g}^{-1}$ ). Last, the maximum simulated  $\omega(\text{NO}_3^-)$  value in the skin layer is  $5332\text{ ng g}^{-1}$ , a value more than 3 times higher than in the observations ( $1400\text{ ng g}^{-1}$ , Erbland et al., 2013).

We recall that the atmospheric nitrate concentrations have been forced with an atmospheric time series idealized from the 2009–2010 measurements at Dome C (Fig. 5d). Concentration maxima in atmospheric nitrate and skin layer nitrate occur with a one-month lag (end of November vs. end of December), consistently with the 3–4 weeks lag observed (Erbland et al., 2013).

Table 5 gives the simulated nitrate mass fluxes and their isotopic composition in the case of the DC realistic simulation. The FA/FPI ratio for this simulation is 2.0 %, which means that a small fraction (2.0 %) of the primary input flux of nitrate is archived below one meter. The remaining fraction ( $\text{FE/FPI} = 1 - \text{FA/FPI} = 98.0\text{\%}$ ) is exported outside the atmospheric box. The photolytic, deposition and export fluxes show a peak whose timing follows the sunlit season. The annual photolytic flux is  $32.0 \times 10^{-6}\text{ kg N m}^{-2}\text{ a}^{-1}$  and it compensated by an annual deposition flux of  $32.2 \times 10^{-6}\text{ kg N m}^{-2}\text{ a}^{-1}$ .

The  $\delta^{15}\text{N}$  value in the photolytic flux is  $2.4\text{\textperthousand}$  on average annually and increases from its minimum ( $-31.4\text{\textperthousand}$ ) at the beginning of the sunlit season to its maximum ( $+16.6\text{\textperthousand}$ ) by the end of January. During most of the sunlit season,  $\delta^{15}\text{N(FD)}$  follows closely  $\delta^{15}\text{N(FP)}$  and its winter value is purely set by  $\delta^{15}\text{N}$  in the primary nitrate.

The  $\Delta^{17}\text{O}$  values in the photolytic, deposition and export fluxes are mostly stable throughout the summer and reach a minimum in the middle of January. The minimum values of  $\Delta^{17}\text{O(FP)}$ ,  $\Delta^{17}\text{O(FD)}$  and  $\Delta^{17}\text{O(FE)}$  are 24.5, 24.7 and  $24.7\text{\textperthousand}$ , respectively.

Title Page

Abstract

Introduction

Conclusions

References

Tables

Figures

◀

▶

◀

▶

Back

Close

Full Screen / Esc

Printer-friendly Version

Interactive Discussion



Figure 6 shows nitrate in snow obtained from the DC realistic simulation. The nitrate mass in the top 50 cm (Fig. 6a) shows an average value of  $(8.3 \pm 1.6)$  mgN (mean  $\pm 1\sigma$ ), a value on the same order of magnitude – although 2.5 times higher – than the observed annual average value  $((3.4 \pm 1.0)$  mgN). The simulated  $m_{50\text{cm}}(\text{NO}_3^-)$  varies in the range 6.3–11.1 mgN with its maximum reached by the end of September and its minimum reached by the end of January. Observed  $m_{50\text{cm}}(\text{NO}_3^-)$  shows a weaker yet significant similar annual variability with winter values (May to November) of  $(3.6 \pm 0.5)$  mgN and summer values (December to April) of  $(3.2 \pm 1.2)$  mgN.

The modeled isotopic composition of nitrate in the top 50 cm shows weighted averages of +89.5‰ and 26.2‰ for  $\delta^{15}\text{N}$  and  $\Delta^{17}\text{O}$ , respectively (Fig. 6c and f). The two time series also show cycles with variations respectively in anti-phase and in phase with variations of  $m_{50\text{cm}}(\text{NO}_3^-)$ .  $\delta^{15}\text{N}_{50\text{cm}}(\text{NO}_3^-)$  and  $\Delta^{17}\text{O}_{50\text{cm}}(\text{NO}_3^-)$  respectively vary in the 68.7–114 and 23.5–29.5‰ ranges. Comparisons to the 3 snow pits show that for one pit  $\delta^{15}\text{N}_{50\text{cm}}(\text{NO}_3^-)$  value is in agreement with the simulated values. The 2 others are off by several tens of ‰. Simulated  $\Delta^{17}\text{O}_{50\text{cm}}(\text{NO}_3^-)$  are 4–6‰ lower than the observed values.

The simulated mass fraction in the archived nitrate is constant throughout the season ( $25.4\text{ ng g}^{-1}$ ) and compares well with the observed values (Fig. 6b). We observe a similar trend with  $\delta^{15}\text{N(FA)}$  with an annual constant value of 292‰ comparable to the observations (Fig. 6f). The simulated  $\Delta^{17}\text{O(FA)}$  is also constant throughout the year (20.6‰) and comparison to the observed values show that this constant value is 6 to 8‰ lower than the observed values (Fig. 6h).

The simulated  $^{15}\text{N}/^{14}\text{N}$  apparent fractionation constant shows an annual average of  $(-48.7 \pm 3.5)$ ‰ with weak annual variations (Fig. 6d). This compares well with the range of observed  $^{15}\varepsilon_{\text{app}}$  values at DC (from  $-40.0$  to  $-74.3$ ‰, Erbland et al., 2013).  $^{17}\varepsilon_{\text{app}}$  shows variations of a greater relative amplitude (from 0.8 to 2.3‰) with an annual average of  $(1.5 \pm 0.5)$ ‰. The comparison to the 3 values observed at DC shows a good agreement (Fig. 6g).

[Title Page](#)[Abstract](#)[Introduction](#)[Conclusions](#)[References](#)[Tables](#)[Figures](#)[◀](#)[▶](#)[◀](#)[▶](#)[Back](#)[Close](#)[Full Screen / Esc](#)[Printer-friendly Version](#)[Interactive Discussion](#)

Figure 7 shows the specific case of the simulated snow nitrate for the week of 24 December in the case of the DC realistic simulation. The realistic simulation reproduces well the variation range of the mass fraction,  $\delta^{15}\text{N}$  and  $\Delta^{17}\text{O}$  in nitrate at depth: nitrate mass fractions decrease by more than two orders of magnitude in the top 10–15 cm and  $\delta^{15}\text{N}$  and  $\Delta^{17}\text{O}$  respectively increases and decreases from 40‰ to a mean background value above 250‰ and from 25‰ to a mean background value below 21‰ at around 20–30 cm depth. The simulated profiles are smooth, consistently with the observations. A small secondary peak can be observed in the mass fraction profile at around 9 cm depth, a depth that corresponds to one year of snow accumulation.

### 3.2.2 Simulation results across East Antarctica

Figure 8 shows the results for the TRANSITS simulations across East Antarctica in which snow accumulation rates only have been varied. The variations of the mass flux and isotopic composition in the archived nitrate are well reproduced by the model (Fig. 8c–e).  $\delta^{15}\text{N(FA)}$  and  $\Delta^{17}\text{O(FA)}$  respectively decrease and increase with the increasing snow accumulation rates. The values of FA and  $\delta^{15}\text{N(FA)}$  are also well reproduced. However, the simulated values of  $\Delta^{17}\text{O(FA)}$  are underestimated by 4‰, on average. TRANSITS produces consistent apparent fractionation constants (Fig. 8a, b) and nitrate mass fraction in the archived nitrate (panel f) for sites on the plateau (characterized by  $A < 50 \text{ kg m}^{-2} \text{ a}^{-1}$ , Erbland et al., 2013). The agreement between the model and observations is less strong above this  $A$  threshold value, especially for  $^{17}\text{F}_{\text{app}}$  (Fig. 8b).

A closer look on Fig. 8c, shows that the model does not seem to reach a maximum in  $\delta^{15}\text{N(FA)}$  with increasing snow accumulation rates. This features seems different than the one drawn by the observed data where  $\delta^{15}\text{N(as.)}$  seems to reach a plateau not exceeding 360‰.

Figure 9 presents the same results in a different way. Panel a is a “modified Rayleigh plot” where  $\ln(\delta^{15}\text{N(FA)} + 1)$  is represented as a function of  $\ln(\text{FA})$  (which equals  $\ln(\omega(\text{FA}) \times A)$ ) instead of  $\ln(\omega(\text{FA}))$ . In this representation, we observe that the two

[Title Page](#)[Abstract](#)[Introduction](#)[Conclusions](#)[References](#)[Tables](#)[Figures](#)[◀](#)[▶](#)[◀](#)[▶](#)[Back](#)[Close](#)[Full Screen / Esc](#)[Printer-friendly Version](#)[Interactive Discussion](#)

datasets fall on comparable lines with slopes of the linear fits being  $-0.065$  and  $-0.061$  for the observed and simulated data, respectively.

When plotting  $\Delta^{17}\text{O}$  in the archived nitrate as a function of  $\delta^{15}\text{N(FA)}$  (Fig. 9b), we observe an anti-correlation which is reproduced by the model. In the same plot, we note that the model slightly underestimates  $\delta^{15}\text{N(FA)}$  at sites with medium/high snow accumulation rates ( $A > 50 \text{ kg m}^{-2} \text{ a}^{-1}$ ).

### 3.3 Evaluation and discussion

Below, we discuss the choice of the adjustment parameters as well as the simulated data in various compartments (atmosphere, skin layer, top snowpack and archive) and fluxes. We note that the results are insensitive to the values used for the model's initialization.

#### 3.3.1 Validation of the choice of the adjustment parameters

In the realistic simulation, the choice of a constant  $f_{\text{exp}} = 0.2$  export flux parameter leads to a net export of  $\text{FE} = 98.0\%$  of the nitrate of primary origin ( $\text{FA/FPI} = 2.0\%$ ).

To the best of our knowledge, there is no observation that could independently corroborate this value because it would require the direct measurement of the export flux. We however point out that a non-zero  $f_{\text{exp}}$  parameter is necessary to reproduce realistic  $\delta^{15}\text{N}$  values both in the atmosphere and skin layer. Indeed, when running the model with  $f_{\text{exp}} = 0$ ,  $\delta^{15}\text{N}$  values in those compartments become highly negative ( $\leq -120\%$ ) which is clearly not realistic when compared to the observations (Fig. 5). Future improvements of the model could aim at a physical parameterization of the nitrate export.

The choice of a non-zero value for  $f_{\text{cage}}$  allows to generate decreasing  $\Delta^{17}\text{O}$  profiles in snow in accordance with the observations in three snow pits from DC (Fig. 7c). On this figure, the decreasing trend in the data overlaps with additional variability in  $\Delta^{17}\text{O}$ .

A better metric to evaluate the changes in  $\Delta^{17}\text{O}$  associated with depth, i.e. with the loss of nitrate, is the apparent  $^{17}\text{O}$ -excess fractionation constant,  ${}^{17}E_{\text{app}}$ . Figure 6g shows

[Title Page](#)[Abstract](#)[Introduction](#)[Conclusions](#)[References](#)[Tables](#)[Figures](#)[Back](#)[Close](#)[Full Screen / Esc](#)[Printer-friendly Version](#)[Interactive Discussion](#)

that the modeled  ${}^{17}E_{\text{app}}$  values at DC are positive, consistently with the observations, confirming the decreasing contribution of cage recombination effects to  $\Delta {}^{17}\text{O}(\text{NO}_3^-)$  (McCabe et al., 2005; Frey et al., 2009). The simulation across East Antarctica confirms the ability of the model to reproduce the sensitivity of  $\Delta {}^{17}\text{O}$  to the nitrate mass loss (Fig. 8). Indeed, for sites with  $A < 33 \text{ kg m}^{-2} \text{ a}^{-1}$ , the model calculates a mean  ${}^{17}E_{\text{app}}$  value of  $(+1.3 \pm 0.2)\%$  for the December/January period while the observed average value is  $(+2.0 \pm 1.2)\%$  (mean  $\pm 1\sigma$ ,  $n = 10$ ). We observe that an  $f_{\text{cage}}$  parameter set to 0 would have led to a mean December/January  ${}^{17}E_{\text{app}}$  value almost nil:  $(+0.3 \pm 0.2)\%$ .

The choice of  ${}^{15}\varepsilon_{\text{dep}}$  allows to reproduce the shift observed between  $\delta {}^{15}\text{N}$  values in atmospheric and skin layer nitrate in winter. The positive sign of  ${}^{15}\varepsilon_{\text{dep}}$  is consistent with a dry deposition of  $\text{HNO}_3$ .

### 3.3.2 Validation of the nitrate mass loss and ${}^{15}\text{N}/{}^{14}\text{N}$ fractionation process

The nitrate mass loss is quantitatively represented in the TRANSITS model. Indeed, Fig. 7a shows that nitrate mass fraction decrease by a factor 10 in the top 10 cm of the snowpack. Also, the simulated archived nitrate mass fractions values are consistent with the observations (Fig. 6). This means that the nitrate mass fraction lost by photolysis ( $f$ ) and calculated from the photolytic rate constant ( $J$ , Eq. 1) is quantitatively simulated by TRANSITS model runs.

Nitrate- $\delta {}^{15}\text{N}$  isotopic profiles in snow also show that the  ${}^{15}\text{N}/{}^{14}\text{N}$  fractionation associated with nitrate photolysis is quantitatively represented. First, the simulated  ${}^{15}\text{N}/{}^{14}\text{N}$  apparent fractionation constants are consistent with the observations for plateau sites ( $A < 50 \text{ kg m}^{-2} \text{ a}^{-1}$ , Figs. 6d and 8). This means that the absorption cross sections used for  ${}^{14}\text{NO}_3^-$  and  ${}^{15}\text{NO}_3^-$  (Berhanu et al., 2014a) and the variables used in the TUV-snow model ( $\text{O}_3$  column), and necessary to calculate  ${}^{15}\varepsilon_{\text{pho}}$  (Eq. 3) allow a quantitative description of the  ${}^{15}\text{N}/{}^{14}\text{N}$  fractionation constant associated with nitrate photolysis. Second, the  $\delta {}^{15}\text{N}$  values in the archived nitrate is well reproduced by the model. This is



a further evidence that the nitrate mass fraction lost by photolysis ( $f$ , Eqs. 4 and 5) are quantitatively simulated by TRANSITS model runs. Indeed, using the same quantum yield than in France et al. (2011) ( $2.1 \times 10^{-3}$  at 246 K) not only leads to unrealistic FA/FPI ratio (70.9 %) and  $\omega(\text{FA})$  value ( $920 \text{ ng g}^{-1}$ ) but also to a very small  $\delta^{15}\text{N}(\text{FA})$  value (17.2 ‰), which clearly reflects a weak recycling and an important trapping of nitrate in snow. The photolytic quantum yield derived from Meusinger et al. (2014) ( $\phi = 0.026$ ) therefore allows to compute a consistent variation range of  $\delta^{15}\text{N}$  in nitrate archived at depth.

In the DC realistic simulation of TRANSITS, the maximum value of the photolytic flux (FP) in the year is  $3.23 \times 10^{-12} \text{ kg N m}^{-2} \text{ s}^{-1}$ , a value around 40 times higher than that obtained by France et al. (2011). This difference is not surprising since we are using a quantum yield 12 times higher than France et al. (2011). The different scaling may be explained by the differences in the complexities of the two models (TRANSITS includes recycling and a net export). The observed median  $\text{NO}_x$  emission fluxes are  $1.6 \times 10^{-13} \text{ kg N m}^{-2} \text{ s}^{-1}$  and  $3.7 \times 10^{-13} \text{ kg N m}^{-2} \text{ s}^{-1}$  over the 22 December 2009 to 28 January 2010 period (Frey et al., 2013) and the 1 December 2011 to 12 January 2012 period (Frey et al., 2014), respectively. Our computed median  $\text{NO}_2$  fluxes over the same periods are  $2.8 \times 10^{-12} \text{ kg N m}^{-2} \text{ s}^{-1}$  and  $3.3 \times 10^{-12} \text{ kg N m}^{-2} \text{ s}^{-1}$ , i.e. values respectively 18 and 9 times higher than in the observations by Frey et al. (2013, 2014). This discrepancy may be explain by the fact that FP represents the potential flux of  $\text{NO}_2$  emitted from the snow to the atmosphere, i.e. an upper limit when comparing to the observed  $\text{NO}_2$  flux. TRANSITS does not take into account various potential processes affecting  $\text{NO}_x$  emission from snow, such as diffusion or chemical conversion prior to emission and forced ventilation from the snowpack (France et al., 2011; Frey et al., 2013; Meusinger et al., 2014). Future improvements of the model could include a more accurate representation of the extraction of  $\text{NO}_2$  from the snowpack with the following processes:  $\text{NO}_x$  diffusion, wind pumping, chemical conversion prior to emission, the latter depending on oxidant levels in firn air ( $\text{HO}_x$ ,  $\text{O}_3$ , and maybe halogens,

[Title Page](#)[Abstract](#)[Introduction](#)[Conclusions](#)[References](#)[Tables](#)[Figures](#)[◀](#)[▶](#)[Back](#)[Close](#)[Full Screen / Esc](#)[Printer-friendly Version](#)[Interactive Discussion](#)

Zatko et al., 2013). Another improvement could be the modeling of two nitrate domains (photolabile and buried nitrate, Meusinger et al., 2014).

We note that if HONO production is greater than assumed at Dome C, following the recent laboratory study of Scharko et al. (2014), this will not change the main conclusions of this study. Indeed, the photolytically produced HONO will be photolyzed to form NO in the atmosphere and this NO would simply enter the NO/NO<sub>2</sub> cycles where oxygen isotopes are reset.

### 3.3.3 Validation of nitrate mass repartition in each compartment

The TRANSITS simulation for East Antarctica shows that the primary inputs of nitrate to the air–snow system is realistic ( $FPI = 8.2 \times 10^{-6} \text{ kgNm}^{-2} \text{ a}^{-1}$ ). Indeed, changing FPI leads to the horizontal shift of the simulated data in Fig. 9a. We note that our simulation in East Antarctica is very simple because it only takes into account changes in snow accumulation rates which are large on the D10–DC–Vostok route. A more sophisticated simulation along this line is beyond the scope of the present study because it would require including a radiative transfer model such as TUV-snow (or such as TARTES, Llibois et al., 2014) in TRANSITS in order to deal with latitudinal and elevation changes. Also, the simulation should take into account boxes from Vostok to D10 with the exchange of nitrate horizontally exported from the center of the continent towards the coast.

The model simulates annual averages of  $\omega(\text{NO}_3^-)$  in skin layer nitrate approximately 7 times higher than in the observations. Fully resolving this discrepancy is beyond the scope of this paper. We however note that it could be linked to heterogeneities in sampling the skin layer (whose thickness is  $(4 \pm 2) \text{ mm}$ , Erbland et al., 2013), especially when considering that different overwintering people were involved in this task. For instance, sampling 6 instead of 4 mm could lead to the sampling of a more diluted skin layer. Another explanation would invoke that a fraction of the skin layer is eroded by the wind.

<a href="#">Title Page</a>	
<a href="#">Abstract</a>	<a href="#">Introduction</a>
<a href="#">Conclusions</a>	<a href="#">References</a>
<a href="#">Tables</a>	<a href="#">Figures</a>
<a href="#"></a>	<a href="#"></a>
<a href="#"></a>	<a href="#"></a>
<a href="#">Full Screen / Esc</a>	
<a href="#">Printer-friendly Version</a>	
<a href="#">Interactive Discussion</a>	



The simulated annual average  $m_{50\text{ cm}}(\text{NO}_3^-)$  value is on the same order of magnitude than the observed annual average value ( $(8.3 \pm 1.6) \text{ mgN}$  vs.  $(3.4 \pm 1.0) \text{ mgN}$ ), which is already very satisfactory. We observe that the discrepancy (annual  $m_{50\text{ cm}}(\text{NO}_3^-)$ ) is 2.5 times higher in the model) could be linked to the response time of the modeled snowpack to changes in primary input fluxes.

- 5 Indeed, when run in the DC realistic simulation with a multiplication of FPI by a factor 10 after 25 years of simulation, TRANSITS shows a response time of approximately 21 years. This means that the snowpack requires 21 years to reach stable  $m_{50\text{ cm}}(\text{NO}_3^-)$  values again. As a consequence, the different  $m_{50\text{ cm}}(\text{NO}_3^-)$  value observed today at Dome C could reflect changes in primary input 10 flux conditions as far back as 21 years in the past.

Simulated nitrate mass in the top 50 cm of snow has been shown to increase in winter and to decrease during the sunlit season (Fig. 6a). This feature can also be seen in the observed data, which is a strong support of the TRANSITS model and the processes included in it. In winter, the input and output to the nitrate reservoir in 15 the top 50 cm of snow are the deposition and archiving fluxes, respectively. During this season, the deposition flux is greater than the archiving flux which leads to an increase in  $m_{50\text{ cm}}(\text{NO}_3^-)$ . When the sunlit season starts, the additional photolysis output flux starts, leading the sum FA + FP to exceed FD and thus decreasing  $m_{50\text{ cm}}(\text{NO}_3^-)$ .

### 3.3.4 Discussion on the $\delta^{15}\text{N}$ values in different nitrate compartments

- 20 Overall, TRANSITS reproduces well the observed  $\delta^{15}\text{N}$  values in skin layer and in the atmosphere nitrate. At the air–snow interface, the observed  $\delta^{15}\text{N}$  values become lower than the simulated ones in spring. We have also observed that the recovery is faster. This would be consistent with an erosion of a fraction of the skin layer as discussed 25 above. Another possible explanation is that the average ozone column profile used for the DC realistic simulation does not well represent that observed in spring/summer 2009.

<a href="#">Title Page</a>	
<a href="#">Abstract</a>	<a href="#">Introduction</a>
<a href="#">Conclusions</a>	<a href="#">References</a>
<a href="#">Tables</a>	<a href="#">Figures</a>
<a href="#">◀</a>	<a href="#">▶</a>
<a href="#">◀</a>	<a href="#">▶</a>
<a href="#">Back</a>	<a href="#">Close</a>
<a href="#">Full Screen / Esc</a>	
<a href="#">Printer-friendly Version</a>	
<a href="#">Interactive Discussion</a>	



Observations of  $\delta^{15}\text{N}$  of nitrate in skin layer shows large variations  $\delta^{15}\text{N}$  (Erbland et al., 2013), which are not reproduced by the model. This could be the result of sampling effects for the observed dataset and/or wind erosion at the surface.

Figure 5e and h shows the recovery of the  $\delta^{15}\text{N}$  in both skin layer and atmospheric compartments in spring/early summer. This return of  $\delta^{15}\text{N}(\text{NO}_3^-)$  to positive values in summer is faster at Dome C than it has been observed at DDU and this feature has been attributed to longer exposure time of nitrate at the snow surface at Dome C (Savarino et al., 2007; Frey et al., 2009). TRANSITS confirms this suggestion when run with the higher snow accumulation rate which characterizes DDU. At Dome C, shortly after the decrease,  $\delta^{15}\text{N}$  values rapidly start to rise again because the nitrate in snow becomes more enriched in  $^{15}\text{N}$  and the extracted  $\text{NO}_2$  has rising  $\delta^{15}\text{N}$  values as well. With large  $\theta$  at the end of the summer, the apparent ozone column crossed by the UV rays is more important and the photolytic fractionation constant ( ${}^{15}\varepsilon_{\text{pho}}$ ) becomes more negative (Fig. 6d). This leads to decreasing  $\delta^{15}\text{N}$  values extracted from the snowpack even if the enrichment does not stop there. Finally, wintertime values of  $\delta^{15}\text{N}$  are reached back by the end of April/beginning of May when the nitrate photolysis stops.

The simulated  $\delta^{15}\text{N}$  values of nitrate in the top 50 cm of snow are higher than the observed ones (Fig. 6c). However, observations are very variable and may be affected by heterogeneities at the surface of the snowpack (erosion, deposition of snow) and more data are required in order to better constrain the model in this compartment. Last, we recall that simulated  $\delta^{15}\text{N}_{50\text{cm}}$  values can also be strongly affected by the residence time of nitrate in this zone (more than 20 years as discussed above). In particular, we observe that the higher  $\delta^{15}\text{N}_{50\text{cm}}$  values in the observations are consistent with observed  $m_{50\text{cm}}(\text{NO}_3^-)$  values lower than in the simulations.

<a href="#">Title Page</a>	
<a href="#">Abstract</a>	<a href="#">Introduction</a>
<a href="#">Conclusions</a>	<a href="#">References</a>
<a href="#">Tables</a>	<a href="#">Figures</a>
<a href="#">◀</a>	<a href="#">▶</a>
<a href="#">◀</a>	<a href="#">▶</a>
<a href="#">Back</a>	<a href="#">Close</a>
<a href="#">Full Screen / Esc</a>	
<a href="#">Printer-friendly Version</a>	
<a href="#">Interactive Discussion</a>	



### 3.3.5 Discussion on the $\Delta^{17}\text{O}$ values in different nitrate compartments

Overall, TRANSITS reproduces qualitatively well the  $\Delta^{17}\text{O}$  in nitrate from each compartment. Concurring variations in  $\Delta^{17}\text{O}$  in atmospheric and skin layer nitrate indicate equilibrium at the air–snow interface. However, differences in  $\Delta^{17}\text{O}$  can be observed throughout the year and this difference varies with time. It is the result of the different sizes of the atmospheric and skin layer nitrate reservoirs and indicates that the equilibrium is dynamic. One other evidence for the different reservoir effects is that the isotope time series in the skin layer are smoother than in the atmosphere (Fig. 5).

One feature cannot be reproduced by TRANSITS: the negative difference between  $\Delta^{17}\text{O}$  in atmospheric and skin layer nitrate. Unraveling this issue is beyond the scope of this study because we anticipate that this shift has a very weak impact on  $\Delta^{17}\text{O}$  in the archived nitrate since nitrate mass in the atmosphere is very small compared to the nitrate mass in the snow.

Quantitatively, the oxygen data observed at DC cannot be fully reproduced by the TRANSITS simulation. Indeed, the simulated  $\Delta^{17}\text{O}$  values are overall lower than the observed values. A quantitative transcription of the information harbored by the oxygen isotopes is not achieved yet in TRANSITS. We however recall that a number of simplifying choices have been made in the description of the local cycling and oxidation of  $\text{NO}_2$ . For instance, the competition of  $\text{O}_3$  with OH in the oxidation of  $\text{NO}_2$  at the beginning and end of the sunlit season was not taken into account. Also, the small contribution of ozone photolysis in the production of OH was neglected. All in all, taking into account these small contributions would lead to a more efficient transfer of the  $^{17}\text{O}$ -excess of ozone to  $\text{HNO}_3$  and a better agreement of the model and the observations.

We also recall that the  $\text{NO}_x/\text{HO}_x$  chemistry at Dome C is not yet completely understood (Kukui et al., 2014 and OPALE special issue). A nitrogen species ( $\text{HNO}_4$  or an unknown species) is expected to perturb the  $\text{NO}_x$  photochemical cycle and lead to the high observed  $\text{NO}_2/\text{NO}$  ratio (Frey et al., 2014).

<a href="#">Title Page</a>	
<a href="#">Abstract</a>	<a href="#">Introduction</a>
<a href="#">Conclusions</a>	<a href="#">References</a>
<a href="#">Tables</a>	<a href="#">Figures</a>
<a href="#">◀</a>	<a href="#">▶</a>
<a href="#">◀</a>	<a href="#">▶</a>
<a href="#">Back</a>	<a href="#">Close</a>
<a href="#">Full Screen / Esc</a>	
<a href="#">Printer-friendly Version</a>	
<a href="#">Interactive Discussion</a>	



Integrating a more realistic chemistry in TRANSITS will probably amplify the intense NO/NO<sub>2</sub> cycling in the atmosphere and not fundamentally change the nature of the processes at play at the air–snow interface of DC. We also anticipate that the type of archived information below the photic zone will not change.

5 Last, we also observe that TRANSITS reproduces well the  $\Delta^{17}\text{O}(\text{FA})/\delta^{15}\text{N}(\text{FA})$  anti-correlation and general trend in the case of the simulation across East Antarctica (Fig. 9c). However, on Fig. 9c, the observations show a large scattering around the trend reproduced by TRANSITS with differences of more than 5‰. One reason for that is the inability of the model to reproduce variations of  $\Delta^{17}\text{O}$  in nitrate below 20 cm  
10 whose variability can be as high as 5‰ (Fig. 7c). Such variations may be linked to variability in ozone column, snow accumulation, local atmospheric chemistry, primary inputs of nitrate from one year to another which are not accounted for by TRANSITS. McCabe et al. (2007) first observed such 2–3 years period cycles in a 6 m snow pit from South Pole and attributed these cycles to variability in the stratospheric ozone column;  
15 the same periodicity in  $\Delta^{17}\text{O}$  is found in DC surface snow (Frey et al., 2009; Erblan et al., 2013). Future work should investigate the impact of the variations in the ozone column on the  $\Delta^{17}\text{O}$  in the archived nitrate.

### 3.3.6 Validation of the local atmospheric processing of NO<sub>2</sub>

The photolytic and deposition fluxes in summer show that there is an intense nitrate recycling at the air–snow interface in this season (Fig. 5a). The local signature of NO<sub>2</sub> cycling and oxidation harbored by  $\Delta^{17}\text{O}$  is therefore incorporated in skin layer nitrate. Given the good qualitative agreement between the simulated and observed  $\Delta^{17}\text{O}$  in skin layer nitrate throughout the year, we conclude that TRANSITS has a realistic representation of the local cycling and oxidation of NO<sub>2</sub> in the atmosphere. We note that the hypothesis that summer conditions in the NO/NO<sub>2</sub> cycling prevail during the whole sunlit season is hypothesis verified for mid-October when using TUV to calculate the appropriate  $J(\text{NO}_2)$  and calculation the reaction rate of NO + O<sub>3</sub>.  
25

<a href="#">Title Page</a>	
<a href="#">Abstract</a>	<a href="#">Introduction</a>
<a href="#">Conclusions</a>	<a href="#">References</a>
<a href="#">Tables</a>	<a href="#">Figures</a>
<a href="#">◀</a>	<a href="#">▶</a>
<a href="#">◀</a>	<a href="#">▶</a>
<a href="#">Back</a>	<a href="#">Close</a>
<a href="#">Full Screen / Esc</a>	
<a href="#">Printer-friendly Version</a>	
<a href="#">Interactive Discussion</a>	



<a href="#">Title Page</a>	
<a href="#">Abstract</a>	<a href="#">Introduction</a>
<a href="#">Conclusions</a>	<a href="#">References</a>
<a href="#">Tables</a>	
<a href="#">Figures</a>	
<a href="#">◀</a>	<a href="#">▶</a>
<a href="#">◀</a>	<a href="#">▶</a>
<a href="#">Back</a>	<a href="#">Close</a>
<a href="#">Full Screen / Esc</a>	
<a href="#">Printer-friendly Version</a>	
<a href="#">Interactive Discussion</a>	



For the realistic simulation, the computed  $\alpha$  variable varies in the range 0.80–1 with the minimum value calculated a few weeks after summer solstice when  $O_3$  mixing ratios reach their minimum (Legrand et al., 2009), and the maximum value calculated at the beginning and at the end of the sunlit season. The FP-weighted annual average value of  $\alpha$  is 0.86 which shows that the Leighton cycle is significantly perturbed by  $HO_2$  and  $CH_3O_2$  and the transfer of the  $^{17}O$ -excess harbored by ozone to  $NO_2$  is not 100 % efficient. The hypothesis of an annually constant BrO mixing ratio of 2.5 pptv is crude because it must be lower and the beginning and end of the sunlit season. However, we observe that BrO marginally contributes to  $\alpha$  at these periods.

We observe that a TRANSITS simulation with  $\alpha$  set to 1 allows a better agreement with the observations. For instance, the minimum summertime  $\Delta^{17}O$  values in skin layer, atmospheric and archived nitrate are 28.7, 29.9 and 23.2‰, respectively. The model will benefit future concurring year-round measurements of mixing ratios of  $O_3$  and species ( $BrO$ ,  $HO_2$ ,  $RO_2$  or additional species) perturbing the Leighton cycle in order to obtain the best input for  $\alpha$ . Also, accurate simulations at Dome C will also benefit the measurement of  $\Delta^{17}O(O_3)_{bulk}$  at this location.

In TRANSITS, the local oxidation of  $NO_2$  has been assumed to only occur through the daytime channel, i.e. through the oxidation by OH. In order to verify this hypothesis, we calculate  $r(OH \text{ vs. } O_3) = v(OH)/(v(OH) + v(O_3))$ , the relative apportioning of the daytime and nighttime  $NO_2$  oxidation channel, with the assumption that the latter occurs through  $NO_2 + O_3$ . For the calculation of  $r(OH \text{ vs. } O_3)$ , we use kinetic rate constants from Atkinson et al. (2004), ozone mixing ratios from Legrand et al. (2009) and OH mixing ratios are extrapolated from  $J(NO_2)$  calculated by TRANSITS and using the relationship  $[OH]/(\text{molecule cm}^{-3}) = 2.5 \times 10^8 \times J(NO_2)/\text{s}^{-1}$  given in Fig. 3a, Kukui et al. (2014). For the realistic DC simulation,  $r(OH \text{ vs. } O_3)$  is higher than 0.95 from the fourth week after sunrise to the second week before sunset, i.e. for more than 90 % of the sunlit season. We also note that for the periods when  $r(OH \text{ vs. } O_3) < 0.95$ , the actinic flux is at maximum 6 % of the maximum actinic flux calculated for summer solstice. One consequence is our calculation of a FP-weighted average of  $r(OH \text{ vs. } O_3)$  of

99 % which means that over the sunlit season, the daytime oxidation channel of NO<sub>2</sub> is almost 100 times faster than the nighttime oxidation channel, a result which supports our choice of a simple representation of NO<sub>2</sub> oxidation in TRANSITS.

### 3.3.7 Validation of the nitrate deposition and diffusion processes

- 5 The parameterization of HNO<sub>3</sub> deposition is simplistic since it solves the mass balance equation (Eq. 6) in order to reproduce the nitrate concentration in the atmosphere. A sensitivity test of TRANSITS has been run using nitrate atmospheric concentrations 10 times higher than the ideal DC time series used for the DC realistic simulation. The higher nitrate concentration in the atmosphere had no significant impact on any of  
10 the nitrate reservoirs both in terms of mass and isotopic composition. Indeed, in this case, the atmospheric nitrate mass would represent a 1/150 and 1/800 nitrate mass in the skin layer and in the top 50 cm, respectively. Future improvements of the model could use a physical description of the deposition of HNO<sub>3</sub> using for example a vertical deposition velocity.

15 Taking nitrate diffusion into account leads to the computation of smooth profiles such as those observed in the field (Fig. 7). However, it is important to note that the diffusion routine is time-consuming since it is modeled by solving the diffusion equations in a sub-routine at a 4 h time step. When nitrate diffusion is turned off, the simulated mass fraction and isotope profiles in the snow show unrealistic variations.

20 The secondary peak observed in simulated nitrate mass fraction profiles (at 8 cm depth) represents nitrate residual from the previous year's skin layer. This is consistent with secondary peaks observed in some snow pits on the Antarctic plateau (e.g. DC07–2, S2 and S3 in Supplementary Information, Erbland et al., 2013). Since TRANSITS is able to reproduce such a feature, we conclude that a simplified description of nitrate diffusion (i.e. constant diffusion coefficient) is not detrimental.  
25

<a href="#">Title Page</a>	
<a href="#">Abstract</a>	<a href="#">Introduction</a>
<a href="#">Conclusions</a>	<a href="#">References</a>
<a href="#">Tables</a>	<a href="#">Figures</a>
<a href="#">◀</a>	<a href="#">▶</a>
<a href="#">◀</a>	<a href="#">▶</a>
<a href="#">Back</a>	<a href="#">Close</a>
<a href="#">Full Screen / Esc</a>	
<a href="#">Printer-friendly Version</a>	
<a href="#">Interactive Discussion</a>	



## 4 A framework for the interpretation of nitrate isotope records in ice cores

Potentially measurable quantities in ice cores are  $\omega(\text{FA})$ ,  $\delta^{15}\text{N}(\text{FA})$  and  $\Delta^{17}\text{O}(\text{FA})$  (e.g. Hastings et al., 2005; Frey et al., 2009). Given snow accumulation rates derived independently, one can also obtain  $\text{FA} = \omega(\text{FA}) \times A$ . In this section, we develop a framework for the interpretation of nitrate records in ice cores. To this end, a larger number of sensitivity tests of the TRANSITS model were run.

### 4.1 Parameters and variables controlling FA and $\delta^{15}\text{N}(\text{FA})$

#### 4.1.1 Sensitivity tests: description and results

The sensitivity of the model is tested in simple cases where single variables and parameters are changed. For each simulation, the model was run for 25 years (i.e. until convergence). The realistic simulation for DC is used as the reference simulation. Table 7 provides an overview of the variations imposed on the tested variables and parameters. The four following variables and parameters have been set to 0 (Table 7):  $\varepsilon_{\text{dep}}^{15}$ ,  $\Delta^{17}\text{O}(\text{FS})$ ,  $\Delta^{17}\text{O}(\text{FT})$  and  $\Delta^{17}\text{O}(\text{O}_3)_{\text{bulk}}$ . The  $\delta^{15}\text{N}(\text{FS})$  and  $\delta^{15}\text{N}(\text{FT})$  parameters have been changed to 119 and 100 ‰, respectively. The parameters FPI and  $h_{\text{AT}}$  were multiplied by a factor 10. The mixing ratios of  $[\text{BrO}]$ ,  $[\text{O}_3]$ ,  $[\text{HO}_2]$  and  $[\text{CH}_3\text{O}_2]$  were multiplied by a factor 2. The nine following variables and parameters have been changed by +20 %: FS/FPI,  $f_{\text{cage}}$ ,  $f_{\text{exp}}$ ,  $A$ ,  $\rho$ ,  $k$ ,  $q$ ,  $\phi$  and  $D$ . The sensitivity to the snow accumulation repartition in the year has been tested by running the model with summer snow accumulation rates two times higher than the winter ones and conversely. The sensitivity to  $T$  has been tested by shifting the observed atmospheric temperature time series by  $-10\text{ K}$ . The model sensitivity to the ozone column has been run for four simulations: with constant ozone columns of 100, 300 and 500 DU as well as with an ozone hole of 100 DU from August to November and an ozone column of 300 DU the rest of the time. Last, the sensitivity of the model to the atmospheric nitrate concentrations has been tested by running it with concentrations ten times higher than in the

[Title Page](#)[Abstract](#)[Introduction](#)[Conclusions](#)[References](#)[Tables](#)[Figures](#)[◀](#)[▶](#)[◀](#)[▶](#)[Back](#)[Close](#)[Full Screen / Esc](#)[Printer-friendly Version](#)[Interactive Discussion](#)

realistic DC simulation. The total number of simulations is then 30, which includes the reference simulation.

For each test, the following outputs (FA, FA/FPI,  $\delta^{15}\text{N}(\text{FA})$  and  $\Delta^{17}\text{O}(\text{FA})$ ) were calculated. The description and results of the tests scenarios are given in Table 7. As an example and a guideline to read Table 7, we describe the result for the test where the snow accumulation rate was changed. The value used in the reference simulation is  $28 \text{ kg m}^{-2} \text{ a}^{-1}$  and that of the tested scenario is 20 % greater (i.e.  $33.6 \text{ kg m}^{-2} \text{ a}^{-1}$ ). Table 7 indicates that such an increase in  $A$  leads to an increase of the archived nitrate mass flux from 2.04 to 4.32 % of the primary nitrate mass flux.  $\Delta^{17}\text{O}$  in the archived nitrate is increased by 0.9 %. Conversely,  $\delta^{15}\text{N}$  in the archived nitrate is decreased by 48.7 from 287.4 to 238.7 %.

Table 7 shows that three parameters and variables have no impact on the archived nitrate:  $h_{\text{AT}}$ ,  $\gamma(\text{NO}_3^-)$  and  $^{15}\varepsilon_{\text{dep}}$ . The reason for these observations is that the nitrate mass in the atmospheric box is negligible when compared to the nitrate reservoir in snow as discussed previously (Sect. 3.3.7). The parameter FPI is the only one affecting FA, while FA and FPI are linearly linked (i.e. FA/FPI remains constant), but this does not modify  $\delta^{15}\text{N}(\text{FA})$ . The  $\delta^{15}\text{N}$  signatures in the primary nitrate sources ( $\delta^{15}\text{N}(\text{FS})$  and  $\delta^{15}\text{N}(\text{FT})$ ) have an impact on  $\delta^{15}\text{N}(\text{FA})$ . In contrast, some parameters only impact  $\Delta^{17}\text{O}(\text{FA})$  such as the  $\Delta^{17}\text{O}$  signature in the primary nitrate sources ( $\Delta^{17}\text{O}(\text{FS})$  and  $\Delta^{17}\text{O}(\text{FT})$ ),  $\Delta^{17}\text{O}$  of bulk ozone and parameters and variables driving the local cycling and oxidation of  $\text{NO}_2$ :  $[\text{O}_3]$ ,  $[\text{BrO}]$ ,  $[\text{HO}_2]$ ,  $[\text{CH}_3\text{O}_2]$  and  $T$ .

The other parameters and variables impact at the same time FA, FA/FPI,  $\delta^{15}\text{N}(\text{FA})$  and  $\Delta^{17}\text{O}(\text{FA})$ . These are:  $f_{\text{cage}}$ ,  $f_{\text{exp}}$ ,  $A$ ,  $\rho$ ,  $k$ ,  $q$ ,  $\phi$ ,  $D$ , FS/FPI, the snow accumulation repartition and the  $\text{O}_3$  column.

#### 4.1.2 Modified Rayleigh plots

In this section, we use a data representation which we term “modified Rayleigh plot” where  $\ln(\delta^{15}\text{N}(\text{FA}) + 1)$  is plotted against  $\ln(\text{FA})$  rather than  $\ln(\omega(\text{FA}))$ , since it includes the variability in  $A$  in contrast to  $\omega(\text{FA})$ . Figure 10 summarizes the results obtained for

[Title Page](#)

[Abstract](#)

[Introduction](#)

[Conclusions](#)

[References](#)

[Tables](#)

[Figures](#)

◀

▶

[Back](#)

[Close](#)

[Full Screen / Esc](#)

[Printer-friendly Version](#)

[Interactive Discussion](#)



most of the sensitivity tests which impact FA/FPI, FA and  $\delta^{15}\text{N}(\text{FA})$ , i.e. tests where the following variables are changed:  $\phi$ ,  $A$ ,  $\rho$ ,  $k$ ,  $q$ ,  $f_{\text{cage}}$ ,  $f_{\text{exp}}$ ,  $D$ , FS/FPI, FPI, O<sub>3</sub> column and the snow accumulation repartition in the year. The thick black dashed curve in Fig. 10 represents the DC realistic simulation in which  $\phi$  is varied to obtain changes in FA and  $\delta^{15}\text{N}(\text{FA})$ . The curve is almost linear with a slope of  $-0.061$  passing through the “starting point” whose coordinates are  $(\ln(\text{FPI}), \ln(\delta^{15}\text{N}(\text{FPI}) + 1))$ . For instance, this means that a decrease in the archived flux (FA, i.e. changes in FA/FPI) corresponds to an increase in  $\delta^{15}\text{N}(\text{FA})$ .

Most of the sensitivity simulation outputs fall on the thick black dashed curve which represents the DC realistic simulation. We also observe from Fig. 10 that some simulations fall on curves which have different slopes or which have the same slope but different starting points. The parameters and variables are therefore sorted in 3 groups: those which control the “starting point”, those which control the slope in the modified Rayleigh plot and those which control the horizontal and vertical distances from the starting point, i.e. the final position on the curve.

#### 4.1.3 Controls on the “starting point”

Figure 10 shows that the starting point is determined by FPI and  $\delta^{15}\text{N}(\text{FT})$  and  $\delta^{15}\text{N}(\text{FS})$ . On one hand, changes in FPI lead to a horizontal shift of the starting point (green star in Fig. 10) and, all other things being equal, to a horizontal shift of the entire line in this plot. On the other hand, changes in the  $\delta^{15}\text{N}$  value in the primary input ( $\delta^{15}\text{N}(\text{FT})$  and  $\delta^{15}\text{N}(\text{FS})$ ) lead to a vertical shift of the starting point and the entire curve. Changes in the  $f_{\text{exp}}$  also result in a slight horizontal shift of the simulated “archived point”. Indeed,  $f_{\text{exp}}$  sets the net horizontal export of nitrate from the atmospheric box, which results in more or less of the primary input flux lost through this process. In the case of an increasing  $f_{\text{exp}}$  parameter, the “apparent” FPI is therefore shifted to lower FPI values.

[Title Page](#)[Abstract](#)[Introduction](#)[Conclusions](#)[References](#)[Tables](#)[Figures](#)[|◀](#)[▶|](#)[◀](#)[▶](#)[Back](#)[Close](#)[Full Screen / Esc](#)[Printer-friendly Version](#)[Interactive Discussion](#)

Sensitivity tests where  $\delta^{15}\text{N(FT)}$  and  $\delta^{15}\text{N(FS)}$  were shifted by +100‰ show that significant amounts of the nitrogen signatures of the primary nitrate inputs are preserved (72 and 56‰, respectively, Table 7), even if the recycling of nitrate has led to a 270‰ increase in  $\delta^{15}\text{N(FA)}$ . Therefore,  $\delta^{15}\text{N(FA)}$  harbours a fraction of the nitrogen isotopic signature of the primary inputs of nitrate but we note that it remains almost insignificant given the observed low variability of  $\delta^{15}\text{N(FS)}$  ([+20, +30]‰, Brizzi et al., 2009) and  $\delta^{15}\text{N(FT)}$  ([-10, +10]‰, Morin et al., 2009).

#### 4.1.4 Controls on the slope

Only the ozone column controls the slope of the curve (Fig. 10). The spectral distribution of the actinic flux determines the  $^{15}\text{N}/^{14}\text{N}$  fractionation constant associated with nitrate photolysis ( $^{15}\varepsilon_{\text{pho}}$ ) (Frey et al., 2009) and hence the slope of the curve. In the case of the DC reference simulation, a yearly mean apparent fractionation constant ( $^{15}\varepsilon_{\text{app}}$ ) of -55.1‰ was calculated for  $^{15}\varepsilon_{\text{pho}}$  ranging from -52.9 to -78.8‰ (Table 6). The variability of the curvature of the thick back curve representing the DC reference simulation in Fig. 10 is linked to the greater incorporating of the summertime value of  $^{15}\varepsilon_{\text{pho}}$  (Fig. 6d): when FA/FPI increases,  $^{15}\varepsilon_{\text{pho}}$  gets less negative and the curvature decreases. Therefore, the slope of the thick dashed lines in the modified Rayleigh plots is slightly more negative (-0.061 = -61‰) than  $^{15}\varepsilon_{\text{app}}$ .

Lower ozone columns have a strong impact on FA and  $\delta^{15}\text{N(FA)}$ : FA is lower while  $\delta^{15}\text{N(FA)}$  is higher (Fig. 10). The first effect is explained by higher UV radiations which reach the ground and so higher photolytic rates. The second effect is linked to the fact that a lower ozone column leads to higher values of the fractionation constant, as observed in spring during the ozone hole period (Fig. 6d). Indeed, a lower ozone column allows UV radiations of shorter wavelengths in the 280–350 nm range to reach the ground, i.e. a shift to the blue of the UV spectra, therefore resulting in higher  $^{15}\varepsilon_{\text{pho}}$  values (Frey et al., 2009). Referring to Eq. (4) and our sensitivity tests reveals that changes in the ozone column result in changes in UV flux ( $f$ ) which overweights the

<a href="#">Title Page</a>	
<a href="#">Abstract</a>	<a href="#">Introduction</a>
<a href="#">Conclusions</a>	<a href="#">References</a>
<a href="#">Tables</a>	<a href="#">Figures</a>
<a href="#">◀</a>	<a href="#">▶</a>
<a href="#">◀</a>	<a href="#">▶</a>
<a href="#">Back</a>	<a href="#">Close</a>
<a href="#">Full Screen / Esc</a>	
<a href="#">Printer-friendly Version</a>	
<a href="#">Interactive Discussion</a>	



changes in UV spectra ( $^{15}\varepsilon_{\text{pho}}$ ). From our sensitivity tests, we also observe that an ozone hole in late winter/spring (August to November) significantly imprints  $\delta^{15}\text{N(FA)}$  (Fig. 10). Therefore, we suggest that  $\delta^{15}\text{N(FA)}$  archived over the last decades at Dome C and other East Antarctic plateau sites could potentially be imprinted by changes in the ozone column, especially in Spring when stratospheric ozone destruction processes are at play.

#### **4.1.5 Controls on the distance from the starting point and along the slope**

Hereafter, the ratio FA/FPI is termed the “nitrate trapping efficiency” because it reflects the fraction of nitrate which is trapped below the photic zone.

In the modified Rayleigh plot, the horizontal distance from the starting point is  $\ln(\text{FA}/\text{FPI}) = \ln(\text{FA}) - \ln(\text{FPI})$ , i.e. the horizontal distance from the starting point is directly linked to the trapping efficiency. This quantity is therefore equivalent to the  $f$  term used in Eq. (4) because it reflects the nitrate fraction remaining in snow below the photic zone. The trapping efficiency and the intensity of the photolysis are linked because a more intense photolysis is necessary to lead to a lower nitrate trapping efficiency.

In the modified Rayleigh plot, the vertical distance from the starting point is  $\ln(\delta^{15}\text{N(FA)} + 1) - \ln(\delta^{15}\text{N(FPI)} + 1)$ . Figure 10 shows that, at first order, the vertical and horizontal distance from the starting point are linked by the slope. This means that at a given slope in the modified Rayleigh plot, i.e. at a given spectral distribution of the actinic flux,  $\ln(\delta^{15}\text{N(FA)} + 1)$  is linearly linked with  $\ln(\text{FA/FPI})$ , i.e.  $\delta^{15}\text{N(FA)}$  is linked with the trapping efficiency.

Our sensitivity tests have shown that the nitrate trapping efficiency is controlled by  $\phi$ ,  $A$ ,  $\rho$ ,  $k$ ,  $q$ ,  $f_{\text{cage}}$ ,  $f_{\text{exp}}$ ,  $D$ , FS/FPI,  $O_3$  column and the snow accumulation repartition in the year. Indeed,  $\phi$ ,  $f_{\text{cage}}$ ,  $q$  and  $O_3$  column are key parameters and variables in controlling the photolytic mass loss while  $A$ ,  $\rho$ ,  $k$ ,  $D$  and the seasonality in snow accumulation determine nitrate exposure time to the actinic flux. Considering the sea-



<a href="#">Title Page</a>	
<a href="#">Abstract</a>	<a href="#">Introduction</a>
<a href="#">Conclusions</a>	<a href="#">References</a>
<a href="#">Tables</a>	<a href="#">Figures</a>
<a href="#"></a>	<a href="#"></a>
<a href="#">Back</a>	<a href="#">Close</a>
<a href="#">Full Screen / Esc</a>	
<a href="#">Printer-friendly Version</a>	
<a href="#">Interactive Discussion</a>	



sonality of snow accumulation, we observe that it plays a minor role in setting FA/FPI and hence  $\delta^{15}\text{N(FA)}$ . The reason is that, in DC conditions, nitrate residence time in the photic zone is very long and set by the other parameters and variables at play in the photolytic process. The same applies to the FS/FPI ratio: the impact on nitrate trapping efficiency is small.

The case of the export flux parameter,  $f_{\text{exp}}$ , is different. Indeed, it does not impact the residence time of nitrate in the photic zone, nor does it impact its photolytic loss. However, an increase in  $f_{\text{exp}}$  results in a greater export of atmospheric nitrate, which is depleted in  $^{15}\text{N}$  with respect to nitrate in snow (data not shown in Table 7). In fact, the increase in  $f_{\text{exp}}$  also leads to higher  $\delta^{15}\text{N(FA)}$  and  $\delta^{15}\text{N(FE)}$  values. In the two simulations tested,  $\delta^{15}\text{N(FE)}$  is always smaller than  $\delta^{15}\text{N(FPI)}$ , which means that the “removal” of nitrate featuring  $\delta^{15}\text{N(FE)} \leq \delta^{15}\text{N(FPI)}$  is compensated by the increase of  $^{15}\text{N}$  in the archived nitrate. This increase in  $\delta^{15}\text{N(FA)}$  is therefore not due to an increased photolysis intensity but to the isotopic mass balance.

The parameters and variables  $\phi$ ,  $k$ ,  $A$ ,  $\rho$  and  $q$  have the largest impact on the nitrate trapping efficiency (FA/FPI), with mostly equivalent impacts on  $\delta^{15}\text{N(FA)}$ . That they control FA/FPI and  $\delta^{15}\text{N(FA)}$  to a similar extent is not surprising since  $k$ ,  $A$ ,  $\rho$  and  $q$  are intimately linked together in determining the residence time in the photic layer and so the exposure time of nitrate to near-surface conditions.

In this paper, the model does not aim at representing the counter ion of nitrate. However, we acknowledge that the diffusion of nitrate may be different depending on the nature of its counter ion ( $\text{H}^+$  or, e.g.  $\text{Ca}^{2+}$ ), especially when glacial conditions are considered (Röthlisberger et al., 2000).

#### 4.1.6 Method to interpret FA and $\delta^{15}\text{N(FA)}$ measured in ice cores

In this section we summarize our recommended approach to interpret nitrate isotope records in ice cores. The approach is valid provided that evidence show that the nitrate

recycling observed today has also occurred in the past. The measurement of elevated  $\delta^{15}\text{N(FA)}$  values could be such a piece of evidence.

Information potentially accessible from ice cores are  $\omega$  (FA) and  $\delta^{15}\text{N(FA)}$ . Knowledge on the past snow accumulation rates (assumed or deduced from other proxies) allow the calculation of  $\text{FA} = \omega(\text{FA}) \times A$ . If FA and  $\delta^{15}\text{N(FA)}$  data align in the modified Rayleigh plot, the previous sections have shown that it is possible to retrieve information on the ozone column. In this case one can deduce that the ozone column is likely to have remained constant through time and its value can be inferred from the slope of the curve (e.g. lower right panel in Fig. 10). In this case as well, FPI is likely to have remained constant through time and its value can be retrieved provided that  $\delta^{15}\text{N(FPI)}$  have remained constant as well and that one can assume its value. If the data do not align in the modified Rayleigh plot, it is likely that either or both the ozone column and FPI have varied over time. If an assumption on the ozone column can be made or if this information can be obtained from other considerations, one can determine past changes in FPI provided that an assumption on  $\delta^{15}\text{N(FPI)}$  can be made. Figure 12 gives a schematic of the method to determine FPI from the measurement of  $\omega$  (FA) and  $\delta^{15}\text{N(FA)}$  in ice cores. As discussed above, a fraction of  $\delta^{15}\text{N(FT)}$  and  $\delta^{15}\text{N(FS)}$  is left in  $\delta^{15}\text{N(FA)}$ . However,  $\delta^{15}\text{N(FT)}$  and  $\delta^{15}\text{N(FS)}$  are small when compared to the 250+ ‰ added under the effect of nitrate recycling at the air–snow interface, thereby erasing information on  $\delta^{15}\text{N(FT)}$  and  $\delta^{15}\text{N(FS)}$ .

## 4.2 Parameters and variables controlling $\Delta^{17}\text{O(FA)}$

The parameters and variables controlling  $\Delta^{17}\text{O(FA)}$  can be sorted in four groups:

- $f_{\text{cage}}$ , which controls the cage effects,
- those which impact FA/FPI, which sets the magnitude of loss and hence the magnitude of the cage effects,
- $\Delta^{17}\text{O(FT)}$  and  $\Delta^{17}\text{O(FS)}$ , which set  $\Delta^{17}\text{O}$  in the primary source of nitrate,

Title Page

Abstract

Introduction

Conclusions

References

Tables

Figures

|◀

▶|

◀

▶

Back

Close

Full Screen / Esc

Printer-friendly Version

Interactive Discussion



- $\Delta^{17}\text{O}(\text{O}_3)_{\text{bulk}}$ , [BrO], [HO<sub>2</sub>], [CH<sub>3</sub>O<sub>2</sub>], [O<sub>3</sub>] and  $T$  which set  $\Delta^{17}\text{O}$  in the secondary source of nitrate (i.e. NO<sub>2</sub> which is cycled in the atmosphere),  $\Delta^{17}\text{O}(\text{NO}_2)$ , PSS).

#### 4.2.1 Correction of the reduction in $\Delta^{17}\text{O}(\text{FA})$ imposed by cage effects

We have shown that cage recombination effects following nitrate photolysis in snow 5 lead to positive simulated  $\Delta^{17}\text{E}_{\text{app}}$  values in snow. For instance, for DC realistic conditions (i.e. for  $f_{\text{cage}} = 0.15$  and FA/FPI = 2.0 %),  $\Delta^{17}\text{O}(\text{FA})$  is reduced by  $\approx 7\%$  because of cage effects. To calculate the reduction in  $\Delta^{17}\text{O}(\text{FA})$  as a result of cage recombination effects, we have run TRANSITS in the DC realistic simulation by varying  $\phi$  from 10 0 to 0.036 and with an  $f_{\text{cage}}$  parameter set to 0 and 0.15 in order to switch the cage effects on and off, respectively.

We denote  $\Delta^{17}\text{O}(\text{FA, corr.})$ , the  $\Delta^{17}\text{O}(\text{FA})$  value corrected from cage effects, which was estimated here by setting  $f_{\text{cage}} = 0$ . Figure 11d shows that for  $\ln(\text{FA/FPI}) < -1.2$  (i.e., FA/FPI < 30 %), the  $\Delta^{17}\text{O}(\text{FA, corr.})/\Delta^{17}\text{O}(\text{FA})$  ratio is linear with  $\ln(\text{FA/FPI})$ :  $\Delta^{17}\text{O}(\text{FA, corr.})/\Delta^{17}\text{O}(\text{FA}) = -0.066 \times \ln(\text{FA/FPI}) + 1.076$ . In Sect. 4.1.6, we have shown 15 that the FA/FPI ratio can be retrieved from the measurement of  $\delta^{15}\text{N}(\text{FA})$  given an hypothesis on the O<sub>3</sub> column and  $\delta^{15}\text{N}(\text{FPI})$ .

From Fig. 11c, we observe that  $\Delta^{17}\text{O}(\text{FA, corr.})$  reaches a plateau at around 27 % for low nitrate trapping efficiencies ( $\ln(\text{FA/FPI}) < -3$ , i.e. FA/FPI < 5 %). Although we anticipate that,  $\Delta^{17}\text{O}(\text{FA, corr.})$  is mostly controlled by the local cycling of NO<sub>2</sub> (as 20 previously observed from sensitivity tests), there is still the need to separate the  $\Delta^{17}\text{O}$  impact of local cycling of NO<sub>2</sub> from those of  $\Delta^{17}\text{O}(\text{FT})$  and  $\Delta^{17}\text{O}(\text{FS})$ .

#### 4.2.2 Contributors to $\Delta^{17}\text{O}(\text{FA, corr.})$

In this section, we consider  $\Delta^{17}\text{O}(\text{FT})$ ,  $\Delta^{17}\text{O}(\text{FS})$ ,  $\Delta^{17}\text{O}(\text{NO}_2)$ , PSS. which impact 25  $\Delta^{17}\text{O}(\text{FA, corr.})$ . To determine the scaled contributions of the variable  $\underline{\Delta^{17}\text{O}(X)}$ , we have run the TRANSITS model with this variable set to 0. We denote  $\Delta^{17}\text{O}(\text{FA})$  the 6934

<a href="#">Title Page</a>	
<a href="#">Abstract</a>	<a href="#">Introduction</a>
<a href="#">Conclusions</a>	<a href="#">References</a>
<a href="#">Tables</a>	<a href="#">Figures</a>
<a href="#">◀</a>	<a href="#">▶</a>
<a href="#">◀</a>	<a href="#">▶</a>
<a href="#">Back</a>	<a href="#">Close</a>
<a href="#">Full Screen / Esc</a>	
<a href="#">Printer-friendly Version</a>	
<a href="#">Interactive Discussion</a>	



$\Delta^{17}\text{O}(\text{FA})$  value obtained when  $\Delta^{17}\text{O}(X)$  has been set to 0. From the previous section, we can calculate  $\Delta^{17}\text{O}(\text{FA, corr.})$  based on the computed FA/FPI value. For  $\Delta^{17}\text{O}(X)$ , we calculate the scaled contribution to  $\Delta^{17}\text{O}(\text{FA, corr.})$  as  $(\Delta^{17}\text{O}(\text{FA, corr.}) - \Delta^{17}\text{O}(\text{FA, corr.})) / \Delta^{17}\text{O}(X)$ .

Figure 11e shows the obtained scaled contributions to  $\Delta^{17}\text{O}(\text{FA, corr.})$ . For example, for  $\ln(\text{FA/FPI}) < -2$ , we observe that  $\Delta^{17}\text{O}(\text{NO}_2, \text{PSS})$  contributes to  $\Delta^{17}\text{O}(\text{FA, corr.})$  by 62 % of  $\Delta^{17}\text{O}(\text{NO}_2, \text{PSS})$ , which means that if  $\Delta^{17}\text{O}(\text{NO}_2, \text{PSS}) = 20\text{\textperthousand}$ , then this variable will contribute to  $\Delta^{17}\text{O}(\text{FA, corr.})$  by as much as  $0.62 \times 20 = 12.4\text{\textperthousand}$ . For the same nitrate trapping efficiency,  $\Delta^{17}\text{O}(\text{FT})$  contributes much less, i.e. by 16 % of  $\Delta^{17}\text{O}(\text{FT})$ , which is to say by 4.8 % for  $\Delta^{17}\text{O}(\text{FT}) = 30\text{\textperthousand}$ . From Fig. 11e, we observe that for  $\ln(\text{FA/FPI}) < -1.2$ , the scaled contributions of  $\Delta^{17}\text{O}(\text{NO}_2, \text{PSS})$  to  $\Delta^{17}\text{O}(\text{FA, corr.})$  is higher than 56 % of  $\Delta^{17}\text{O}(\text{NO}_2, \text{PSS})$ , i.e. more than twice the sum of those of  $\Delta^{17}\text{O}(\text{FT})$  (< 20 % of  $\Delta^{17}\text{O}(\text{FT})$ ) and  $\Delta^{17}\text{O}(\text{FS})$  (< 5 % of  $\Delta^{17}\text{O}(\text{FS})$ ). This means that, in the conditions tested (i.e. low trapping efficiencies which characterize the Antarctic plateau),  $\Delta^{17}\text{O}(\text{FA, corr.})$  is poorly controlled by  $\Delta^{17}\text{O}(\text{FS})$  and  $\Delta^{17}\text{O}(\text{FT})$  and dominated by local cycling of  $\text{NO}_2$ . We note that, for very low nitrate trapping efficiencies, the scaled contributions of  $\Delta^{17}\text{O}(\text{NO}_2, \text{PSS})$  and the sum of those of  $\Delta^{17}\text{O}(\text{FS})$  and  $\Delta^{17}\text{O}(\text{FT})$  reach plateaus at 65 % of  $\Delta^{17}\text{O}(\text{NO}_2, \text{PSS})$  and 22 % of  $\Delta^{17}\text{O}(\text{FS})$  and  $\Delta^{17}\text{O}(\text{FT})$ , respectively. From Fig. 11b, we observe that the plateaus are consistent with that of the ratio FD/FPI at a value of 4, i.e. the primary inputs of nitrate only annually contribute to 1/4 of the deposited flux, the rest being the deposition of locally recycled nitrate (secondary inputs of nitrate). This is consistent with the 3 : 1 ratio in the scaled contributions of  $\Delta^{17}\text{O}(\text{NO}_2, \text{PSS})$  and the sum of those of  $\Delta^{17}\text{O}(\text{FS})$  and  $\Delta^{17}\text{O}(\text{FT})$ .

For low nitrate trapping efficiencies, we also observe that the scaled contribution of  $\Delta^{17}\text{O}(\text{FT})$  increases while that of  $\Delta^{17}\text{O}(\text{FS})$  decreases. This is linked to the preferential incorporation of the local  $\Delta^{17}\text{O}$  signature on the summertime primary source of nitrate.

Figure 11f represents an application of what precedes in the case of Dome C, i.e. using  $\Delta^{17}\text{O}(\text{FT}) = 30\text{\textperthousand}$ ,  $\Delta^{17}\text{O}(\text{FS}) = 42\text{\textperthousand}$  and  $\Delta^{17}\text{O}(\text{NO}_2, \text{PSS}) = 31.3\text{\textperthousand}$ . Figure 11g

<a href="#">Title Page</a>	
<a href="#">Abstract</a>	<a href="#">Introduction</a>
<a href="#">Conclusions</a>	<a href="#">References</a>
<a href="#">Tables</a>	<a href="#">Figures</a>
<a href="#">◀</a>	<a href="#">▶</a>
<a href="#">◀</a>	<a href="#">▶</a>
<a href="#">Back</a>	<a href="#">Close</a>
<a href="#">Full Screen / Esc</a>	
<a href="#">Printer-friendly Version</a>	
<a href="#">Interactive Discussion</a>	



reproduces the relationship between  $\delta^{15}\text{N}(\text{FA})$  and FA/FPI as a function of ozone column. In the case of the present-day DC conditions (realistic DC O<sub>3</sub> column and  $\delta^{15}\text{N}(\text{FA}) = 287\text{\textperthousand}$ ), we find that the relative contribution of  $\Delta^{17}\text{O}(\text{NO}_2, \text{PSS})$ ,  $\Delta^{17}\text{O}(\text{FT})$  and  $\Delta^{17}\text{O}(\text{FS})$  to  $\Delta^{17}\text{O}(\text{FA, corr.})$  are 63, 27 and 10 %, respectively. In DC conditions,  $\Delta^{17}\text{O}(\text{FA, corr.})$  therefore harbors almost two third of the oxygen isotope signature of the local cycling of NO<sub>2</sub> and the remaining signature of primary inputs of nitrate is small. This is such because nitrate undergoes more than 150 cycles (defined as the ratio FP/FA) before being ultimately trapped in snow below the photic zone (Fig. 11a).

#### 4.2.3 Method to interpret $\Delta^{17}\text{O}(\text{FA, corr.})$ derived from ice cores measurements

From Sect. 4.1.6, we provided a framework for the interpretation of  $\omega$  (FA) and  $\delta^{15}\text{N}(\text{FA})$  which can be measured from ice cores. The variation in nitrate trapping efficiency (FA/FPI) could be determined from  $\delta^{15}\text{N}(\text{FA})$  and hypothesis on past variations in  $\delta^{15}\text{N}(\text{FPI})$  and in the ozone column (see also Fig. 12). Knowledge of the variations in nitrate trapping efficiency allows to determine the variations in the  $\Delta^{17}\text{O}(\text{FA, corr.})/\Delta^{17}\text{O}(\text{FA})$  ratio. Therefore, variations in  $\Delta^{17}\text{O}(\text{FA, corr.})$  can be retrieved from  $\Delta^{17}\text{O}(\text{FA})$  and the correction ratio. In this way, we obtain a time series of  $\Delta^{17}\text{O}(\text{FA, corr.})$  in the past, a variable which is only influenced by past changes in  $\Delta^{17}\text{O}(\text{NO}_2, \text{PSS})$ ,  $\Delta^{17}\text{O}(\text{FT})$  and  $\Delta^{17}\text{O}(\text{FS})$  and that of their scaled contributions.

To determine the variations in the scaled contributions of  $\Delta^{17}\text{O}(\text{NO}_2, \text{PSS})$ ,  $\Delta^{17}\text{O}(\text{FT})$  and  $\Delta^{17}\text{O}(\text{FS})$ , we use the nitrate trapping efficiency determined in Sect. 4.1.6. Assumptions or evidences on past changes in two of the three variable controlling  $\Delta^{17}\text{O}(\text{FA, corr.})$  (i.e.  $\Delta^{17}\text{O}(\text{NO}_2, \text{PSS})$ ,  $\Delta^{17}\text{O}(\text{FT})$  and  $\Delta^{17}\text{O}(\text{FS})$ ) allow to determine past changes in the last one. For instance, assuming that  $\Delta^{17}\text{O}(\text{FT})$  and  $\Delta^{17}\text{O}(\text{FS})$  have remained constant over time allows to determine past changes in the local cycling of NO<sub>2</sub> above the East Antarctic plateau.

<a href="#">Title Page</a>	
<a href="#">Abstract</a>	<a href="#">Introduction</a>
<a href="#">Conclusions</a>	<a href="#">References</a>
<a href="#">Tables</a>	<a href="#">Figures</a>
<a href="#"></a>	<a href="#"></a>
<a href="#"></a>	<a href="#"></a>
<a href="#">Full Screen / Esc</a>	
<a href="#">Printer-friendly Version</a>	
<a href="#">Interactive Discussion</a>	



Figure 12 gives a schematic of the method to determine  $\Delta^{17}\text{O}(\text{FA, corr.})$  as well as in the scaled contributions of  $\Delta^{17}\text{O}(\text{NO}_2, \text{PSS})$ ,  $\Delta^{17}\text{O}(\text{FT})$  and  $\Delta^{17}\text{O}(\text{FS})$  from the measurement of  $\omega$  (FA),  $\delta^{15}\text{N}(\text{FA})$  and  $\Delta^{17}\text{O}(\text{FA})$  in ice cores.

If we assume that modern conditions in East Antarctica have prevailed in the past,  
5 we anticipate from Fig. 11 that almost two third of the variations  $\Delta^{17}\text{O}(\text{FA, corr.})$  are the result of variations in  $\Delta^{17}\text{O}(\text{NO}_2, \text{PSS})$ . In this case, the potential for  $\Delta^{17}\text{O}(\text{FA, corr.})$  to trace past changes in atmospheric oxidation at the global scale is weak. However, we would have in this case a tool to document past changes in the local atmospheric oxidation above the East Antarctic plateau.

## 10 5 Summary and conclusions

The TRANSITS model is a conceptual, multi-layer, 1-D isotopic model which represents the air–snow transfer of nitrate and its isotopic composition on the Antarctic plateau at around a one-week time resolution. It rests on the conceptual model initially proposed by Davis et al. (2008) and on the fact that nitrate photolysis is the process dominating nitrate mass loss at the low accumulation sites which characterize the Antarctic plateau  
15 (Frey et al., 2013; Erbland et al., 2013). The particularity of TRANSITS is its representation of the isotopic composition of nitrate ( $\delta^{15}\text{N}$  and  $\Delta^{17}\text{O}$ ).

When using a realistic scenario representing the Dome C conditions, the model reproduces well the variations in concentrations and isotopic time series observed in the atmospheric and skin layer compartments. While the nitrogen isotope ratio is well reproduced by the model, the simulated  $\Delta^{17}\text{O}$  data in the air–snow interface are lower than the observations. This has been attributed to simplifications in the description of the local cycling and oxidation of  $\text{NO}_2$ . One consequence is that  $\Delta^{17}\text{O}$  values in the snowpack and in the archived nitrate are lower than the observations as well. However, cage recombination effects occurring in snow are well reproduced by the model as shown by the agreement between the simulated and observed values of the apparent fractionation constant ( ${}^{17}\text{E}_{\text{app}}$ ). The representation of nitrate diffusion within the  
20

[Title Page](#)

[Abstract](#)

[Introduction](#)

[Conclusions](#)

[References](#)

[Tables](#)

[Figures](#)

[◀](#)

[▶](#)

[◀](#)

[▶](#)

[Back](#)

[Close](#)

[Full Screen / Esc](#)

[Printer-friendly Version](#)

[Interactive Discussion](#)



snowpack allows simulating nitrate mass fraction and isotope depth profiles, which are consistent with observations. Under the DC realistic simulation conditions, the quantum yield ( $\phi = 0.026$ ) necessary to reproduce the observations transicts that nitrate lies in two different domains in or on the snow ice matrix (Meusinger et al., 2014). The comparison of the simulated and observed  $\text{NO}_2$  shows that the simulated  $\text{NO}_2$  flux is 9 to 18 times higher than the observed  $\text{NO}_2$  flux at Dome C in 2009–2010 and 2011–2012, which could be due to simplifying assumptions made in the model regarding the product of nitrate photolysis.

TRANSITS has been used to investigate the spatial variability in the mass and isotopic composition of the nitrate archived from the Antarctic coast to the plateau (Dome C to Vostok) obtained from 21 snow pits collected from 2007 to 2010 (Erbland et al., 2013). Using the realistic simulation and snow accumulation rates varying in a range observed on the zone of interest (from 20 to  $600 \text{ kg m}^{-2} \text{ a}^{-1}$ ), we have shown that, in present-day conditions, changes in snow accumulation rates are enough to explain the first order variations in the  $\delta^{15}\text{N}$  in the archived nitrate. This suggests that functioning principles at the base of the model (the principles of photolytic mass loss, isotopic fractionation and exposure time of nitrate) are realistic. Moreover, the use of a nitrate primary input flux of  $8.2 \times 10^{-6} \text{ kg N m}^{-2} \text{ a}^{-1}$  is consistent with the observations.

The model has shown a 21 years response time to changes in the primary input flux of nitrate, which could explain the difference between the observed and simulated nitrate mass in the top 50 cm of snow. Such a response time is the result of the important number of recycling cycles undergone by nitrate at the air–snow interface of DC (> 150 cycles). This effect must be taken into account for future analysis of firn and ice cores.

We propose some improvements and guidelines for future work on the TRANSITS model. For example, the model would benefit the measurement of  $\Delta^{17}\text{O}(\text{O}_3)_{\text{bulk}}$  on the East Antarctic plateau (Vicars and Savarino, 2014) as well as the measurement of  $\Delta^{17}\text{O}(\text{NO})$ ,  $\Delta^{17}\text{O}(\text{NO}_2)$  or  $\Delta^{17}\text{O}$  in other key species participating in the oxidation scheme ( $\text{HO}_2$ ,  $\text{RO}_2$ ,  $\text{BrO}$ ). Additional processes or mechanisms could be implemented, such as nitrate pools featuring different photolytic availabilities that could be modeled

<a href="#">Title Page</a>	
<a href="#">Abstract</a>	<a href="#">Introduction</a>
<a href="#">Conclusions</a>	<a href="#">References</a>
<a href="#">Tables</a>	<a href="#">Figures</a>
<a href="#">◀</a>	<a href="#">▶</a>
<a href="#">◀</a>	<a href="#">▶</a>
<a href="#">Back</a>	<a href="#">Close</a>
<a href="#">Full Screen / Esc</a>	
<a href="#">Printer-friendly Version</a>	
<a href="#">Interactive Discussion</a>	



using a quantum yield which would vary with space and time. Some additional parameters could also be taken into account such as the latitude of the simulated site to better represent plateau sites other than Dome C. The radiative transfer model TARTES (Lobois et al., 2013) could be explicitly incorporated into TRANSITS. This would allow the modeling of the e-folding attenuation depth dependence to the vertical profile of the physical properties and the impurity content of the snowpack. The explicit representation of the export and depositions fluxes (using horizontal and vertical air mass velocities, respectively) could be also explored.

A framework for the interpretation of nitrate isotope records in ice cores has been proposed. From ice cores, the following data are measurable:  $\omega$  (FA),  $\delta^{15}\text{N}(\text{FA})$  and  $\Delta^{17}\text{O}(\text{FA})$ . The interpretation framework described in this paper will be applicable to ice core records which display proofs of significant nitrate recycling, e. g. on the basis of elevated  $\delta^{15}\text{N}(\text{FA})$  values. In this case, sensitivity tests have shown that  $\delta^{15}\text{N}(\text{FA})$  is the result of a  $^{15}\text{N}/^{14}\text{N}$  fractionation constant which is set by the spectral repartition of the UV radiation (i.e. set by the ozone column above the site of interest). Indeed, the ozone column controls the slope in the “modified Rayleigh plot” introduced in this study. At a given ozone column,  $\delta^{15}\text{N}(\text{FA})$  is at last controlled by the nitrate trapping efficiency (i.e. the ratio of the archived flux vs. the primary nitrate inputs, FA/FPI) which is determined by the exposure time of nitrate and the intensity of nitrate recycling, and the  $\delta^{15}\text{N}$  in the primary inputs of nitrate whose variations are negligible when compared to the  $\delta^{15}\text{N}$  imprinted by nitrate recycling. We have observed that the major controls on FA/FPI are the photolytic quantum yield ( $\phi$ ), the annual snow accumulation rate ( $A$ ), the snow density ( $\rho$ ), the photic zone compression factor ( $k$ ) and the actinic flux enhancement factor ( $q$ ), with equivalent relative impacts.

Given a constant spectral repartition of the actinic flux, the archived flux (FA) is primarily controlled by the primary input flux and the trapping efficiency. Therefore, the (FA,  $\delta^{15}\text{N}(\text{FA})$ ) couples plotted in the modified Rayleigh plot are good candidates to track modern or past changes in the spectral distribution of the UV received at ground, i.e. changes in the ozone column but also changes in the solar UV spectra. At a given

[Title Page](#)[Abstract](#)[Introduction](#)[Conclusions](#)[References](#)[Tables](#)[Figures](#)[|◀](#)[▶|](#)[◀](#)[▶](#)[Back](#)[Close](#)[Full Screen / Esc](#)[Printer-friendly Version](#)[Interactive Discussion](#)

spectral distribution of the actinic flux, past variations in FPI can be reconstructed from (FA,  $\delta^{15}\text{N}(\text{FA})$ ) data and an assumption on variations in  $\delta^{15}\text{N}(\text{FPI})$ .

From the nitrate trapping efficiency (FA/FPI), we have shown that we can deduce  $\Delta^{17}\text{O}(\text{FA, corr.})$  which represents the  $\Delta^{17}\text{O}$  value in the archived flux corrected from the cage recombination effects. The variable  $\Delta^{17}\text{O}(\text{FA, corr.})$  is controlled by  $\Delta^{17}\text{O}(\text{NO}_2, \text{PSS})$ ,  $\Delta^{17}\text{O}(\text{FT})$  and  $\Delta^{17}\text{O}(\text{FS})$  and the scaled contributions of each of these three variable has been determined as a function of FA/FPI. We have shown that these contributions are independent of the ozone column. Under the modern DC conditions, we have shown that 63, 27 and 10 % of  $\Delta^{17}\text{O}(\text{FA, corr.})$  are due to  $\Delta^{17}\text{O}(\text{NO}_2, \text{PSS})$ ,  $\Delta^{17}\text{O}(\text{FT})$  and  $\Delta^{17}\text{O}(\text{FS})$ , respectively. These are the result of the important number of recycling cycles undergone by nitrate at the air–snow interface. Therefore, if the modern DC conditions applied in the past as well, the determination of  $\Delta^{17}\text{O}(\text{FA, corr.})$  from ice cores drilled on the East Antarctic plateau are expected to deliver mostly information about the local oxidative chemistry.

**Acknowledgements.** This research has received the financial support of the Agence Nationale de la Recherche (ANR), through the VANISH (contract ANR-07-VULN-013) and OPALE (contract ANR-09-BLAN-0226) projects (J. Erblanc, J. Savarino). J. L. France and M. D. King gratefully acknowledge NERC for support through grants NE/F0004796/1 and NE/F010788, NERC FSF for support and expertise through grants 555.0608 and 584.0609 and Royal Holloway Earth Sciences research strategy fund awards. Partial funding has also been received from LICENCE (LEFE-CHAT), a scientific program of the Institut National des Sciences de l'Univers (INSU/CNRS), as well as from the IPICS program (CNRS) and from IPEV (program NITEDC – 1011) (J. Erblanc, J. Savarino). LGGE and CNRM-GAME/CEN are part of LabEx OSUG@2020 (ANR10 LABX56). We thank F. Dominé, G. Picard and D. Voisin for helpful discussions on light penetration in snow and modeling. The authors are grateful to C. Carmagnola, G. Picard, F. Dupont and N. Champollion who shared their knowledge on Python. J. Erblanc thanks G. Krinner and S. Parouty for providing the snow accumulation data used in this work. Last, we thank the overwintering people, S. Lafont, I. Bourgeois, S. Aubin, A. Barbero and C. Lenormant, for the samples collection at Concordia – Dome C from 2010 to 2013.

<a href="#">Title Page</a>	
<a href="#">Abstract</a>	<a href="#">Introduction</a>
<a href="#">Conclusions</a>	<a href="#">References</a>
<a href="#">Tables</a>	<a href="#">Figures</a>
<a href="#">◀</a>	<a href="#">▶</a>
<a href="#">◀</a>	<a href="#">▶</a>
<a href="#">Back</a>	<a href="#">Close</a>
<a href="#">Full Screen / Esc</a>	
<a href="#">Printer-friendly Version</a>	
<a href="#">Interactive Discussion</a>	



## References

- Alexander, B., Hastings, M. G., Allman, D. J., Dachs, J., Thornton, J. A., and Kunasek, S. A.: Quantifying atmospheric nitrate formation pathways based on a global model of the oxygen isotopic composition ( $\Delta^{17}\text{O}$ ) of atmospheric nitrate, *Atmos. Chem. Phys.*, 9, 5043–5056, doi:10.5194/acp-9-5043-2009, 2009.
- Atkinson, R., Baulch, D. L., Cox, R. A., Crowley, J. N., Hampson, R. F., Hynes, R. G., Jenkin, M. E., Rossi, M. J., and Troe, J.: Evaluated kinetic and photochemical data for atmospheric chemistry: Volume I – gas phase reactions of  $\text{O}_x$ ,  $\text{HO}_x$ ,  $\text{NO}_x$  and  $\text{SO}_x$  species, *Atmos. Chem. Phys.*, 4, 1461–1738, doi:10.5194/acp-4-1461-2004, 2004.
- Atkinson, R., Baulch, D. L., Cox, R. A., Crowley, J. N., Hampson, R. F., Hynes, R. G., Jenkin, M. E., Rossi, M. J., Troe, J., and IUPAC Subcommittee: Evaluated kinetic and photochemical data for atmospheric chemistry: Volume II – gas phase reactions of organic species, *Atmos. Chem. Phys.*, 6, 3625–4055, doi:10.5194/acp-6-3625-2006, 2006.
- Atkinson, R., Baulch, D. L., Cox, R. A., Crowley, J. N., Hampson, R. F., Hynes, R. G., Jenkin, M. E., Rossi, M. J., and Troe, J.: Evaluated kinetic and photochemical data for atmospheric chemistry: Volume III – gas phase reactions of inorganic halogens, *Atmos. Chem. Phys.*, 7, 981–1191, doi:10.5194/acp-7-981-2007, 2007.
- Berhanu, T. A., Meusinger, C., Erbland, J., Jost, R., Bhattacharya, S. K., Johnson, M. S., and Savarino, J.: Laboratory study of nitrate photolysis in Antarctic snow. II. Isotope effects and wavelength dependence, *J. Chem. Phys.*, 140, 244306, doi:10.1063/1.4882899, 2014a.
- Berhanu, T. A., Savarino, J., Erbland, J., Vicars, W. C., Preunkert, S., Martins, J. F., and Johnson, M. S.: Isotopic effects of nitrate photochemistry in snow: a field study at Dome C, Antarctica, *Atmos. Chem. Phys. Discuss.*, 14, 33045–33088, doi:10.5194/acpd-14-33045-2014, 2014b.
- Blunier, T., Floch, G. L., Jacobi, H.-W., and Quansah, E.: Isotopic view on nitrate loss in Antarctic surface snow, *Geophys. Res. Lett.*, 32, L13501, doi:10.1029/2005GL023011, 2005.
- Boxe, C. S. and Saiz-Lopez, A.: Multiphase modeling of nitrate photochemistry in the quasi-liquid layer (QLL): implications for  $\text{NO}_x$  release from the Arctic and coastal Antarctic snowpack, *Atmos. Chem. Phys.*, 8, 4855–4864, doi:10.5194/acp-8-4855-2008, 2008.
- Brizzi, G., Arnone, E., Carlotti, M., Dinelli, B. M., Flaud, J.-M., Papandrea, E., Pererin, A., and Ridolfi, M.: Retrieval of atmospheric  $\text{H}^{15}\text{NO}_3/\text{H}^{14}\text{NO}_3$  isotope ratio profile

[Title Page](#)[Abstract](#)[Introduction](#)[Conclusions](#)[References](#)[Tables](#)[Figures](#)[◀](#)[▶](#)[◀](#)[▶](#)[Back](#)[Close](#)[Full Screen / Esc](#)[Printer-friendly Version](#)[Interactive Discussion](#)

from MIPAS/ENVISAT limb-scanning measurements, *J. Geophys. Res.*, 114, D16301, doi:10.1029/2008JD011504, 2009.

Chance, K. and Kurucz, R. L.: An improved high-resolution solar reference spectrum for Earth's atmosphere measurements in the ultraviolet, visible, and near infrared, *J. Quant. Spectrosc. Ra.*, 111, 1289–1295, 2010.

Chu, L. and Anastasio, C.: Quantum yields of hydroxyl radical and nitrogen dioxide from the photolysis of nitrate on ice, *J. Phys. Chem. A*, 107, 9594–9602, 2003.

Chu, L. and Anastasio, C.: Temperature and wavelength dependence of nitrite photolysis in frozen and aqueous solutions, *Environ. Sci. Technol.*, 41, 3626–3632, 2007.

Davis, D. D., Seelig, J., Huey, G., Crawford, J., Chen, G., Wang, Y., Buhr, M., Helmig, D., Neff, W., Arimoto, D. B. R., and Eisele, F.: A reassessment of Antarctic plateau reactive nitrogen based on ANTCI 2003 airborne and ground based measurements, *Atmos. Environ.*, 42, 2831–2848, doi:10.1016/j.atmosenv.2007.07.039, 2008.

Dominé, F. and Shepson, P. B.: Air–snow interactions and atmospheric chemistry, *Science*, 297, 1506–1510, 2002.

Dominé, F., Taillandier, A.-S., Houdier, S., Parrenin, F., Simpson, W. R., and Douglas, T. A.: Interactions between snow metamorphism and climate physical and chemical aspects, in: *Physics and Chemistry of Ice*, edited by: Kuhs, W. F., Royal Society of Chemistry, Cambridge, UK, 27–46, 2007.

Domine, F., Albert, M., Huthwelker, T., Jacobi, H.-W., Kokhanovsky, A. A., Lehning, M., Picard, G., and Simpson, W. R.: Snow physics as relevant to snow photochemistry, *Atmos. Chem. Phys.*, 8, 171–208, doi:10.5194/acp-8-171-2008, 2008.

EPICA community members: Eight glacial cycles from an Antarctic ice core, *Nature*, 429, 623–628, doi:10.1038/nature02599, 2004.

Erbländ, J., Vicars, W. C., Savarino, J., Morin, S., Frey, M. M., Frosini, D., Vince, E., and Martins, J. M. F.: Air–snow transfer of nitrate on the East Antarctic Plateau – Part 1: Isotopic evidence for a photolytically driven dynamic equilibrium in summer, *Atmos. Chem. Phys.*, 13, 6403–6419, doi:10.5194/acp-13-6403-2013, 2013.

France, J. L., King, M. D., Frey, M. M., Erbländ, J., Picard, G., Preunkert, S., MacArthur, A., and Savarino, J.: Snow optical properties at Dome C (Concordia), Antarctica; implications for snow emissions and snow chemistry of reactive nitrogen, *Atmos. Chem. Phys.*, 11, 9787–9801, doi:10.5194/acp-11-9787-2011, 2011.

[Title Page](#)

[Abstract](#)

[Introduction](#)

[Conclusions](#)

[References](#)

[Tables](#)

[Figures](#)

◀

▶

◀

▶

[Back](#)

[Close](#)

[Full Screen / Esc](#)

[Printer-friendly Version](#)

[Interactive Discussion](#)



## Air–snow transfer of nitrate on the East Antarctic plateau

J. Erbland et al.

- Frey, M. M., Savarino, J., Morin, S., Erbland, J., and Martins, J. M. F.: Photolysis imprint in the nitrate stable isotope signal in snow and atmosphere of East Antarctica and implications for reactive nitrogen cycling, *Atmos. Chem. Phys.*, 9, 8681–8696, doi:10.5194/acp-9-8681-2009, 2009.
- 5 Frey, M. M., Brough, N., France, J. L., Anderson, P. S., Traulle, O., King, M. D., Jones, A. E., Wolff, E. W., and Savarino, J.: The diurnal variability of atmospheric nitrogen oxides (NO and NO<sub>2</sub>) above the Antarctic Plateau driven by atmospheric stability and snow emissions, *Atmos. Chem. Phys.*, 13, 3045–3062, doi:10.5194/acp-13-3045-2013, 2013.
- 10 Frey, M. M., Roscoe, H. K., Kukui, A., Savarino, J., France, J. L., King, M. D., Legrand, M., and Preunkert, S.: Atmospheric nitrogen oxides (NO and NO<sub>2</sub>) at Dome C, East Antarctica, during the OPALe campaign, *Atmos. Chem. Phys. Discuss.*, 14, 31281–31317, doi:10.5194/acpd-14-31281-2014, 2014.
- Freyer, H. D., Kobel, K., Delmas, R. J., Kley, D., and Legrand, M. R.: First results of <sup>15</sup>N/<sup>14</sup>N ratios in nitrate from alpine and polar ice cores, *Tellus B*, 48, 93–105, 1996.
- 15 Frezzotti, M., Pourchet, M., Flora, O., Gandolfi, S., Gay, M., Urbini, S., Vincent, C., Becagli, S., Gragnani, R., Proposito, M., Severi, M., Traversi, R., Udisti, R., and Fily, M.: New estimations of precipitation and surface sublimation in East Antarctica from snow accumulation measurements, *Clim. Dynam.*, 23, 803–813, doi:10.1007/s00382-004-0462-5, 2004.
- Gallée, H., Preunkert, S., Argentini, S., Frey, M. M., Genthon, C., Jourdain, B., Pietroni, I., Casasanta, G., Barral, H., Vignon, E., and Legrand, M.: Characterization of the boundary layer at Dome C (East Antarctica) during the OPALe summer campaign, *Atmos. Chem. Phys. Discuss.*, 14, 33089–33116, doi:10.5194/acpd-14-33089-2014, 2014.
- 20 Grannas, A. M., Jones, A. E., Dibb, J., Ammann, M., Anastasio, C., Beine, H. J., Bergin, M., Bottenheim, J., Boxe, C. S., Carver, G., Chen, G., Crawford, J. H., Dominé, F., Frey, M. M., Guzmán, M. I., Heard, D. E., Helmig, D., Hoffmann, M. R., Honrath, R. E., Huey, L. G., Hutterli, M., Jacobi, H. W., Klán, P., Lefer, B., McConnell, J., Plane, J., Sander, R., Savarino, J., Shepson, P. B., Simpson, W. R., Sodeau, J. R., von Glasow, R., Weller, R., Wolff, E. W., and Zhu, T.: An overview of snow photochemistry: evidence, mechanisms and impacts, *Atmos. Chem. Phys.*, 7, 4329–4373, doi:10.5194/acp-7-4329-2007, 2007.
- 25 Hastings, M. G., Sigman, D. M., and Steig, E. J.: Glacial/Interglacial changes in the isotopes of nitrate from the GISP2 ice core, *Global Biogeochem. Cy.*, 19, GB4024, doi:10.1029/2005GB002502, 2005.

<a href="#">Title Page</a>	
<a href="#">Abstract</a>	<a href="#">Introduction</a>
<a href="#">Conclusions</a>	<a href="#">References</a>
<a href="#">Tables</a>	<a href="#">Figures</a>
<a href="#">◀</a>	<a href="#">▶</a>
<a href="#">◀</a>	<a href="#">▶</a>
<a href="#">Back</a>	<a href="#">Close</a>
<a href="#">Full Screen / Esc</a>	
<a href="#">Printer-friendly Version</a>	
<a href="#">Interactive Discussion</a>	



- Huey, L. G., Tanner, D. J., Slusher, D. L., Dibb, J. E., Arimoto, R., Chen, G., Davis, D., Buhr, M. P., Nowak, J. B., Mauldin III, R. L., Eisele, F. L., and Kosciuch, E.: CIMS measurements of  $\text{HNO}_3$  and  $\text{SO}_2$  at the South Pole during ICAT 2000, *Atmos. Environ.*, 38, 5411–5421, doi:10.1016/j.atmosenv.2004.04.037, 2004.
- 5 Jacob, D. J.: *Introduction to Atmospheric Chemistry*, Princeton University Press, Princeton, NJ, USA, 1999.
- Jarvis, J. C., Steig, E. J., Hastings, M. G., and Kunasek, S. A.: Influence of local photochemistry on isotopes of nitrate in Greenland snow, *Geophys. Res. Lett.*, 35, L21804, doi:10.1029/2008GL035551, 2008.
- 10 Jarvis, J. C., Hastings, M. G., Steig, E. J., and Kunasek, S. A.: Isotopic ratios in gas-phase  $\text{HNO}_3$  and snow nitrate at Summit, Greenland, *J. Geophys. Res.*, 114, D17301, doi:10.1029/2009JD012134, 2009.
- Kaempfer, T. U. and Plapp, M.: Phase-field modeling of dry snow metamorphism, *Phys. Rev. E*, 79, 031502, doi:10.1103/PhysRevE.79.031502, 2009.
- 15 King, M. D. and Simpson, W. R.: Extinction of UV radiation in Arctic snow at Alert, Canada ( $82^\circ\text{N}$ ), *J. Geophys. Res.*, 106, 12499–12507, 2001.
- Kukui, A., Legrand, M., Preunkert, S., Frey, M. M., Loisil, R., Gil Roca, J., Jourdain, B., King, M. D., France, J. L., and Ancellet, G.: Measurements of OH and  $\text{RO}_2$  radicals at Dome C, East Antarctica, *Atmos. Chem. Phys.*, 14, 12373–12392, doi:10.5194/acp-14-12373-2014, 2014.
- 20 Kunasek, S. A., Alexander, B., Steig, E. J., Hastings, M. G., Gleason, D. J., and Jarvis, J. C.: Measurements and modeling of  $\Delta^{17}\text{O}$  of nitrate in snowpits from Summit, Greenland, *J. Geophys. Res.*, 113, D24302, doi:10.1029/2008JD010103, 2008.
- Lee-Taylor, J. and Madronich, S.: Calculation of actinic fluxes with a coupled atmosphere–snow radiative transfer model, *J. Geophys. Res.*, 107, 4796, doi:10.1029/2002JD002084, 2002.
- 25 Legrand, M. R. and Delmas, R. J.: Relative contributions of tropospheric and stratospheric sources to nitrate in Antarctic snow, *Tellus B*, 38, 236–249, 1986.
- Legrand, M. R. and Kirchner, S.: Origins and variations of nitrate in South Polar precipitation, *J. Geophys. Res.*, 95, 3493–3507, 1990.
- 30 Legrand, M., Preunkert, S., Jourdain, B., Galle, H., Goutail, F., Weller, R., and Savarino, J.: Year-round record of surface ozone at coastal (Dumont d'Urville) and inland (Concordia) sites in East Antarctica, *J. Geophys. Res.-Atmos.*, 114, D20306, doi:10.1029/2008JD011667, 2009.

[Title Page](#)[Abstract](#)[Introduction](#)[Conclusions](#)[References](#)[Tables](#)[Figures](#)[◀](#)[▶](#)[◀](#)[▶](#)[Back](#)[Close](#)[Full Screen / Esc](#)[Printer-friendly Version](#)[Interactive Discussion](#)

## Air–snow transfer of nitrate on the East Antarctic plateau

J. Erbland et al.

[Title Page](#)

[Abstract](#)

[Introduction](#)

[Conclusions](#)

[References](#)

[Tables](#)

[Figures](#)

[◀](#)

[▶](#)

[◀](#)

[▶](#)

[Back](#)

[Close](#)

[Full Screen / Esc](#)

[Printer-friendly Version](#)

[Interactive Discussion](#)



- Liao, W. and Tan, D.: 1-D Air-snowpack modeling of atmospheric nitrous acid at South Pole during ANTCI 2003, *Atmos. Chem. Phys.*, 8, 7087–7099, doi:10.5194/acp-8-7087-2008, 2008.
- Libois, Q., Picard, G., France, J. L., Arnaud, L., Dumont, M., Carmagnola, C. M., and King, M. D.: Influence of grain shape on light penetration in snow, *The Cryosphere*, 7, 1803–1818, doi:10.5194/tc-7-1803-2013, 2013.
- 5 Libois, Q., Picard, G., Arnaud, L., Morin, S., and Brun, E.: Modeling the impact of snow drift on the decameter-scale variability of snow properties on the Antarctic Plateau, *J. Geophys. Res. Atmos.*, 119, 11662–11681, doi:10.1002/2014JD022361, 2014.
- McCabe, J. R., Boxe, C. S., Colussi, A. J., Hoffman, M. R., and Thiemens, M. H.: Oxygen isotopic fractionation in the photochemistry of nitrate in water and ice, *J. Geophys. Res.*, 110, D15310, doi:10.1029/2004JD005484, 2005.
- 10 McCabe, J. R., Thiemens, M. H., and Savarino, J.: A record of ozone variability in South Pole Antarctic snow: the role of nitrate oxygen isotopes, *J. Geophys. Res.*, 112, D12303, doi:10.1029/2006JD007822, 2007.
- 15 Meusinger, C., Berhanu, T. A., Erbland, J., Savarino, J., and Johnson, M. S.: Laboratory study of nitrate photolysis in Antarctic snow. I. Observed quantum yield, domain of photolysis, and secondary chemistry, *J. Chem. Phys.*, 140, 244–305, doi:10.1063/1.4882898, 2014.
- Michalski, G., Scott, Z., Kabiling, M., and Thiemens, M. H.: First measurements and modeling of  $\Delta^{17}\text{O}$  in atmospheric nitrate, *Geophys. Res. Lett.*, 30, 1870, doi:10.1029/2003GL017015, 2003.
- 20 Morin, S., Savarino, J., Bekki, S., Gong, S., and Bottenheim, J. W.: Signature of Arctic surface ozone depletion events in the isotope anomaly ( $\Delta^{17}\text{O}$ ) of atmospheric nitrate, *Atmos. Chem. Phys.*, 7, 1451–1469, doi:10.5194/acp-7-1451-2007, 2007.
- Morin, S., Savarino, J., Frey, M. M., Yan, N., Bekki, S., Bottenheim, J. W., and Martins, J. M. F.: 25 Tracing the origin and fate of  $\text{NO}_x$  in the Arctic atmosphere using stable isotopes in nitrate, *Science*, 322, 730–732, doi:10.1126/science.1161910, 2008.
- Morin, S., Savarino, J., Frey, M. M., Dominé, F., Jacobi, H. W., Kaleschke, L., and Martins, J. M. F.: Comprehensive isotopic composition of atmospheric nitrate in the Atlantic Ocean boundary layer from 65°S to 79°N, *J. Geophys. Res.*, 114, D05303, doi:10.1029/2008JD010696, 2009.
- 30 Morin, S., Sander, R., and Savarino, J.: Simulation of the diurnal variations of the oxygen isotope anomaly ( $\Delta^{17}\text{O}$ ) of reactive atmospheric species, *Atmos. Chem. Phys.*, 11, 3653–3671, doi:10.5194/acp-11-3653-2011, 2011.

## Air–snow transfer of nitrate on the East Antarctic plateau

J. Erbland et al.

- Muscaria, G. and de Zafra, R. L.: Evolution of the  $\text{NO}_y\text{-N}_2\text{O}$  correlation in the Antarctic stratosphere during 1993 and 1995, *J. Geophys. Res.*, 108, 4428, doi:10.1029/2002JD002871, 2003.
- Röhlisberger, R., Hutterli, M. A., Sommer, S., Wolff, E. W., and Mulvaney, R.: Factors controlling nitrate in ice-cores: evidence from the Dome C deep ice core, *J. Geophys. Res.*, 105, 20565–20572, 2000.
- Savarino, J., Kaiser, J., Morin, S., Sigman, D. M., and Thiemens, M. H.: Nitrogen and oxygen isotopic constraints on the origin of atmospheric nitrate in coastal Antarctica, *Atmos. Chem. Phys.*, 7, 1925–1945, doi:10.5194/acp-7-1925-2007, 2007.
- Savarino, J., Bhattacharya, S. K., Morin, S., Baroni, M., and Doussin, J.-F.: The  $\text{NO} + \text{O}_3$  reaction: a triple oxygen isotope perspective on the reaction dynamics and atmospheric implications for the transfer of the ozone isotope anomaly, *J. Chem. Phys.*, 128, 194–303, doi:10.1063/1.2917581, 2008.
- Scharko, N. K., Berke, A. E., and Raff, J. D.: Release of nitrous acid and nitrogen dioxide from nitrate photolysis in acidic aqueous solutions, *Environ. Sci. Technol.*, 48, 11991–12001, doi:10.1021/es503088x, 2014.
- Seinfeld, J. and Pandis, S.: *Atmospheric Chemistry and Physics*, Wiley Interscience, New York, 1998.
- Swain, M. R. and Gallée, H.: Antarctic boundary layer seeing, *Publ. Astron. Soc. Pac.*, 118, 1190–1197, 2006.
- Thibert, E. and Dominé, F.: Thermodynamics and kinetics of the solid solution of  $\text{HNO}_3$  in ice, *J. Phys. Chem. B*, 102, 4432–4439, 1998.
- Thomas, J. L., Stutz, J., Lefer, B., Huey, L. G., Toyota, K., Dibb, J. E., and von Glasow, R.: Modeling chemistry in and above snow at Summit, Greenland – Part 1: Model description and results, *Atmos. Chem. Phys.*, 11, 4899–4914, doi:10.5194/acp-11-4899-2011, 2011.
- Traversi, R., Udisti, R., Frosini, D., Becagli, S., Ciardini, V., Funke, B., Lanconelli, C., Petkov, B., Scarchilli, C., Severi, M., and Vitale, V.: Insights on nitrate sources at Dome C (East Antarctic Plateau) from multi-year aerosol and snow records, *Tellus B*, 66, 22550, doi:10.3402/tellusb.v66.22550, 2014.
- Vicars, W. C. and Savarino, J.: Quantitative constraints on the  $^{17}\text{O}$ -excess ( $\Delta^{17}\text{O}$ ) signature of surface ozone: ambient measurements from 50° N to 50° S using the nitrite-coated filter technique, *Geochim. Cosmochim. Ac.*, 135, 270–287, doi:10.1016/j.gca.2014.03.023, 2014.

[Title Page](#)

[Abstract](#)

[Introduction](#)

[Conclusions](#)

[References](#)

[Tables](#)

[Figures](#)

◀

▶

◀

▶

[Back](#)

[Close](#)

[Full Screen / Esc](#)

[Printer-friendly Version](#)

[Interactive Discussion](#)



**Air–snow transfer of nitrate on the East Antarctic plateau**

J. Erbland et al.

Wagenbach, D., Graf, W., Minikin, A., Trefzer, U., Kipfstuhl, J., Oerter, H., and Blindow, N.: Reconnaissance of chemical and isotopic firn properties on top of Berkner Island, Antarctica, *Ann. Glaciol.*, 20, 307–312, 1994.

5 Wang, Y., Choi, Y., Zeng, T., Davis, D., Buhr, M., Huey, L. G., and Neff, W.: Assessing the photochemical impact of snow NO<sub>x</sub> emissions over Antarctica during ANTCI 2003, *Atmos. Environ.*, 41, 3944–3958, doi:10.1016/j.atmosenv.2007.01.056, 2007.

Wolff, E.: Ice core studies of global biogeochemical cycles, chap. Nitrate in Polar Ice, Springer-Verlag, New York, 195–224, 1995.

10 Wolff, E. W., Jones, A. E., Martin, T. J., and Grenfell, T. C.: Modelling photochemical NO<sub>x</sub> production and nitrate loss in the upper snowpack of Antarctica, *Geophys. Res. Lett.*, 29, 1944, doi:10.1029/2002GL015823, 2002.

15 Wolff, E. W., Jones, A. E., Bauguitte, S. J.-B., and Salmon, R. A.: The interpretation of spikes and trends in concentration of nitrate in polar ice cores, based on evidence from snow and atmospheric measurements, *Atmos. Chem. Phys.*, 8, 5627–5634, doi:10.5194/acp-8-5627-2008, 2008.

20 Wolff, E. W., Barbante, C., Becagli, S., Bigler, M., Boutron, C. F., Castellano, E., de Angelis, M., Federer, U., Fischer, H., Fundel, F., Hansson, M., Hutterli, M., Jonsell, U., Karlin, T., Kaufmann, P., Lambert, F., Littot, G. C., Mulvaney, R., Röhlisberger, R., Ruth, U., Severi, M., Siggaard-Andersen, M. L., Sime, L. C., Steffensen, J. P., Stocker, T. F., Traversi, R., Twarloh, B., Udisti, R., Wagenbach, D., and Wegner, A.: Changes in environment over the last 800000 years from chemical analysis of the EPICA Dome C ice core, *Quaternary Sci. Rev.*, 29, 285–295, doi:10.1016/j.quascirev.2009.06.013, 2010.

25 Zatko, M. C., Grenfell, T. C., Alexander, B., Doherty, S. J., Thomas, J. L., and Yang, X.: The influence of snow grain size and impurities on the vertical profiles of actinic flux and associated NO<sub>x</sub> emissions on the Antarctic and Greenland ice sheets, *Atmos. Chem. Phys.*, 13, 3547–3567, doi:10.5194/acp-13-3547-2013, 2013.

[Title Page](#)[Abstract](#)[Introduction](#)[Conclusions](#)[References](#)[Tables](#)[Figures](#)[Back](#)[Close](#)[Full Screen / Esc](#)[Printer-friendly Version](#)[Interactive Discussion](#)

**Table 1.** List of the acronyms used in this paper.

Compartment	Acronym	Definition
Atmosphere	FS	Stratospheric input flux
	FT	Tropospheric input flux
	FPI	Primary input flux ( $FPI = FS + FT$ )
	FE	Exported flux ( $FE = FPI - FA$ )
	FA	Archived flux
	FD	Deposited flux
	FP	Photolytic flux
	$\delta^{15}\text{N}(FX)$	$\delta^{15}\text{N}$ in flux FX
	$\Delta^{17}\text{O}(FX)$	$\Delta^{17}\text{O}$ in flux FX
	$\gamma(\text{NO}_3^-)$	Atmospheric nitrate concentration
	$h_{\text{AT}}$	Height of the ABL
	$f_{\text{exp}}$	Exported fraction of the incoming fluxes to the atmospheric box
	$T$	Near ground atmospheric temperature
	$P$	Near ground atmospheric pressure
	${}^{15}\varepsilon_{\text{dep}}$	${}^{15}\text{N}/{}^{14}\text{N}$ fractionation constant associated with nitrate deposition
	$J(\text{NO}_2)$	Photolytic rate constant of $\text{NO}_2$
	$\alpha$	Leighton cycle perturbation factor
	$\Delta^{17}\text{O}(\text{O}_3)_{\text{bulk}}$	${}^{17}\text{O}$ -excess in bulk ozone
	$\theta$	Solar zenith angle
	$I$	Actinic flux
	$q$	Actinic flux enhancement factor
Snow	$A$	Annual snow accumulation rate
	$\rho$	Snow density
	$f_{\text{cage}}$	Cage effect factor
	$D$	Diffusion coefficient
	$\omega(\text{NO}_3^-)$	Nitrate mass fraction
	$m_{50\text{cm}}(\text{NO}_3^-)$	Nitrate mass fraction in the top 50 cm
	$\Delta^{17}\text{O}(50\text{cm})$	$\Delta^{17}\text{O}$ in the top 50 cm
	$\delta^{15}\text{N}(50\text{cm})$	$\delta^{15}\text{N}$ in the top 50 cm
	$\phi$	Quantum yield in nitrate photolysis
	$\sigma$	Absorption cross section of ${}^{14}\text{NO}_3^-$
	$\sigma'$	Absorption cross section of ${}^{15}\text{NO}_3^-$
	$k$	Photic zone compression factor
	$J$	Photolytic rate constant of ${}^{14}\text{NO}_3^-$
	$J'$	Photolytic rate constant of ${}^{15}\text{NO}_3^-$
	$\eta$	E-folding attenuation depth
	${}^{15}\varepsilon_{\text{app}}$	Apparent ${}^{15}\text{N}/{}^{14}\text{N}$ fractionation constant
	${}^{17}\varepsilon_{\text{app}}$	${}^{17}\text{O}$ -excess apparent fractionation constant
	${}^{15}\varepsilon_{\text{pho}}$	${}^{15}\text{N}/{}^{14}\text{N}$ fractionation constant associated with nitrate photolysis

## Air–snow transfer of nitrate on the East Antarctic plateau

J. Erbland et al.

Title Page

Abstract

Introduction

Conclusions

References

Tables

Figures

|◀

▶|

◀

▶

Back

Close

Full Screen / Esc

Printer-friendly Version

Interactive Discussion



## Air–snow transfer of nitrate on the East Antarctic plateau

J. Erbland et al.

**Table 2.** List of the physical and chemical processes included and excluded in TRANSITS. Physical and chemical processes are written in straight and bold font, respectively.

	Processes included	Processes excluded
Snow	Snow accumulation Nitrate diffusion	Snow densification Snow metamorphism (sublimation, melting) Snow erosion Snowpack ventilation
	<b>Nitrate UV-photolysis</b> <b>Cage recombination effects</b>	<b>Dissociation of the deposited HNO<sub>3</sub></b> <b>Nitrate location changes</b> <b>Nitrate saturation</b> <b>Physical release of HNO<sub>3</sub></b>
Atmosphere	Nitrate export  <b>Primary nitrate inputs (strato. and tropo.)</b> <b>HNO<sub>3</sub> dry deposition</b> <b>Local cycling of NO<sub>2</sub> (conceptual)</b> <b>Location oxidation of NO<sub>2</sub> by OH (conceptual)</b>	Variation of ABL  <b>Nitrate wet deposition</b> Formal atmospheric chemistry

- [Title Page](#)
- [Abstract](#) | [Introduction](#)
- [Conclusions](#) | [References](#)
- [Tables](#) | [Figures](#)
- [◀](#) | [▶](#)
- [◀](#) | [▶](#)
- [Back](#) | [Close](#)
- [Full Screen / Esc](#)
- [Printer-friendly Version](#)
- [Interactive Discussion](#)



**Table 3.** Parameters and variables used for the realistic simulation of TRANSITS. Input time-variables and fixed parameters are written in bold.

Process		Realistic, DC	Realistic, EAP
Snow accumulation	$\rho /(\text{kg m}^{-3})$ $\mathbf{A}/(\text{kg m}^{-2} \text{a}^{-1})$ Accu repartition	300 28 Constant throughout the year	[20 to 600]
$\text{HNO}_3$ deposition	$10^3 \times \varepsilon_{\text{dep}}$	-10	
Nitrate diffusion in snow	$D/(\text{m}^2 \text{s}^{-1})$	$1.3 \times 10^{-11}$ at $T = 237 \text{ K}$	
TUV-snow parameters and variables	<b>Optical and physical prop. snowpack</b> $O_3$ column $k$	DC snowpack, from France et al. (2011) DC observations 2000–2009 1	
Nitrate photolysis	$\phi$ $\sigma$ and $\sigma'$ $q$	0.026 From Berhanu et al. (2014a) 1	
Cage effect	$f_{\text{cage}}$ $10^3 \times \Delta^{17}\text{O}(\text{H}_2\text{O})$	0.15 0	
Cycling of $\text{NO}_2$	$[\text{BrO}] / \text{pptv}$ $[\text{RO}_2] / (\text{molecule cm}^{-3})$  $[\text{HO}_2]/[\text{RO}_2]$ $[\text{O}_3] / \text{ppbv}$ $10^3 \times \Delta^{17}\text{O}(\text{O}_3)_{\text{bulk}}$	2.5 (Frey et al., 2014) $= 7.25 \times 10^9 \times (J(\text{NO}_2)/\text{s}^{-1})$ (Kukui et al., 2014) 0.7 (Kukui et al., 2014) From Legrand et al. (2009) 25.2 (Vicars and Savarino, 2014)	
Atmospheric properties	$T/\text{K}$ $P/\text{mbar}$	Concordia AWS (8989) in 2009–2010 Concordia AWS (8989) in 2009–2010	
Nitrate export	$f_{\text{exp}}$	20 %	
Mass balance in the atmosphere	$\text{FPI}/(\text{kg N m}^{-2} \text{a}^{-1})$ $\text{FS/FPI}$ FS repartition FT repartition $h_{\text{AT}}/\text{m}$ $\gamma(\text{NO}_3^-)$ $10^3 \times \Delta^{17}\text{O}(\text{FS})$ $10^3 \times \delta^{15}\text{N}(\text{FS})$ $10^3 \times \Delta^{17}\text{O}(\text{FT})$ $10^3 \times \delta^{15}\text{N}(\text{FT})$	$8.2 \times 10^{-6}$ (Muscati and de Zafra, 2003) 50 % Plateau from 16 May to 18 Oct Constant throughout the year 50 Idealized DC 42 19 30 0	

**Table 4.** Simulated nitrate concentration and isotopic composition at the air–snow interface in the case of the DC realistic simulation.

	Atmosphere			Skin layer		
	$\gamma(\text{NO}_3^-)/(\text{ng m}^{-3})$	$10^3 \times \delta^{15}\text{N}$	$10^3 \times \Delta^{17}\text{O}$	$\omega(\text{NO}_3^-)/(\text{ng g}^{-1})$	$10^3 \times \delta^{15}\text{N}$	$10^3 \times \Delta^{17}\text{O}$
Average	31.9			2953		
Weighted average		-9.8	27.6		26.3	28.6
Min	5.0	-25.3	24.7	772	4.2	24.3
Max	110.0	5.7	39.3	5332	45.4	38.7

- [Title Page](#)
- [Abstract](#) | [Introduction](#)
- [Conclusions](#) | [References](#)
- [Tables](#) | [Figures](#)
- [◀](#) | [▶](#)
- [◀](#) | [▶](#)
- [Back](#) | [Close](#)
- [Full Screen / Esc](#)
- [Printer-friendly Version](#)
- [Interactive Discussion](#)



**Table 5.** Simulated nitrate mass fluxes and their isotopic composition in the case of the DC realistic simulation.

Flux	Annual flux/ ( $10^{-6}$ kg N $m^{-2} a^{-1}$ )	Seasonal flux/ ( $10^{-12}$ kgNm $^{-2}$ s $^{-1}$ )			Seasonal $10^3 \times \delta^{15}\text{N}$			Seasonal $10^3 \times \Delta^{17}\text{O}$		
		Mean	Min	Max	Mean	Min	Max	Mean	Min	Max
FP	32.00	1.01	0.00	3.26	2.4	-31.4	16.6	26.2	24.5	30.2
FD	32.16	1.02	0.10	2.71	3.9	-15.3	15.7	28.4	24.7	39.3
FE	8.04	0.25	0.03	0.68	3.9	-15.3	15.7	28.2	24.7	39.3
FA	0.16	0.01	0.01	0.01	291.6	291.5	291.7	20.6	20.6	20.6
FS	4.10	0.13	0.00	0.45	19.0	19.0	19.0	42.0	42.0	42.0
FT	4.10	0.13	0.13	0.13	0.0	0.0	0.0	30.0	30.0	30.0

<a href="#">Title Page</a>	<a href="#">Abstract</a>	<a href="#">Introduction</a>
<a href="#">Conclusions</a>	<a href="#">References</a>	
<a href="#">Tables</a>	<a href="#">Figures</a>	
<a href="#">◀</a>	<a href="#">▶</a>	
<a href="#">◀</a>	<a href="#">▶</a>	
<a href="#">Back</a>	<a href="#">Close</a>	
<a href="#">Full Screen / Esc</a>		
	<a href="#">Printer-friendly Version</a>	
	<a href="#">Interactive Discussion</a>	



**Table 6.** Simulated nitrate mass, concentration and isotopic composition in the top 50 cm of snow and in the archived flux as well as the apparent fractionation constants.

	Nitrate in top 50 cm			Nitrate in archived flux			Fractionation constants		
	$m_{50\text{cm}}(\text{NO}_3^-)/\text{mgN}$	$10^3 \times \delta^{15}\text{N}$	$10^3 \times \Delta^{17}\text{O}$	$\omega(\text{NO}_3^-)/(\text{ng g}^{-1})$	$10^3 \times \delta^{15}\text{N}$	$10^3 \times \Delta^{17}\text{O}$	$10^3 \times \varepsilon_{\text{app}}$	$10^3 \times E_{\text{app}}$	$10^3 \times \varepsilon_{\text{pho}}$
Average	$8.3 \pm 1.6$			$25.4 \pm 0.0$			$-48.7 \pm 3.5$	$1.5 \pm 0.5$	
Weighted average		89.5	26.2		291.6	20.6			-55.1
Min	6.3	68.7	23.5	25.3	291.5	20.6	-52.3	0.8	-78.8
Max	11.1	114.2	29.5	25.4	291.7	20.6	-42.5	2.3	-52.9

- [Title Page](#)
- [Abstract](#) | [Introduction](#)
- [Conclusions](#) | [References](#)
- [Tables](#) | [Figures](#)
- [◀](#) | [▶](#)
- [◀](#) | [▶](#)
- [Back](#) | [Close](#)
- [Full Screen / Esc](#)
- [Printer-friendly Version](#)
- [Interactive Discussion](#)



## Air–snow transfer of nitrate on the East Antarctic plateau

J. Erbland et al.

[Title Page](#)

[Abstract](#)

[Introduction](#)

[Conclusions](#)

[References](#)

[Tables](#)

[Figures](#)

[◀](#)

[▶](#)

[◀](#)

[▶](#)

[Back](#)

[Close](#)

[Full Screen / Esc](#)

[Printer-friendly Version](#)

[Interactive Discussion](#)



**Table 7.** Overview of the TRANSITS results for the sensitivity tests.

Tested variable	Tested values (reference value)	FA/ ( $10^{-6}$ kg m $^{-2}$ a $^{-1}$ ) (abs. diff.)	FA/FPI in % (abs. diff.)	$10^3 \times$ $\delta^{15}\text{N(FA)}$ (abs. diff.)	$10^3 \times$ $\Delta^{17}\text{O(FA)}$ (abs. diff.)
<b>Realistic simulation</b>	<b>for DC (reference)</b>	<b>0.17</b>	<b>2.04</b>	<b>287.4</b>	<b>20.7</b>
$h_{\text{AT}}/\text{m}$	500 (50)	0.17 (=)	2.04 (=)	287.4 (=)	20.7 (=)
$10^3 \times \varepsilon_{\text{dep}}$	0 (+10)	0.17 (=)	2.04 (=)	287.4 (=)	20.7 (=)
$\gamma(\text{NO}_3^-)$	Real. ideal. DC $\times 10$ <b>(Real. ideal. DC)</b>	0.17 (=)	2.04 (=)	287.4 (=)	20.7 (=)
FPI/( $10^{-6}$ kg N m $^{-2}$ a $^{-1}$ )	82 (8.2)	1.67 (+1.5)	2.04 (=)	287.4 (=)	20.7 (=)
$10^3 \times \delta^{15}\text{N(FS)}$	+119 (+19)	0.17 (=)	2.04 (=)	359.5 (+72.1)	20.7 (=)
$10^3 \times \delta^{15}\text{N(FT)}$	+100 (0)	0.17 (=)	2.04 (=)	343.0 (+55.6)	20.7 (=)
$10^3 \times \Delta^{17}\text{O(FS)}$	0 (42)	0.17 (=)	2.04 (=)	287.4 (=)	18.6 (-2.1)
$10^3 \times \Delta^{17}\text{O(FT)}$	0 (30)	0.17 (=)	2.04 (=)	287.4 (=)	17.2 (-3.5)
$10^3 \times \Delta^{17}\text{O(O}_3\text{)}_{\text{bulk}}$	0 (25.2)	0.17 (=)	2.04 (=)	287.4 (=)	8.3 (-12.4)
[BrO]/pptv	5.0 (2.5)	0.17 (=)	2.04 (=)	287.4 (=)	21.2 (+0.5)
[HO <sub>2</sub> ]	Est. DC $\times 10$ <b>(Est. DC)</b>	0.17 (=)	2.04 (=)	287.4 (=)	19.3 (-1.4)
[CH <sub>3</sub> O <sub>2</sub> ]	Est. DC $\times 10$ <b>(Est. DC)</b>	0.17 (=)	2.04 (=)	287.4 (=)	20.1 (-0.6)
[O <sub>3</sub> ]/ppbv	Obs. DC $\times 10$ <b>(Obs. DC)</b>	0.17 (=)	2.04 (=)	287.4 (=)	21.6 (+0.9)
T/K	Obs. DC -10 <b>(Obs. DC)</b>	0.17 (=)	2.04 (=)	287.4 (=)	20.4 (-0.3)
FS/FPI	0.6 (0.5)	0.16 (-0.0)	1.98 (-0.06)	292.5 (+5.0)	20.8 (+0.1)
$f_{\text{cage}}$	0.18 (0.15)	0.20 (+0.03)	2.41 (+0.37)	276.5 (-10.9)	19.5 (-1.2)
$f_{\text{exp}}$	0.24 (0.2)	0.13 (-0.04)	1.59 (-0.45)	290.8 (+3.4)	21.0 (+0.3)
$A/(\text{kg m}^{-2} \text{ a}^{-1})$	33.6 (28)	0.35 (+0.19)	4.32 (+2.29)	238.7 (-48.7)	21.6 (+0.9)
$\rho/(\text{kg m}^{-3})$	360 (300)	0.07 (-0.1)	0.87 (-1.16)	337.2 (+49.8)	19.9 (-0.8)
$k$	1.2 (1.0)	0.40 (+0.23)	4.82 (+2.78)	225.6 (-61.9)	21.8 (+1.1)
$q$	1.2 (1.0)	0.07 (-0.1)	0.85 (-1.19)	338.5 (+51.1)	19.8 (-0.9)
$\phi$	0.0336 ( <b>0.026</b> )	0.07 (-0.1)	0.85 (-1.19)	338.5 (+51.1)	19.8 (-0.9)
$D/(10^{-11} \text{ m}^2 \text{ s}^{-1})$	1.56 (1.3)	0.18 (+0.01)	2.20 (+0.17)	278.3 (-9.1)	20.9 (+0.2)
Accumulation repartition	Winter = 2 $\times$ summer	0.19 (+0.02)	2.29 (+0.25)	276.2 (-11.2)	20.9 (+0.2)
	Summer = 2 $\times$ winter <b>(flat)</b>	0.15 (-0.01)	1.88 (-0.15)	295.5 (+8.1)	20.6 (-0.1)
$\text{O}_3$ column	100 DU flat	0.01 (-0.16)	0.11 (-1.92)	304.7 (+17.3)	18.0 (-2.7)
	300 DU flat	0.22 (+0.05)	2.64 (+0.61)	280.0 (-7.4)	21.0 (+0.3)
	500 DU flat	0.75 (+0.59)	9.20 (+7.17)	229.8 (-57.6)	22.7 (+2.0)
	300 DU/100 DU hole <b>(real. DC)</b>	0.08 (-0.09)	0.92 (-1.12)	295.4 (+7.9)	19.7 (-1.0)

## Air–snow transfer of nitrate on the East Antarctic plateau

J. Erbland et al.

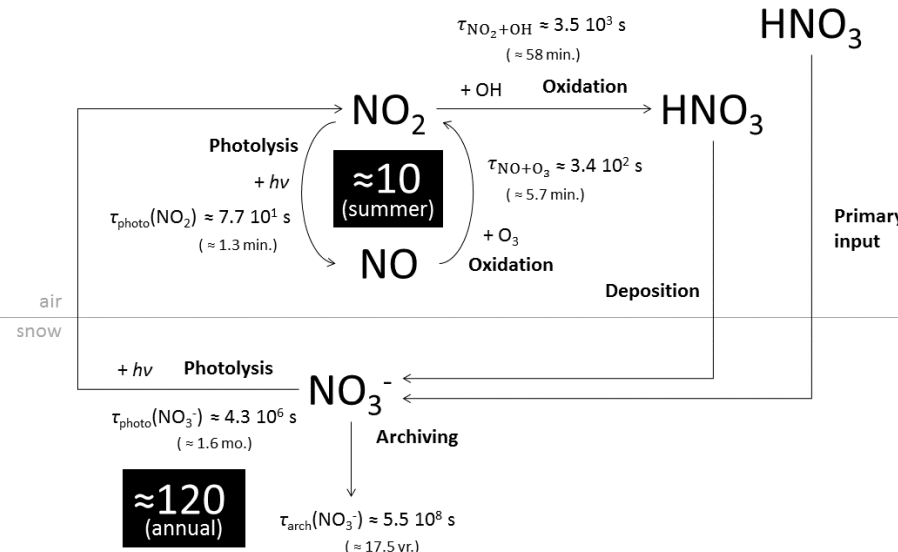


**Figure 1.** Two cycles overlapping at the air–snow interface of Dome C in summer. The calculation of the photochemical, chemical and archiving lifetimes of NO<sub>2</sub> and NO<sub>3</sub><sup>-</sup> for summer solstice conditions are explained in the text. Numbers in the black boxes represent the number of cycles undergone by NO<sub>2</sub> and NO<sub>3</sub><sup>-</sup> before their oxidation and archiving, respectively.

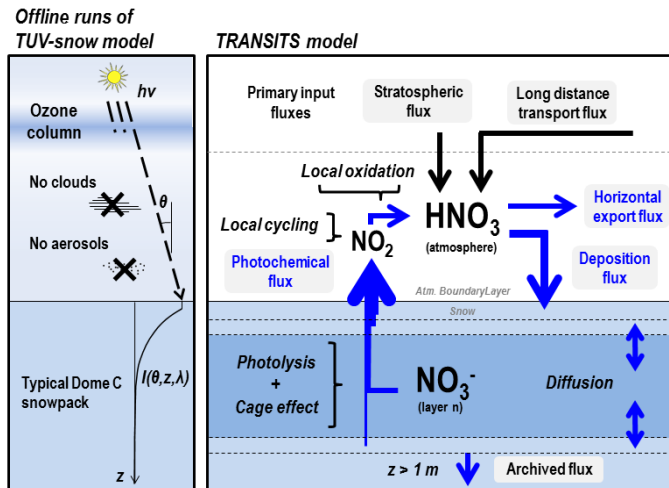


**Figure 2.** Overview of the TRANSITS model.

Title Page	
ostract	Introduction
clusions	References
ables	Figures
◀	▶
◀	▶
Back	Close
Full Screen / Esc	
rinter-friendly Version	
nteractive Discussion	



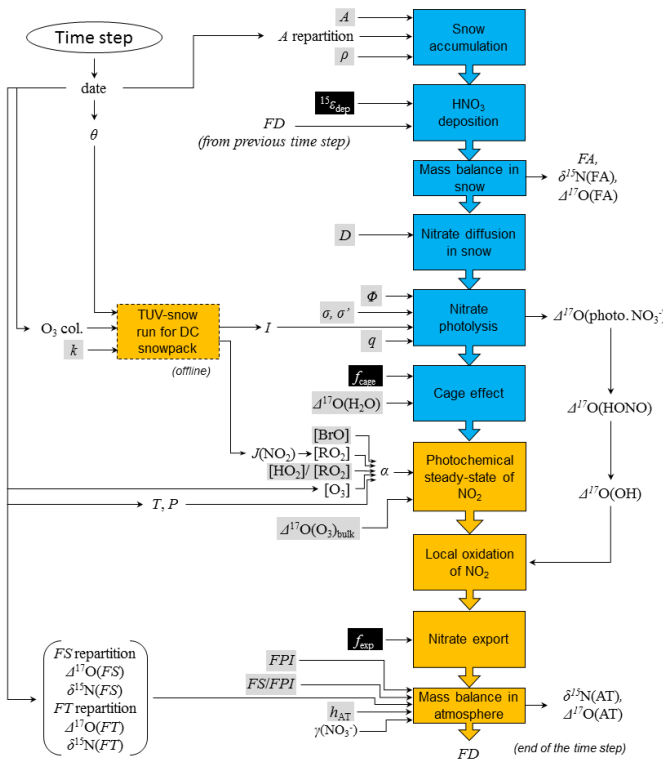


**Figure 3.** Schematic view of the processes included in TRANSITS (one time step is shown). The orange and blue boxes represent processes occurring in the atmosphere and the snowpack, respectively. Arrows entering from left and right sides of each box represent required inputs to the calculation of each process. For the sake of clarity, we only display the input time-variables (black font on white background), the fixed parameters (black on grey) and the tuned parameters (white on black).

**Air–snow transfer of nitrate on the East Antarctic plateau**

J. Erbland et al.

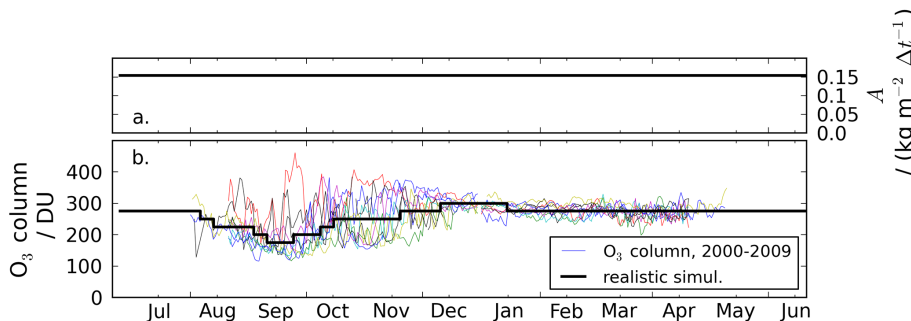


**Figure 4.** Driving data for the DC realistic simulation. **(a)** Snow accumulation rates shared over the 52 time steps ( $A$  is set to  $28 \text{ kg m}^{-2} \text{ a}^{-1}$ ). **(b)** Ozone column. The ozone column scenarios are given with the annual cycles measured at a daily time resolution over the period 2000–2009.

<a href="#">Title Page</a>	<a href="#">Abstract</a>	<a href="#">Introduction</a>
<a href="#">Conclusions</a>	<a href="#">References</a>	
<a href="#">Tables</a>	<a href="#">Figures</a>	
<a href="#">◀◀</a>	<a href="#">▶▶</a>	
<a href="#">◀</a>	<a href="#">▶</a>	
<a href="#">Back</a>	<a href="#">Close</a>	
<a href="#">Full Screen / Esc</a>		
	<a href="#">Printer-friendly Version</a>	
	<a href="#">Interactive Discussion</a>	



## Air–snow transfer of nitrate on the East Antarctic plateau

J. Erbland et al.

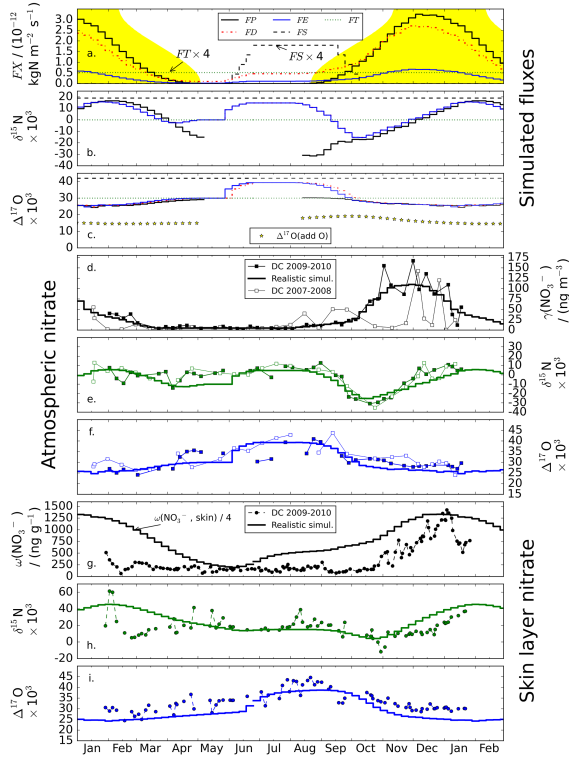


**Figure 5.** Realistic simulation results and comparison to the observations at Dome C. **(a–c)** Simulated fluxes (mass and isotopic composition) and  $\Delta^{17}\text{O}$  in the additional O atom (panel **c**). The yellow filled curve in panel **(a)** represents the day length at Dome C. Note that  $\delta^{15}\text{N}$  and  $\Delta^{17}\text{O}$  in FE and FD are equal. **(d–f)** Simulated and observed concentrations.  $\delta^{15}\text{N}$  and  $\Delta^{17}\text{O}$  in atmospheric nitrate. **(g–i)** Simulated and observed mass fractions.  $\delta^{15}\text{N}$  and  $\Delta^{17}\text{O}$  in skin layer nitrate. The 2007–2008 and 2009–2010 observed data originate from Frey et al. (2009) and Erbland et al. (2013) respectively.

## Air–snow transfer of nitrate on the East Antarctic plateau

J. Erblund et al.

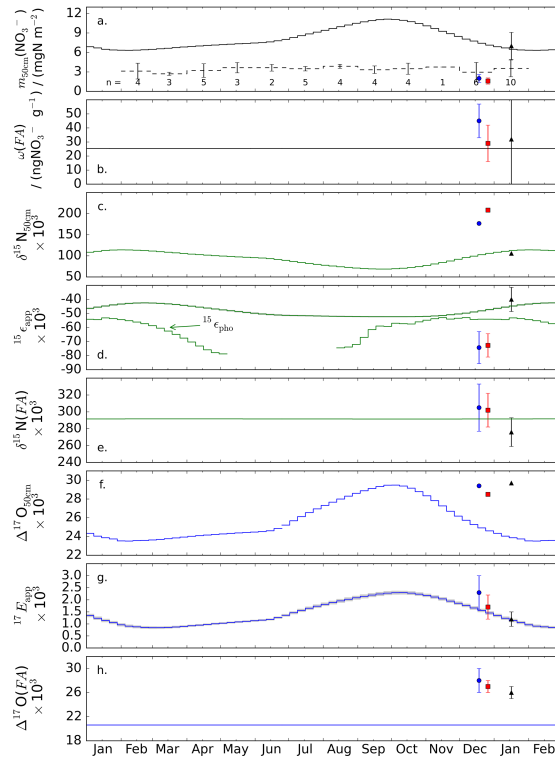


**Figure 6.** Realistic simulation results for the snowpack and comparison to the observations at Dome C. **(a)** Nitrate mass in the top 50 cm (the dashed curve represents the observed monthly values), **(b)** archived nitrate mass fractions, **(c)**  $\delta^{15}\text{N}$  of nitrate in the top 50 cm, **(d)** apparent and photolytic  $^{15}\epsilon$  fractionation constants (in grey the range  $\pm 1\sigma$ ), **(e)**  $\delta^{15}\text{N}$  in the archived nitrate, **(f)**  $\Delta^{17}\text{O}$  of nitrate in the top 50 cm, **(g)** apparent  $^{17}\text{E}$  fractionation constant (in grey the range  $\pm 1\sigma$ ) and **(h)**  $\Delta^{17}\text{O}$  in the archived nitrate. In each panels, the observed data from the three DC snowpits (Frey et al., 2009; Erblund et al., 2013) are represented the same symbols as in Fig. 7).

**Air–snow transfer of nitrate on the East Antarctic plateau**

J. Erblund et al.

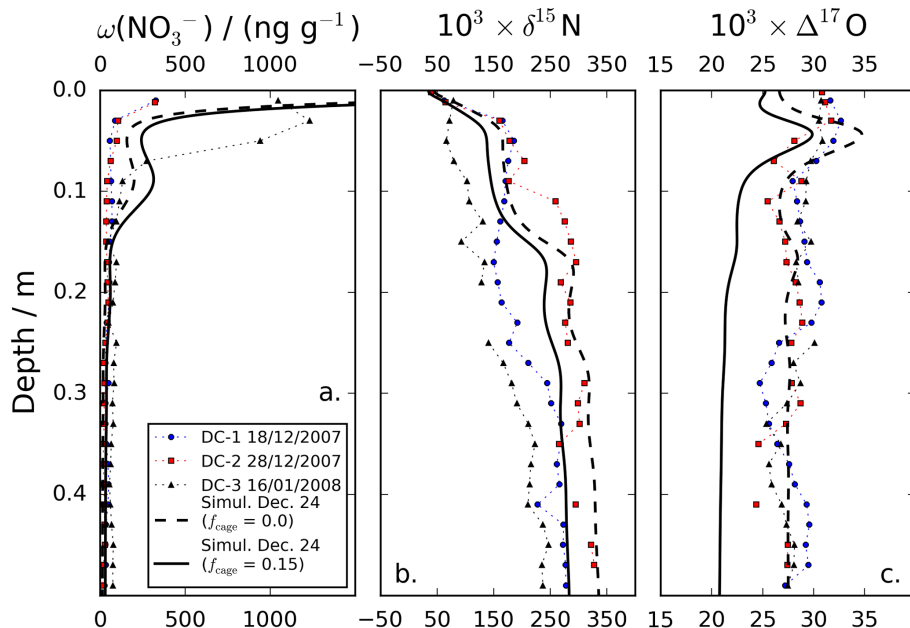


**Figure 7.** Realistic simulation results: nitrate in the 50 top cm of the snowpack on 24 December and comparison to the three observed profiles at Dome C in summer 2007–2008 (Frey et al., 2009; Erblund et al., 2013). **(a)** Nitrate mass fractions, **(b)**  $\delta^{15}\text{N}$  in nitrate and **(c)**  $\Delta^{17}\text{O}$  in nitrate.

- [Title Page](#)
- [Abstract](#) [Introduction](#)
- [Conclusions](#) [References](#)
- [Tables](#) [Figures](#)
- [◀](#) [▶](#)
- [Back](#) [Close](#)
- [Full Screen / Esc](#)
- [Printer-friendly Version](#)
- [Interactive Discussion](#)



Air–snow transfer of  
nitrate on the East  
Antarctic plateau

J. Erbland et al.

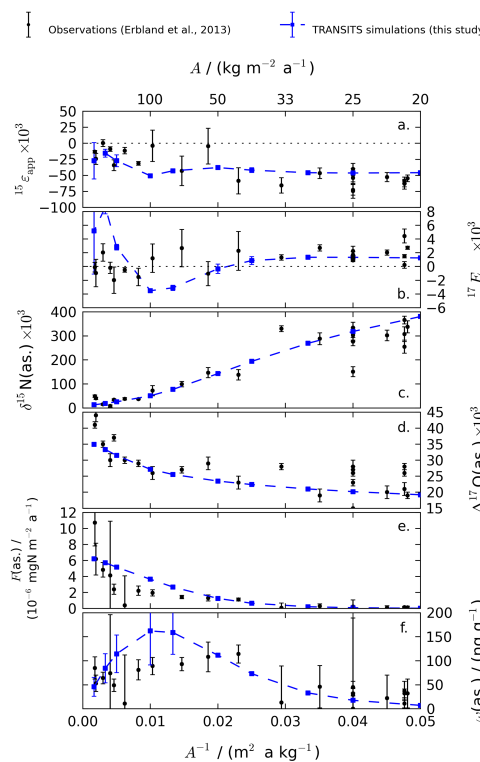


**Figure 8.** Reduced data in the TRANSITS simulations across East Antarctica and in the observations (Erbland et al., 2013) as a function of the snow accumulation rates (top x axis) and their inverse (bottom x axis). (**a–b**)  $^{15}\text{N}/^{14}\text{N}$  and  $^{17}\text{O}$ -excess apparent fractionation constants (simulated dots and errors bars represent the mean and SD values over the December/January period), (**c–d**) asymptotic (observed) and archived (modeled)  $\delta^{15}\text{N}$  and  $\Delta^{17}\text{O}$  values (simulated dots represent annual average values), (**e**) asymptotic and archived nitrate mass, (**f**) asymptotic and archived nitrate mass fractions (simulated dots and errors bars represent the mean and SD values over the whole year).

## Air–snow transfer of nitrate on the East Antarctic plateau

J. Erbland et al.

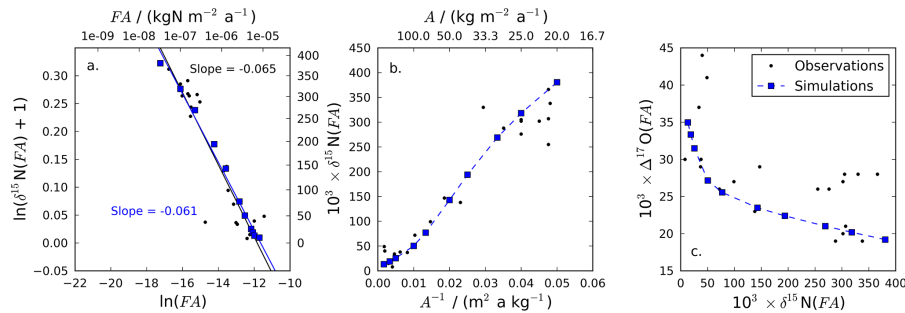


**Figure 9.** Realistic simulation with varying snow accumulation rates (blue squares) vs. observations along the D10–Dome C–Vostok route (black dots). **(a)** Modified Rayleigh plot. The two lines are linear fit to the data and the slopes are given in the respective colors. **(b)**  $\delta^{15}\text{N}(\text{FA})$  vs. the inverse of the snow accumulation rates, **(c)**  $\Delta^{17}\text{O}(\text{FA})$  vs.  $\delta^{15}\text{N}(\text{FA})$ .

## Air–snow transfer of nitrate on the East Antarctic plateau

J. Erbland et al.

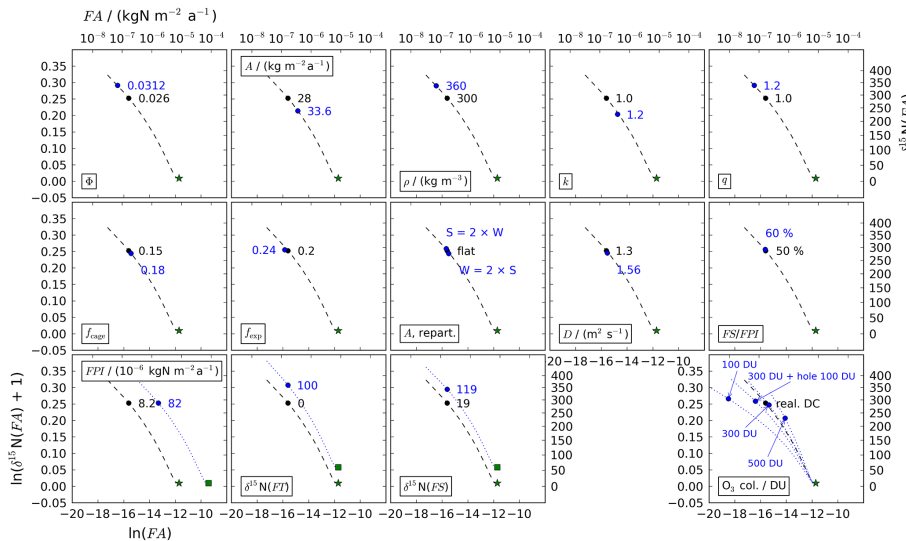


**Figure 10.** Modified Rayleigh plots of the sensitivity tests to the TRANSITS model. Only the tests which imply significant changes in FA and  $\delta^{15}\text{N}(\text{FA})$  are shown. The green star represents the starting point whose coordinates are ( $\ln(\text{FPI})$ ,  $\ln(\delta^{15}\text{N}(\text{FA}) + 1)$ ) and thick dashed lines represent the curve which is obtained for the realistic DC simulation ( $\phi$  varied). The other blue dashed curves represent the consequences of a change in the starting point (squares) or in the ozone column.

## Air–snow transfer of nitrate on the East Antarctic plateau

J. Erbland et al.

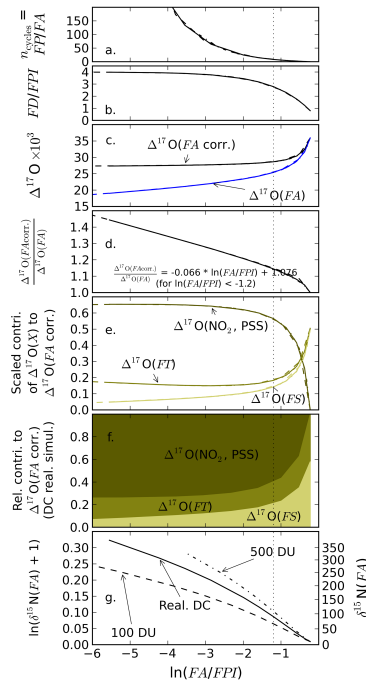


**Figure 11.** TRANSITS simulations of the reduction in  $\Delta^{17}\text{O}(FA)$  under the cage recombination effects and scaled contributions to  $\Delta^{17}\text{O}(FA, \text{corr.})$  as a function of nitrate trapping efficiency ( $\ln(FA/FPI)$ ). **(a)** Number of recycling cycles undergone by nitrate at the air–snow interface, **(b)** deposition ratio ( $FD/FPI$ ), **(c)**  $\Delta^{17}\text{O}(FA)$  with and without cage effect and **(d)** the associated  $\Delta^{17}\text{O}(FA, \text{corr.})/\Delta^{17}\text{O}(FA)$  ratio, **(e)** the scaled contributions of  $\Delta^{17}\text{O}(\text{NO}_2, \text{PSS})$ ,  $\Delta^{17}\text{O}(FT)$  and  $\Delta^{17}\text{O}(FS)$ , **(f)** the relative contributions to  $\Delta^{17}\text{O}(FA, \text{corr.})$  in the DC case ( $\Delta^{17}\text{O}(\text{NO}_2, \text{PSS}) = 31.3\%$ ,  $\Delta^{17}\text{O}(FT) = 30\%$  and  $\Delta^{17}\text{O}(FS) = 42\%$ ), and **(g)** the  $\delta^{15}\text{N}(FA)$  as a function of the ozone column. Note that for the **(a–f)** panels, the curves for the three  $\text{O}_3$  column case superimpose. The vertical dashed line at  $\ln(FA/FPI) = -1.2$  represents a threshold value below which  $\Delta^{17}\text{O}(FA, \text{corr.})/\Delta^{17}\text{O}(FA)$  ratio is linear with  $\ln(FA/FPI)$ .

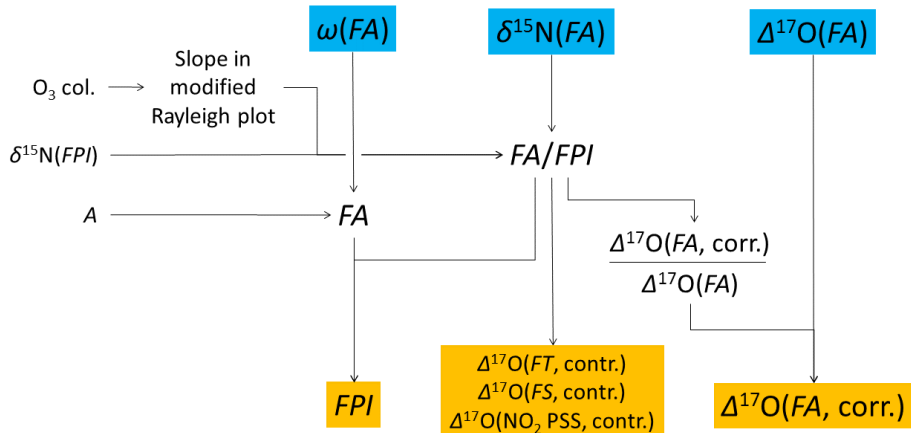


**Figure 12.** Schematic of the methods to retrieve information from  $\omega$  (FA),  $\delta^{15}\text{N}(FA)$  and  $\Delta^{17}\text{O}(FA)$  in ice cores. Orange boxes at the bottom of the figure represent the variable. which can be retrieved from variables measured in ice cores.